R 695

Technical Report

DYNAMIC SHEAR STRENGTH OF REINFORCED CONCRETE BEAMS—PART III

September 1970

Sponsored by

DEFENSE ATOMIC SUPPORT AGENCY

NAVAL FACILITIES ENGINEERING COMMAND

NAVAL CIVIL ENGINEERING LABORATORY

Port Hueneme, California

187

DYNAMIC SHEAR STRENGTH OF REINFORCED CONCRETE BEAMS—PART III

Technical Report R 695

Y-F008 08 02 110, DASA SC3318

by

Richard H Seabold

ABSTRACT

Theoretical and experimental work was done at NCEL to study shear and diagonal tension in rectangular reinforced concrete beams on simple supports and subjected to uniformly distributed dynamic and static loads The objective was to determine criteria for the minimum amount of web reinforcement required for developing the ultimate flexural resistance of beams, and to determine the difference between these criteria for static and dynamic loading

The main portion of the experimental work consisted of testing 53 beams, 29 were loaded dynamically and 24 were loaded statically Emphasis was placed on effectiveness of web reinforcement, 47 beams contained web reinforcement and six had none All of the beams were tested in the NCEL blast simulator Static loads were applied using compressed air, and dynamic loads were applied using the expanding gas from detonation of Primacord explosive All of the beams were slender, and all of them were rectangular except 10 that were I shaped

It was found that the shear and the shear strength in the beams were greater under dynamic load than under the same amount of load applied statically Furthermore, it was found that a beam with enough web reinforcement to force flexural failure under static loading might not have enough to force flexural failure under dynamic loading The theory was found to predict behavior up to the usable ultimate shear strength within normal engineering accuracy and to provide a fair estimate of the time, location, and mode of failure

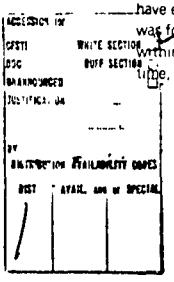

CONTENTS

INTRODUCTION

Objectives

In order to design structures to withstand the effects of nuclear weapons, there is a need for knowledge of the resistance and behavior in shear of reinforced concrete beams under dynamic load The objectives of the work reported here were to determine criteria for the minimum amount of web reinforcement required for developing the ultimate flexural resistance of beams, and to determine the difference between these criteria for static and dynamic loading

Background

Failure and Design Criteria. The major difference between design criteria for protective construction and conventional construction has been stated by Hammer and Dill in the following paragraph [1]

> When considering the atomic defense problem, the usual concept of failure of a structure must be extended Superimposed on the usual considerations are those of military and emergency operation In some cases major damage can be accepted and in other cases the acceptable damage is only minor. The structure must be thought of as having an assigned primary or secondary function Performance of this function may be required immediately or a time for recovery may be allowable.

Army,[2] Navy,[3] and Air Force[4] manuals and a book[5] are available to designers for use as guides for designing structures to resist the effects of nuclear weapons. They contain discussions indicating that depending on the mission of a structure that structure might be designed to behave elastically, elasto plastically, or plastically Further, the design criteria for elements might be based on absolute displacements, relative displacements, stresses, strains, accelerations, and/or velocities. These references provide little or no information about the economical design in shear of reinforced concrete beams under dynamic load. The information that is provided is based on static testing of beams and is projected to the dynamic case using logical reasoning and data from dynamic tests on engineering materials

The following important statement is part of a discussion of failure and design criteria in the Air Force Design Manual [6]

> It is usually desirable to insure that if failure does occur it will be in a predicted fashion This can be decided either with the aim of reducing the violence of suddenness of failure or of controlling failure in a manner which is well understood.

From this statement, it is deduced that reinforced concrete beams should be proportioned in such a way that if failure does occur the mode of failure will be ductile flexure since flexural behavior is the best understood behavior and ductile failures are less violent than brittle ones. Also, if large shear cracks are to be allowed, beams should be proportioned in such a way that shear behavior will tend toward the most favorable mode of shear failure

Beams Failing in Shear Under Static Loads. Researchers have been active during the last 15 years advancing theories about static shear behavior and testing beams which failed in shear under static loads. In Germany, Leonhardt and Walther[7 8] conducted an extensive long-term program. Their theoretical studies included the concepts of truss analogy, tied arch analogy, and shear failure moment They performed a large number of tests on reinforced concrete beams which included uniform and concentrated loads, simple supports, rectangular sections and T-sections, various web thicknesses, a wide range of span-to-depth ratio, high-strength steel, high-strength concrete, and various types and arrangements of web reinforcement Uniform load was obtained by placing pressurized fire hoses between a loading beam and the test beam Some of the beams had no web reinforcement, others had web reinforcement consisting of bent-up inclined bars, vertical stirrups, or inclined stirrups. The results of the tests indicated that stirrups, when functioning at high stresses as shear reinforcement, are more suitable than bent-up inclined bars, and if failure results from destruction of the shear-compression zone, it may be advantageous to use vertical stirrups with their relieving effect upon the compression flange.

Ojha, also working in Germany, presented a paper[10] in which he gave a method of calculating the shear strength of reinforced and prestressed concrete rectangular beams under one- or two-point loads. The behavior of the concrete in the compression zone is considered in the method by use of a distortion energy principle similar to the shear rotation concept. In both distortion energy and shear rotation concepts, (1) it is assumed that there is a point of rotation at or near the head of the main shear crack and (2) the end portion of the beam, which tends to break away from the remainder of the beam, is considered as a free body. In the free-body diagram given by

Ojha, force vectors are shown for the reaction at the support, tension in the longitudinal reinforcement, horizontal and vertical components for stirrups, horizontal and vertical components of compression in the concrete, and vertical shear in the concrete. The method could be expanded to include other loading conditions by adding force vectors to the diagram and introducing additional terms to the equations.

Concurrent with the German work mentioned above, Krefeld and Thurston[11] conducted a program at Columbia University. This investigation included the testing of some 200 simply supported beams, with and without stirrups, having a range of concrete strengths, steel ratios, and span subjected to both concentrated and uniform loads. Most of the beams with stirrups were subjected to a center concentrated load. Uniform load was simulated by eight-point concentrated loading. Dowel action by the longitudinal tension reinforcement was one of the main items being studied, and it was found that stirrups function in dowel action by providing support for the longitudinal reinforcement. The theoretical work is based mostly on the shear rotation concept and presupposes that after the shear crack has extended a short distance into the compression zone, further propagation due to shear depends upon the ability of the beam to resist the dowel force at the level of the longitudinal bars. The following equation was developed for computing the shear resistance in beams without web reinforcement.

$$\frac{V_x}{bh} = 1.8\sqrt{f'_c} + \frac{2{,}600\,p}{\left[\frac{M}{Vd}\right]_x} \qquad (1)$$

where V_x = shear resistance at the critical section (lb)

b = beam width (in.)

h = beam height (in.)

f'_c = 28-day compressive strength of concrete (psi)

p = steel ratio

d = effective depth of the beam (in.)

x = distance from the support to the critical section (in.)

$[M/V]_x$ = moment-shear ratio at the critical section (in.)

Since the shear and moment distributions along the span are different for the two loading distributions, equations associated with each type of loading were developed for relating shears and moment-shear ratios at the support to those at the critical section. For concentrated loadings

$$V_x = V \tag{1a}$$

$$\left[\frac{M}{V}\right]_x = x \tag{1b}$$

whereas for uniform loadings

$$V_x = \frac{V(L - 2x)}{L} \tag{1c}$$

$$\left[\frac{M}{V}\right]_x = \frac{Lx - x^2}{L - 2x} \tag{1d}$$

where V = shear at the support (lb)

L = span length (in.)

Measurements on test beams indicated that for concentrated loadings

$$x = 0.6a \qquad 2 \leq a/d \leq 5 \tag{1e}$$

$$x = a - 2d \qquad 5 \leq a/d \tag{1f}$$

where a is the shear span in inches, and for uniform loadings

$$x = 0.2L \qquad 4 \leq L/d \leq 10 \tag{1g}$$

$$x = 2d \qquad 10 \leq L/d \tag{1h}$$

The following equations were developed for estimating the maximum shear intensity in beams with stirrups subjected to one and two concentrated loads

$$\frac{V_{ult}}{bh} = v_c + rf_y \qquad 90 \text{ psi} \leq rf_y \tag{2}$$

$$\frac{V_{ult}}{bh} = v_c + 1.5 r f_y - 45 \qquad 30 < r f_y < 90 \text{ psi} \qquad (2a)$$

$$\frac{V_{ult}}{bh} = v_c \qquad r f_y < 30 \text{ psi} \qquad (2b)$$

where V_{ult} = ultimate shear resistance (lb)

v_c = V_x/bh, shear intensity in beam without web reinforcement (psi)

r = reinforcement ratio for web reinforcement

f_y = yield strength of web reinforcement (psi)

Information regarding static shear resistance has been documented by many authors, much of which is summarized in the report of the ACI ASCE Joint Committee 326, "Shear and Diagonal Tension."[12] The following semi-empirical equations, which have been incorporated in the "ACI Building Code,"[13] were selected by Committee 326 as the basis for design criteria for statically loaded beams

$$v_c = \frac{V_c}{bd} = \phi\left(1.9\sqrt{f'_c} + 2{,}500\,\frac{p V d}{M'}\right) \leq 3.5\phi\sqrt{f'_c} \qquad (3)$$

$$v_u = \frac{V_u}{bd} = v_c + \phi(\sin\alpha + \cos\alpha)\frac{A_v f_y}{bs} \leq 10\phi\sqrt{f'_c} \qquad (4)$$

where v_c = shear strength at the critical section contributed by the concrete (psi)

v_u = usable ultimate shear strength at the critical section (psi)

V_c = shear resistance at the critical section contributed by the concrete (lb)

V_u = usable ultimate shear resistance at the critical section (lb)

b = width of the beam (in.)

d = effective depth of the beam (in.)

ϕ = capacity reduction factor

f'_c = 28-day compressive strength of concrete (psi)

p = steel ratio

V/M = shear-moment ratio at the critical section (in^{-1})

α = angle of inclination of web reinforcement (deg)

A_v = area of a stirrup (in^2)

f_y = yield strength of stirrups (psi)

s = horizontal spacing of stirrups (in)

An equation is not given in the Code for calculating the distance from the support to the critical section. It is stated, however, that "the shear at sections between the face of the support and the section a distance, d, therefrom shall not be considered critical." This infers that for simply supported beams of constant cross section subjected to uniform loading, the distance from the face of the support to the critical section may be assumed to be equal to the effective depth of the beam, d. For beams with web reinforcement, the Code provides for a lower limit to the area of web reinforcement as follows

$$A_v > 0.0015bs \qquad (4a)$$

Equation 3 is intended for designing beams without web reinforcement and is based on the following

(1) Diagonal tension is a combined stress involving horizontal tensile stress due to bending as well as shearing stress

(2) Since failure due to shear can occur with the formation of the critical diagonal crack if redistribution of internal forces is not accomplished in design, the load causing the formation of the critical diagonal tension crack is generally considered as the ultimate load carrying capacity of a reinforced concrete member without web reinforcement

Committee 326 studied the data from more than 440 beam tests and concluded that the three significant parameters are percentage of longitudinal reinforcement, p, the dimensionless quantity, M/Vd, and the quality of the concrete, f'_c. The equation was obtained by fitting the parameters to the data from 194 tests on beams with simple supports and concentrated loads. At a later time, data from other tests with different conditions of loading and restraint correlated well with values computed using the equation

Equation 4 is intended for designing beams with web reinforcement and is based on the following

(1) Failure can occur in diagonal tension upon diagonal cracking, in shear-compression upon yielding of the web reinforcement, or in shear-compression prior to yielding of the web reinforcement

(2) Shear-compression is the most common mode of failure in normally proportioned beams.

(3) The ultimate shearing capacity is the sum of the shearing capacity at diagonal cracking plus a contribution from the web reinforcement at the point where yielding of the web reinforcement occurs.

(4) The concept of truss analogy can be used to analyze the stress in the web reinforcement

The equation was obtained by summing the terms for the cracking resistance and for the contribution from web reinforcement From the above concepts and observations, Keenan[14] concluded that the effective amount of web reinforcement required to produce a flexural failure is a function of the difference between the shears corresponding to the ultimate flexural resistance and the diagonal tension cracking resistance Tests on beams with web reinforcement to support Equation 4 were limited both in number and scope.[12]

The Code equations, numbers 3 and 4, are similar to the Krefeld and Thurston equations, numbers 1 and 2 They contain the same dominant parameters, the same general form, and nearly the same values for coefficients. The use of effective depth, **d**, instead of the height of the beam, **h**, and the use of the capacity reduction factor, ϕ, tend to make the Code equations more conservative than the other equations. On the other hand, the distance to the critical section permitted by the Code may tend to make the Code equations less conservative than the others. Another difference in the equations is the lower limit on stirrup effectiveness The Code equations tend to be the less conservative in the case of very small beams with small amounts of web reinforcement where

$$A_v > 0.0015\,b\,s \quad \text{and} \quad r f_y < 30 \text{ psi}$$

Rajagopalan and Ferguson* indicated that the Code equation for the shear strength contributed by the concrete, v_c, is unconservative when the steel ratio, p, is small They performed tests on ten beams having p between

* Unpublished communication "Exploratory shear tests emphasizing percentage of longitudinal steel," by K S Rajagopalan and P M Ferguson University of Texas at Austin, Oct 1967

0.0173 and 0 0025. Also, they analyzed the results of tests by other investigators on 27 beams with p less than 0.012 For the data analyzed, the following equation seemed to define a safe lower bound

$$v_c = (0.8 + 100\,p)\sqrt{f'_c} \qquad p < 0.012 \qquad (5)$$

Dynamic Properties of Materials. The rapid loading of materials causes rapid strain rates which, in turn, affect the stress–strain relationships and the circumstances under which brittle failure can occur. As the rate of strain in steel is increased, (1) the yield stress increases, (2) the yield strain increases, (3) the modulus of elasticity in the elastic range remains essentially constant, (4) the strain at which strain hardening begins increases, and (5) the ultimate strength increases.[5] Since the yield stress increases more rapidly than the ultimate stress, failures in material specimens tend to be more brittle under dynamic load than under static load Concrete under dynamic compression behaves similarly, but the influence of strain rate on the compressive strength of concrete is not as easily determined First, the stress–strain relationship of concrete has no appreciable linear region even under static load. Second, in the Code provisions for static design of beams, the compressive limit (yield) strain, 0 003 in./in , is rather arbitrarily chosen. Third, the effective modulus of elasticity appears to change under dynamic load Attention is also given to the possibility that concrete in control specimens may behave differently than concrete in beams because of boundary effects, size effects, and the presence or absence of bond with compression reinforcement. Dynamic yield stresses for concrete in compression and reinforcing bars in tension are recommended in several sources.[4, 5, 16]

Nagarajo Rao, Lohrmann, and Tall[16] tested specimens of ASTM steels A36, A441, and A514 to determine the effect of strain rate on yield stress in the inelastic range. They presented the following equation to relate the strain rate to the ratio of the dynamic yield stress level and the static yield stress level

$$\frac{\sigma_{yd}}{\sigma_{ys}} = 1 + k\dot{\varepsilon}^n \qquad (6)$$

where σ_{yd} = dynamic yield stress level (psi)

σ_{ys} = static yield stress level (psi)

k = constant peculiar to the material

n = constant peculiar to the material

$\dot{\varepsilon}$ = strain rate (in /in /sec)

The dynamic yield stress level, σ_{yd}, was defined as the average stress during actual yielding in the inelastic range, which remains fairly constant provided the strain rate remains constant. The static yield stress level, σ_{ys}, was defined as the average stress during actual yielding in the inelastic range at zero strain rate, this stress remains fairly constant. When the stress was not constant, it was taken as the stress corresponding to a strain of 0.5%.

Tests were made by Lundeen and Saucier[17] to study the dynamic tensile strength of concrete, otherwise, little or no background information could be found regarding dynamic tensile and shear strengths of concrete and dynamic bond strength.

Beams Failing in Shear Under Impact Loads. Research on the shear and bond strength of high-strength reinforced concrete beams under impact loads has been conducted at the University of Texas under contract with the Air Force Weapons Laboratory (AFWL).[18, 19] The first phase, now complete, included 41 beam tests: 4 flexure tests, 22 shear tests, and 15 anchorage tests. All the beams had 28-day compressive strengths of concrete, f'_c, of about 8,000 psi and longitudinal reinforcing bar yield strengths, f_y, exceeding 75,000 psi. All were simply supported and subjected to concentrated loadings. Twenty-two beams were loaded slowly (static load) and 19 beams were loaded rapidly by means of a falling mass (impact load) that struck the beams through an impulse-controlling cushion. The initial rise time to about 50% of the maximum load was 3 to 5 msec. After the initial rise, the force continued to increase at a slower rate until the specimen failed or absorbed all the energy of the drop. The time from impingement to maximum force varied from 25 to 70 msec. Flexure, shear, and anchorage failures were obtained.

In the 22 shear tests, both deep and slender beams were tested. Eleven beams were loaded dynamically and 11 companions were loaded statically. Punching shear, diagonal tension, and shear-compression failures were obtained. Only three beams with stirrups were tested dynamically, therefore, no quantitative conclusions were made regarding the effectiveness of stirrups under dynamic load.

Scope

Experimental Work. The main portion of the experimental work at NCEL consisted of tests on simply supported reinforced concrete beams subjected to dynamic and static uniformly distributed loads. Of the 53 beams tested, 29 were loaded dynamically and 24 were loaded statically. Emphasis was placed on effectiveness of web reinforcement; 47 beams contained web reinforcement and six had none.

Static uniform loads were applied using compressed air, dynamic uniform loads were applied using the expanding gas from detonation of Primacord. Dynamic loads had rise times of 1 to 2 msec and exponential decays. Dynamic load durations varied from $T/T_n = 1.4$ to $T/T_n = \infty$, where T is the effective load duration and T_n is the natural period of vibration.

The 43 rectangular beams were slender ($L/d \geq 7$) and they had either no web reinforcement or web reinforcement consisting of vertical deformed bars or plain wires. The primary parameters studied were peak load, load duration, and rate of loading, stirrup spacing, area of stirrups, and the yield strength of the stirrups, and concrete strength (Table 1). Length-to-depth ratio and longitudinal steel percentage were studied also, but to a lesser degree.

The 10 I-beams had very thin webs and were of intermediate slenderness ($5 < L/d < 7$), and they had welded wire fabric for web reinforcement. The parameters studied were peak load, rate of loading, stirrup area, yield strength of the stirrups, and longitudinal steel percentage (Table 2). A limited study on the effects of web width on diagonal tension was made by comparing the behavior of the rectangular beams and the I-beams.

The beam tests were supplemented by dynamic and static tests on the materials used in the beams to determine the dynamic properties of the concrete, stirrups, and longitudinal bars in tension, and the concrete in compression. Pull-out tests to study the influence of normal pressure on bond were conducted at the Iowa State University.

The I-beam tests, the pull-out tests, and some of the dynamic tests on concrete were funded by the Naval Facilities Engineering Command under Work Unit Y-F011-05-04-002, Thin Shell Construction. All of the other testing was funded by DASA under Subtask No. SC3318 (formerly Subtask 13.018 and RSS3318).

Theoretical Work. A simplified design method and both simplified and rigorous analysis methods were developed for simply supported rectangular reinforced concrete beams under uniform and concentrated dynamic loads. Many of the equations apply to other conditions of loading and restraint as well. Equations were developed for predicting the maximum dynamic shear at the support (used in the simplified methods), the shear at the support with respect to time (used in the rigorous method), and the dynamic resistance of the beam at the support corresponding to shear cracking, shear yielding, shear failure, flexural yielding, and flexural failure

Table 1 Proportions and Static Material Properties of the Rectangular Beams Tested

Beam No.	Load Type	L/d	b/d	d/d	f'_c (psi)	f_y (psi)	ρ	f_y (psi)	ρ	f_y (psi)	s (in.)	A_v (in.²)	(0.0015) $b_w s$ (in.²)
WA1	static	13.0	0.601	0.116	5,440	71,000	0.0199	77,000	0.0120	b	b	b	b
WA2	static	13.0	0.601	0.116	5,440	71,000	0.0199	76,400	0.0120	b	b	b	b
WA3	static	13.0	0.601	0.116	4,760	71,000	0.0199	77,000	0.0120	72,000	6	0.10	0.0698
WA4	dynamic	13.0	0.601	0.116	4,760	71,000	0.0199	71,700	0.0120	67,100	6	0.10	0.0698
WB1	static	11.2	0.601	0.116	5,440	71,000	0.0199	77,000	0.0120	b	b	b	b
WB3	static	11.2	0.601	0.116	5,440	71,000	0.0199	77,000	0.0120	71,500	6	0.10	0.0698
WB.1	static	11	0.601	0.116	4,750	72,000	0.0199	77,000	0.0120	44,000	6	0.10	0.0698
WD1	static	11.2	0.601	0.116	5,440	70,000	0.0199	66,300	0.0120	41,000	6	0.10	0.0698
WD2	static	11.2	0.601	0.116	5,810	70,100	0.0199	65,500	0.0120	39,000	6	0.10	0.0698
WD3	static	11.2	0.601	0.116	5,760	69,100	0.0199	67,700	0.0120	41,000	6	0.10	0.0698
WD4	dynamic	11.2	0.601	0.116	5,810	70,100	0.0199	64,400	0.0120	34,000	6	0.10	0.0698
WD	dynamic	11.2	0.601	0.116	4,760	70,000	0.0199	66,400	0.0120	31,000	6	0.10	0.0698
WD5	dynamic	11.2	0.601	0.116	5,810	69,500	0.0199	65,900	0.0120	30,000	6	0.10	0.0698
WD7	dynamic	11.2	0.601	0.116	5,760	71,100	0.0199	66,400	0.0120	40,500	6	0.10	0.0698
WD8	dynamic	11.2	0.601	0.116	4,440	69,900	0.0199	65,100	0.0120	37,300	6	0.10	0.0698
WD9	dynamic	11.2	0.601	0.116	5,810	71,400	0.0199	65,200	0.0120	39,500	6	0.10	0.0698
WE 1	dynamic	11.2	0.601	0.116	4,010	70,900	0.0199	66,300	0.0120	36,000	3	0.0346	0.0581
WE 2	dynamic	11.2	0.601	0.116	3,990	68,700	0.0199	65,900	0.0120	35,000	3	0.0346	0.0581
WE 3	dynamic	11.2	0.601	0.116	4,150	69,800	0.0199	66,600	0.0120	36,000	3	0.0346	0.0581
WE 4	dynamic	11.2	0.601	0.116	4,120	67,900	0.0199	64,100	0.0120	34,000	3	0.0346	0.0581
WE 5	dynamic	11.2	0.601	0.116	4,110	68,800	0.0199	67,700	0.0120	36,000	3	0.0346	0.0581
WE 6	dynamic	11.2	0.601	0.116	4,120	68,000	0.0199	64,400	0.0120	34,000	3	0.0346	0.0581
WE 7	static	11.2	0.601	0.116	3,820	70,500	0.0199	68,000	0.0120	36,000	3	0.0346	0.0581
WE 8	static	11.2	0.601	0.116	3,910	67,800	0.0199	64,900	0.0120	36,000	3	0.0346	0.0581
WE 9	static	11.2	0.601	0.116	4,010	68,800	0.0199	67,000	0.0120	36,000	3	0.0346	0.0581
WE 10	static	11	0.601	0.116	3,820	66,200	0.0199	64,100	0.0120	36,000	3	0.0346	0.0581
WE 11	static	11.2	0.601	0.116	3,420	67,100	0.0199	66,800	0.0120	36,000	3	0.0346	0.0581
WE 12	dynamic	11.2	0.601	0.116	3,960	66,000	0.0199	64,400	0.0120	36,000	3	0.0346	0.0581
OE 1	static	11.2	0.601	0.116	3,400	68,900	0.0199	66,000	0.0120	b	b	b	b
OE 2	dynamic	11.2	0.601	0.116	3,690	66,000	0.0199	64,000	0.0120	b	b	b	b
OE 3	static	11.2	0.601	0.116	4,180	66,000	0.0199	64,000	0.0120	b	b	b	b
WF 1	static	11.79	0.446	0.0817	6,210	69,000	0.0182	66,900	0.0109	30,000	3	0.0587	0.0315
WF 2	static	11.79	0.446	0.0817	6,010	68,500	0.0182	70,100	0.0109	30,000	3	0.0587	0.0315
WF 3	dynamic	11.79	0.446	0.0817	5,940	67,000	0.0182	64,100	0.0109	30,000	3	0.0587	0.0315
WF 4	dynamic	11.79	0.446	0.0817	6,290	69,400	0.0182	68,000	0.0109	30,000	3	0.0587	0.0315
WF 6	static	11.79	0.446	0.0817	5,710	69,200	0.0182	68,000	0.0109	30,000	5	0.0587	0.0525
WF 6	static	11.79	0.446	0.0817	5,560	69,700	0.0182	71,200	0.0109	30,000	5	0.0587	0.0525
WF 7	dynamic	11.79	0.446	0.0817	5,540	69,200	0.0182	70,900	0.0109	30,000	5	0.0587	0.0525
WF 8	dynamic	11.79	0.446	0.0817	5,060	69,500	0.0182	68,200	0.0109	30,000	5	0.0587	0.0525
WF 9	static	11.79	0.446	0.0817	3,070	68,800	0.0182	68,400	0.0109	30,000	5	0.0587	0.0525
WF 10	static	11.79	0.446	0.0817	3,470	67,900	0.0182	68,700	0.0109	30,000	5	0.0587	0.0525
WF 11	dynamic	11.79	0.446	0.0817	3,780	68,500	0.0182	68,000	0.0109	30,000	5	0.0587	0.0525
WF 12	dynamic	11.79	0.446	0.0817	3,990	71,900	0.0182	75,800	0.0109	30,000	5	0.0587	0.0525

[a] See List of Symbols on page 178 for notation

[b] No steel across the critical section

[c] Short duration load: $T/T_R < b$

Table 2 Proportions and Static Material Properties of the I Beams Tested[a]

(L/d = 6.57 b'/d = 0.0952 d/d 0.0952)

Beam No	Load Type	f'_c (psi)	f_y (psi)	ρ	ρ_w	f_y (psi)	ρ	f_{yy} (psi)	s (in.)	A_v (in.^{2})	$0.0015 b_w s$ (in.^{2})
H1	static	7,700	47,700	0.0105	0.0314	49,700	0.0059	90,700[b]	2	0.020	0.0040
H2	dynamic	7,510	47,700	0.0105	0.0314	49,700	0.0059	90,700[b]	2	0.020	0.0060
H3	dynamic	7,240	47,700	0.0105	0.0314	49,700	0.0059	90,200[b]	2	0.020	0.0060
H4	dynamic	7,100	47,700	0.0105	0.0314	49,700	0.0059	90,200[b]	2	0.020	0.0060
H5	dynamic	8,450	47,700	0.0105	0.0314	49,700	0.0059	90,700[b]	2	0.020	0.0060
L1	static	7,980	47,700	0.0098	0.0295	49,700	0.0052	60,500	2	0.0072	0.0060
L2	dynamic	8,020	47,700	0.0098	0.0295	49,700	0.0052	60,500	2	0.0072	0.0060
L3	dynamic	8,360	47,700	0.0098	0.0295	49,700	0.0052	60,500	2	0.0072	0.0060
L4	dynamic	7,490	47,700	0.0098	0.0295	49,700	0.0052	60,500	2	0.0072	0.0060
L5	dynamic	7,660	47,700	0.0098	0.0295	49,700	0.0052	60,500	2	0.0072	0.0060

[a] See List of Symbols on page 171 for notation.

[b] Stress at weld fracture.

A computer code was programmed to make calculations using the rigorous analysis procedure The procedure is based on the linear acceleration extrapolation method for numerical analysis of single-degree-of-freedom systems, and for each cycle of the calculation, checks are made for shear and bond The procedure applies in the elastic, elasto-plastic, and plastic regions of response, and the motion parameters (displacement, velocity, and acceleration) are calculated for each cycle, therefore, the procedure applies to all the types of failure and design criteria previously discussed.

Reports. This report contains a summary of the previous work at NCEL, a presentation of the theory used in the computer code, the reporting on the final series of beam tests (Series F), conclusions about all of the work, and recommendations The testing of materials associated with the Series F beams is reported in Appendix A Earlier reports covered Series D and Series E, the beam tests in Series A, B, and C have not been previously reported

Notation

In the Introduction of this report, notation conforms to that of the reference cited, and local lists of symbols are provided with equations. In the body of this report, notation conforms as nearly as practical to that of the ACI designation, and a List of Symbols is provided on page 179 A few notations and definitions are different from those in previous reports on this work unit. Such changes were made in the interest of simplicity, order, and standardization.

In general, uppercase letters are used to indicate forces while lowercase letters indicate forces per unit area. For example, V_u is the usable ultimate shear resistance (total force), while v_u is the usable ultimate shear stress (force per unit area). Where it is necessary to indicate location at the support rather than at the critical section, the subscript s is used to specify location at the support. For example, V_{su} is the ultimate shear resistance at the support while V_u is the usable ultimate shear resistance at the critical section A letter d is added to the subscripts of symbols to denote the dynamic case For instance, f_y is the yield strength of steel in tension and f_{dy} denotes the dynamic yield strength of steel in tension. In order to differentiate between the strengths of stirrups and longitudinal tension and compression steel, the subscript contains a letter v to denote stirrup material and a prime denotes a material in compression Thus, f_{dvy} is the dynamic yield strength of stirrups, f_{dy}' is the dynamic yield strength of steel in compression, and f_{dy} is the dynamic yield strength of steel in tension

Definitions

Behavior. When testing a beam subjected to dynamic load, the experimental engineer does not have time to observe the formation of cracks in order to make judgments regarding change in behavior, nor can he know the moment when the resistance in the beam changes suddenly since the beam is in motion throughout the test. He must use *measured values* instead of *visual observations* to judge behavior. Therefore, it becomes necessary to define changes in behavior such as cracking, yielding, and failure in quantitative as well as qualitative terms.

Critical Strains. It seems logical that values of stress or strain in the materials from which the beam is made should be used instead of motions or forces to define changes in behavior, because critical values of stress and strain can be obtained from tests on specimens of the materials. Furthermore, motion or force parameters cannot or are not easily compared with similar parameters in statically loaded beams. Strain is preferred over stress because it is more easily measured in the beams, and stress is less applicable in the inelastic range of behavior. The traditional practice of using stress criteria in elastic design does not cause a serious problem here. Since the modulus of elasticity of steel does not change an appreciable amount as the strain rate is increased, conversion between stress and strain in the elastic range is easily done. Unless determined otherwise in tests, the modulus of elasticity for steel in the dynamic and static cases can be assumed to be[13]

$$E_s = 29{,}000{,}000 \text{ psi}$$

As mentioned before, the stress–strain relationship of concrete in compression is nonlinear in the elastic range, and the effective modulus of elasticity increases as the strain rate is increased. However, the magnitude of the net effect of the increase in modulus in beams is probably less than the total error due to (1) possible changes in stress block shape, (2) changes in toughness, and (3) approximation of the static modulus used in design. Thus, unless determined otherwise in tests, the modulus of elasticity for concrete in compression in the dynamic and static cases can be assumed to be[13]

$$E_c = \rho^{1.5} 33 \sqrt{f'_c} \qquad (7)$$

where E_c = modulus of elasticity of concrete in compression (psi)

ρ = density of concrete (lb/ft^3)

f'_c = 28-day compressive strength of concrete (psi)

In the computer code, which was used for predicting the behavior of the Series F beams, the increase in concrete modulus was considered by using the dynamic strength of the concrete, f'_{dc}, in place of the static strength, f'_c, in Equation 7. The increase was small since the modulus is proportional to the square root of the compressive strength. All other computations were made using Equation 7 as shown.

Since the stress–strain relationship of concrete in compression is nonlinear, the concepts of yield strength, yield strain, ultimate strength, and ultimate strain do not apply directly. However, when combining concrete and steel to form beams, it becomes necessary to establish effective values of these properties for proportioning the beams and defining the regions of response. The 28-day compressive strength, f'_c, the breaking stress of a control specimen, is used for a criterion in lieu of ultimate stress, and 85% of the compressive strength is normally used in lieu of yield stress in proportioning beams. In addition, the effective modulus of elasticity is estimated by use of Equation 7 as given above. The ACI[13] recommends using a limit strain of 0.003 in./in. to represent yielding. In beams with compressive reinforcement, destruction of the concrete in compression occurs progressively over a range of loads or times. Experience with the flexural testing of beams has shown that in beams with compressive reinforcement, destruction usually occurs after a strain of 0.006 in./in. is reached at the remote fiber, and the change in the crushing strain in beams under dynamic load is unknown. Thus, critical events of concrete behavior in compression are defined here as strains in quantitative terms as

$$\epsilon_{cy} = 0.003 \text{ in./in.} \quad \text{(yield strain of concrete)}$$

$$\epsilon_{cu} = 0.006 \text{ in./in.} \quad \text{(ultimate strain of concrete)}$$

The stresses associated with those strains are

$$f_{cy} = 0.85 f'_c \quad \text{(static yield strength of concrete)}$$

$$f_{dcy} = 0.85 f'_{dc} \quad \text{(dynamic yield strength of concrete)}$$

$$f_{cu} = f'_c \quad \text{(static ultimate strength of concrete)}$$

$$f_{dcu} = f'_{dc} \quad \text{(dynamic ultimate strength of concrete)}$$

Other stresses in the concrete are computed as follows

Static loading, elastic region

$$f_c = \epsilon_c E_c \leq 0.85 f'_c$$

Dynamic loading, elastic region

$$f_c = \epsilon_c E_c \leq 0.85 f'_{dc}$$

Static loading, inelastic region

$$0.85 f'_c < f_c = \epsilon_c E_c \leq f'_c$$

Dynamic loading, inelastic region

$$0.85 f'_{dc} < f_c = \epsilon_c E_c \leq f'_{dc}$$

Flexure. Flexural cracking of the beam occurs when the tensile strength of the concrete is overcome at sections where bending forces are paramount and shear cracks do not already exist. In the accepted methods for flexural analysis, the concrete tensile stress and strain associated with flexural cracking are assumed to be zero. The term cracked section is used to describe this condition

Flexural yielding occurs when the longitudinal tension steel yields or when the yield strain of the concrete is exceeded at the remote fiber If the flexural yielding is governed by yielding of the steel, this is referred to as ductile yielding Yielding of compression steel has some influence on beam behavior, but does not constitute yielding of the beam

Flexural failure occurs when the ultimate strain of the concrete is exceeded at the remote fiber or when the longitudinal tension steel ruptures. If the failure is governed by failure (ultimate strain) of the concrete prior to yielding of the tension steel, this is referred to as brittle failure, otherwise, it is referred to as ductile failure This is to say that ductile failure is always preceded by ductile yielding

Shear. Shear cracking of the beam occurs when the tensile strength of the concrete is overcome at sections where diagonal tension forces are paramount. The critical section is where the diagonal tension stress is largest, and the critical diagonal tension crack, herein called the shear crack, initiates at or nearly at a point in that section In thin-webbed beams, the initiation point is at the critical section, in wide-webbed beams, the shear crack may start from

a flexural crack along the bottom of the beam a short distance away and then propagate rapidly to a point in the critical section. After initiation of the shear crack, increase in load and/or passage of time may cause the crack to progress diagonally upward. The shear-compression zone is located at the head of the shear crack where the concrete area acting in shear and compression is greatly reduced by the crack, and therefore the concrete is subjected to large shearing and bending stresses acting simultaneously.

Shear yielding occurs when the web reinforcement yields at the critical section or when the yield strain of the concrete is exceeded at the remote fiber in the shear-compression zone. Yielding of the longitudinal reinforcement at the critical section is not considered here because it appears that such yielding triggers dowel failure immediately. If the shear yielding is governed by yielding of the web reinforcement, this is referred to as ductile yielding.

Shear failure can occur upon formation of any one of a large number of possible mechanisms generally classified as pure shear, diagonal tension, or shear-compression. Pure shear occurs in deep members and is beyond the scope of this work unit. Diagonal tension failures can occur (1) upon formation of the shear crack if redistribution of stresses is not accomplished, (2) later when the longitudinal tension reinforcement fails to resist the dowel forces, or (3) in rare cases when the stirrups rupture. Diagonal tension failures triggered by cracking and most of those triggered by dowel failure are not preceded by shear yielding, they are rapid and are considered to be brittle failures. Shear-compression failure can occur when the ultimate strain of the concrete is exceeded in the shear-compression zone before or after yielding of the stirrups, or can occur in rare cases when the stirrups rupture. Shear-compression failures are considered to be ductile, the least violent being crushing of the concrete after yielding of the stirrups. If shear failure is caused by stirrup rupture without yielding in the shear-compression zone, that failure is classified as diagonal tension failure. On the other hand, if shear failure is caused by stirrup rupture with yielding in the shear-compression zone, it is classified as shear-compression failure.

Usable ultimate shear strength and usable ultimate shear resistance are defined by Equation 4.

Bond. A detailed study of bond was not attempted, but since some bond failures resemble shear failures, studies were made to insure against bond failures in the beams tested. In those beams, longitudinal tension bar anchorage failure at the support was the most probable type of bond failure.

SUMMARY OF PREVIOUS WORK

Series A Beam Tests

In the Series A beam tests, (1) beams with and without stirrups were tested statically to study the effectiveness of stirrups, (2) beams with stirrups were tested statically and dynamically to study change in the probability of failing in shear or flexure with change in loading rate, and (3) beams with stirrups having small stirrup areas were tested to study the possible conservatism of the limit ($A_v \geq 0.0015\ bs$) given in the ACI Code.[13] These tests were pilot tests to study gross effects and develop techniques.

Details and instrumentation of the four beams designated Series A (OA1, WA1, OA2, and WA4) are shown in Figure 1. The proportions and static material properties are given in Table 1. Two beams had stirrups made from no. 2 deformed reinforcing bars uniformly spaced in the vicinity of the critical section, and the others had no stirrups near the critical section. The beams with stirrups were designated WA, and those without were designated OA. The web reinforcement was slightly more than the minimum allowable by the ACI Code neglecting the capacity reduction factor, ϕ. Beam WA4, with stirrups, was loaded dynamically, the others were loaded statically. Strains were measured in the stirrups in the vicinity of the critical section and in the concrete remote fiber and longitudinal steel both in the vicinity of the critical section and at midspan. The beams without stirrups failed in shear, and those with stirrups failed in flexure.

The stirrups were effective in preventing shear failures under both static and dynamic loads, and the probability of failure in shear or flexure did not appear to change grossly with change in loading rate. The Code provisions for shear were found to be very conservative in the beams tested. The loading equipment and beam reactions performed well, but the method used for detecting and measuring shear cracking was unsatisfactory.

Series B Beam Tests

An attempt was made in the Series B tests to obtain a shear-compression failure under static loading in a beam with stirrups similar to the beams of Series A. The concrete strength and the span length were less to make the shear sensitivity greater. A companion beam without stirrups was tested for comparison.

Details and instrumentation of the two beams designated Series B are shown in Figure 2, and the proportions and material properties are given in Table 1. Beam WB1 had stirrups in the vicinity of the critical section, and beam OB1 had none there. Both beams were tested under static load. The one without stirrups failed in shear, and the one with stirrups failed in flexure.

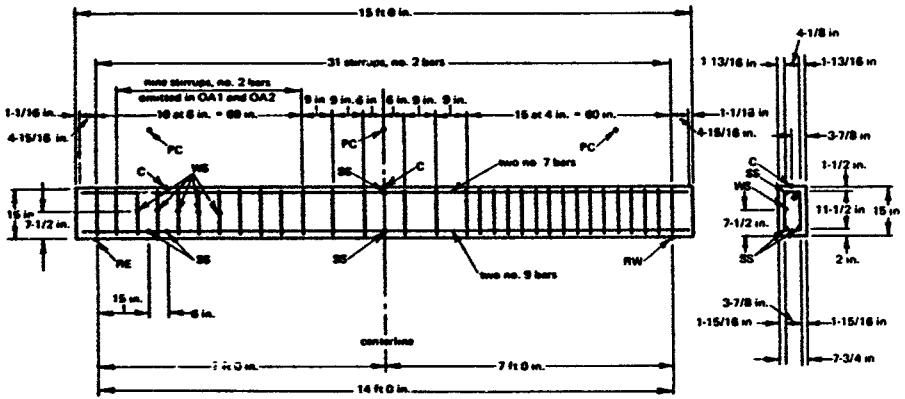

Mark	Measurement
RE	Reaction, east
RW	Reaction, west
SS	Steel strain
PC	Compressure
WS	Stirrup (web steel) strain
C	Concrete strain

Figure 1. Details and instrumentation, Series A beams.

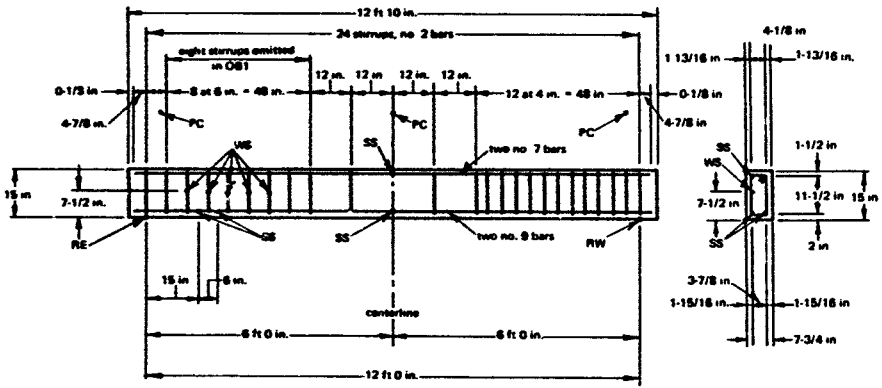

Mark	Measurement
RE	Reaction, east
RW	Reaction, west
SS	Steel strain
WS	Stirrup (web steel) strain
PC	Overpressure

Figure 2. Details and instrumentation, Series B and Series C beams.

The primary objective, to obtain a shear-compression failure, was not achieved The shear crack propagated up to the level of the compression reinforcement, but no crushing occurred at the top surface of the beam in the shear-compression zone

Series C Beam Test

Beam WC1 was the only beam tested in Series C The primary objective of this pilot test was to obtain a shear-compression failure under static load The secondary objective was to test two methods of measuring diagonal cracking

The dimensions of the beam were identical to those of beam WB1 as shown in Figure 2, but concrete strength and stirrup yield strength were less to make the shear sensitivity greater The proportions and material properties are given in Table 1 The low stirrup yield strength was obtained by heat treating the no 2 deformed reinforcing bars All of the measurements which had been made in Series B were repeated in Series C, and two measurements of shear cracking were made also

The beam was loaded statically and failed in flexure Although failure occurred in flexure, a comparison of the various strains indicated that shear failure was nearly achieved The shear crack extended above the level of the compression reinforcement as can be seen in Figure 3 One of the methods of measuring shear cracking was considered to be satisfactory and was used in some of the later beam tests The other method was unsatisfactory.

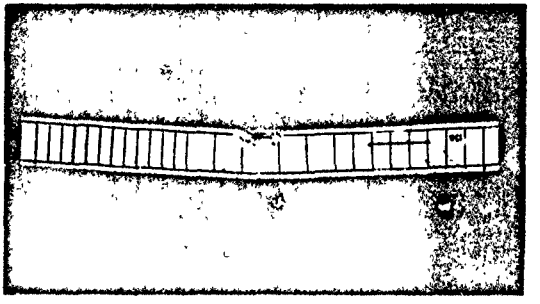

Figure 3. Post test photograph of beam WC1.

Pull-Out Bond Tests

It was conjectured that low bond strength in beams might contribute to dowel failures, and that premature anchorage failures might be difficult to differentiate from diagonal tension failures. Therefore, it was desirable to design shear test specimens with high margins of safety in bond. On the other hand high margins of safety were difficult to achieve in design because (1) high-strength steel was needed to obtain beams of suitable size and proportions for the testing equipment available, and (2) it was desirable to keep the steel arrangement simple, that is, no hooked bars and no extra bars near the support.

The conditions of loading and restraint were such that the longitudinal reinforcement was subjected to normal pressure at the support, and it was supposed that the bond resistance of the beam was increased by the normal pressure. Tests performed under contract with Iowa State University[20] indicated that bond resistance is increased by normal pressure and, also, that the presence of stirrups at the support improves bond resistance. The effect of normal pressure and stirrups was then considered in estimating the margin of safety in bond

The pull-out tests were funded by NAVFAC under Work Unit Y-F011-05-04-002.

Dynamic Testing of Materials

The NCEL dynamic materials testing machine[21] was used to test a variety of steel and concrete specimens at various controlled head velocities. Without the booster, the machine has a maximum static capacity of 50,000 pounds and can be operated at head velocities up to 15 in./sec. The piston stroke is 4 inches. Using the booster, the head velocity can be increased to 30 in./sec, and the static load capacity can be increased to 80,000 pounds. The piston stroke at the higher velocity is 0.75 inch, the head velocity will reduce to 15 in./sec for the remainder of the 4-inch stroke. For typical specimens of reinforcing steel, the maximum strain rate that can be obtained is about 2 in /in /sec.

Dynamic tests were conducted on a specially fabricated chrome-alloy high-strength reinforcing steel,[21] four grades of typical reinforcing steel,[22] and annealed plain wires.[23] The four grades of typical reinforcing steel were ASTM intermediate grade A15, hard grade A15, high-strength A432, and high-strength A431 The reinforcing bar specimens had their deformations machined off. The specimens were tested at various strain rates from about 0 002 to about 2 in /in /sec, and plots were made of increase in yield strength with respect to strain rate. In the tests on 9-gage wire with static yield strength

of 36,000 lb/sq in , a strain rate of 2 5 in /in /sec was obtained, and the yield strength was nearly doubled at that rate Tests on other wire are reported in Appendix A of this report.

Dynamic compression tests and dynamic tensile splitting tests were conducted on circular cylinders made of portland cement concrete.[24] A medium- and a high-strength mix were used, and specimens of each mix were tested at two ages, 28 and 49 days. The compression tests were performed at strain rates from about 0 001 to 1 in./in /sec, and the tension tests were performed at strain rates from about 0 0004 to about 0 2 in./in./sec. Plots were made of increase in strength with respect to strain rate and also with respect to stress rate Dynamic tests on another concrete mix are reported in Appendix A of this report

Dynamic compression tests also were performed on reinforced concrete rectangular prisms.[25] The test members were planar concrete panels reinforced with a single layer of square-meshed welded-wire fabric. Several combinations of panel thickness, reinforcing-wire diameter, and mesh size were investigated, as well as two concrete strengths. A single rate of compressive stress (100,000 psi/sec) was applied

The tests on rectangular concrete prisms were funded by NAVFAC under Work Unit Y-F011-05-04-002. The other testing of materials was funded by DASA under Subtask SC3318.

Modal Analysis

A modal analysis of the elastic response of a simply supported beam under a uniformly distributed load was made (1) to determine the influence of the dynamic parameters (peak load, load duration, and damping) on the transient variation in shear and moment-shear ratio along the span, and (2) to develop a dynamic response chart for quickly determining the maximum shear forces a beam must resist to fail in flexure. Exact solutions for the transient variation in shear and moment at any point along the beam were developed and compared with approximate solutions. From the approximate solutions, a chart for the maximum dynamic shear factor at the supports was developed for various ratios of peak load to dynamic yield resistance and load duration to fundamental period of vibration Figure 4 is the chart for the maximum shear at the supports, and Figure 5 is a plot showing the exact solution for the elastic case and a ratio of load duration to natural period, T/T_n, equal to 6. The modal analysis is discussed in Appendix G of Reference 14

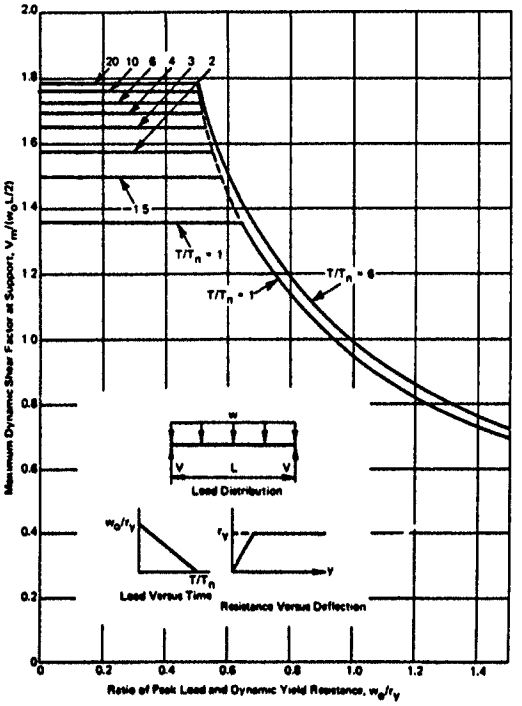

Figure 4. Chart for predicting the maximum shear at the supports of a simply supported beam under uniformly distributed dynamic load.

Series D Beam Tests

The Series D beam tests were reported in NCEL Technical Report R-395, Dynamic Shear Strength of Reinforced Concrete Beams—Part I [14] All nine beams designated Series D contained vertical stirrups made from heat-treated no 2 reinforcing bars which were uniformly spaced in the

vicinity of the critical section The beams were simply supported and subjected to uniformly distributed loads, three were loaded statically and six dynamically Major variables in the experiment plan were stirrup spacing, peak load, load duration, and rate of loading The proportions and static material properties are given in Table 1 Ratios of peak load to static flexural resistance varied from 0 535 to 0 943, and ratios of effective load duration to natural period of vibration varied from 1 4 to 21 2

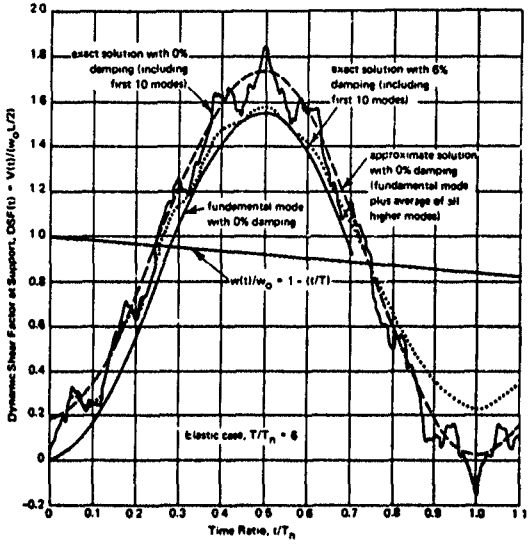

Figure 5. Dynamic shear factor at the supports of a simply supported beam under uniformly distributed dynamic load with $T/T_n = 6$.

One statically loaded beam suffered a premature bond failure, all the other beams failed in flexure after shear yielding In all the beams, shear cracks extended up to or beyond the compression reinforcement as can be seen in Figures 6 and 7 Evaluation of the data produced these findings

1 The maximum dynamic shear at the supports was greater than the shear produced by the same peak load applied statically and increased with peak load and load duration

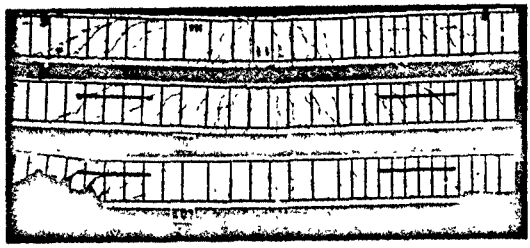

Figure 6. Post test photograph of statically loaded Series D beams.

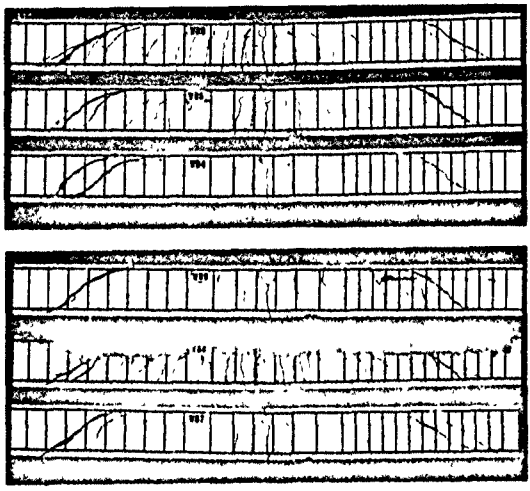

Figure 7 Post test photograph of dynamically loaded Series D beams.

2 The shear at the support did not increase after yielding of the tension reinforcement at midspan

3. Strains in the stirrups were small until shear cracking occurred at which time there was a pronounced increase in rate of straining in stirrups located near the shear crack

4 The pattern of shear cracks and the location of the critical diagonal tension crack were about the same in all of the beams.

5 The maximum strain rates in stirrups in the vicinity of the shear crack were greater than the maximum strain rates in longitudinal tension steel at midspan

6. Flexural failures occurred at midspan under static and dynamic loads.

7 The shears at the supports corresponding to shear cracking and shear yielding were greater under dynamic load than under static load

The following conclusions were based mainly on the comparison of test data with data calculated using the modal analysis equations and modified versions of Equations 3 and 4

1. The modal analysis is satisfactory for predicting shears at supports.

2 The static shear and moment distributions can be used in the dynamic analysis of shear without causing significant error.

3 Yielding at midspan prevents or retards further increase in shear at the support

4. Prior to shear cracking, practically all of the diagonal tension is resisted by the concrete

5. The location of the shear crack is influenced very little by loading rate and stirrup spacing.

6 The ACI provisions for shear are very conservative when applied to dynamic loading.

Series E Beam Tests

The Series E beam tests were reported in NCEL Technical Report R 502, Dynamic Shear Strength of Reinforced Concrete Beams—Part II [23] Appendix A of that report contains equations for computing the distance from the support to the critical section and the shear moment ratio at the

critical section There is a discussion in Appendix B of the same report about the tests that determined the static and dynamic strength properties of the materials in the beams

The variable parameters in the experiment plan were rate of loading, peak load, and stirrup spacing All 15 beams were doubly reinforced, simply supported, and subjected to uniformly distributed loads Three beams had no web reinforcement in the vicinity of the critical section, all the others had vertical stirrups made from 9 gage annealed plain wire The stirrups were spaced uniformly in the vicinity of the critical section Long-duration dynamic loads were applied to eight beams, and static loads were applied to the other seven beams. The proportions and static material properties are given in Table 1

Four different modes of failure occurred in the Series E tests. They were ductile flexure, diagonal tension retarded by dowel action, shear compression with yielding of stirrups, and shear-compression without yielding of stirrups *Under static loads*, the beams without stirrups failed in diagonal tension retarded by dowel action, those with the larger stirrup spacing failed in shear compression with yielding of the stirrups, and those with the smaller stirrup spacing failed in flexure. *Under long-duration dynamic loads with the lower peak load*, the beam without stirrups failed in diagonal tension retarded by dowel action, and those with stirrups (both spacings) failed in shear-compression without yielding of the stirrups. On the other hand, *under long-duration dynamic loads with the higher peak load*, beams with stirrups (both spacings) failed in shear-compression with yielding of the stirrups Thus, differences in mode of failure were brought about by changes in each of the varied parameters—rate of loading, peak load, and stirrup spacing

Comparisons of various measured strains indicated that several beams had nearly equal probability of failing in shear or flexure This is also evident in the full development of both shear and flexure cracks. Figures 8, 9, and 10 are post test photographs of the beams.

One of the objectives of the Series E tests was to determine whether or not the ACI provisions could be modified to apply to dynamic loading The usable ultimate shear strength, v_u, as defined by Equations 3 and 4 was expressed as shown in Equations 8 and 9 assuming a capacity reduction factor, ϕ, of unity for experimental purposes and adding coefficients C_1 and C_2 for the increases under dynamic loading in concrete tensile strength and stirrup yield strength

$$v_c = \frac{V_c}{bd} = 1.9 C_1 \sqrt{f'_c} + 2{,}500 \frac{pVd}{M} \leq 3.5 C_1 \sqrt{f'_c} \quad (8)$$

$$v_u = \frac{V_u}{bd} = v_c + C_2(\sin\alpha + \cos\alpha)\frac{A_v f_{vy}}{bs} \leq 10C_1\sqrt{f'_c} \qquad (9)$$

The coefficients, C_1 and C_2, were unity for statically loaded beams and increased with increasing strain rate. In general, correlation was very good between test results and data computed with the use of the equations. After studying these results, a capacity reduction factor, ϕ, of 0.85 was considered adequate for design in both the dynamic and static cases. However, the upper limit ($10C_1\sqrt{f'_c}$) in Equation 9 was found to be unconservative. This can be seen in the tendency under dynamic load toward shear-compression failures without yielding of stirrups and toward relatively small energy absorption capacities after shear yielding. Therefore, it was recommended that no increase be allowed in that limit. Furthermore, it was conjectured that a safe limit might be slightly less than $10\sqrt{f'_c}$. Note that in Reference 12 the ACI-ASCE Joint Committee 326 originally recommended a limit of $8\sqrt{f'_c}$ for rectangular beams and $10\sqrt{f'_c}$ for T-beams. It appears, then, that the ACI formulas can be modified to include dynamic loading as follows:

$$v_c = \frac{V_c}{bd} = \phi\left(1.9C_1\sqrt{f'_c} + 2{,}500\frac{pVd}{M}\right) \leq 3.5\phi C_1\sqrt{f'_c} \qquad (10)$$

$$v_u = \frac{V_u}{bd} = v_c + \phi C_2(\sin\alpha + \cos\alpha)\frac{A_v f_{vy}}{bs} \qquad (11)$$

$$v_u \leq 8\phi\sqrt{f'_c} \quad \text{(rectangular beams)} \qquad (11a)$$

$$v_u \leq 10\phi\sqrt{f'_c} \quad \text{(T beams)} \qquad (11b)$$

The conclusions drawn from the Series E tests are summarized below.

1. The shear, moment, shear strength, and flexural strength all increase under dynamic load with respect to the same load applied statically. Both the shear strength contributions from the concrete and the web reinforcement increase.

2. The shear and moment increase in about the same proportions with respect to the loading rate.

3. The usable shear strength and the flexural strength increase in different proportions. Furthermore, the contributions to the usable shear strength from the concrete and the web reinforcement increase in different proportions, depending mainly on the material used for stirrups and the rate

of strain in the stirrups. Therefore, the mass of the beam and the characteristics of the dynamic load influence the relative increases in the flexural strength, shear strength from the concrete, and shear strength from stirrups.

4. The additional shear resistance beyond shear yielding tends to be less under dynamic than under static loading. Thus, in general, dynamic shear failures tend to be more brittle than static failures.

5. A beam containing adequate web reinforcement to force flexural failure under static conditions might not have sufficient web reinforcement to force flexural failure under dynamic conditions.

6. It is possible for a beam to fail in flexure after the usable ultimate shear resistance has been exceeded. In other words, the additional shear resistance beyond yielding in shear might be enough to force flexural failure.

7. In beams which fail in diagonal tension, collapse might be retarded or prevented by dowel action.

8. If failure occurs after yielding of the web reinforcement under static loading, it might occur before yielding of web reinforcement under dynamic loading. This difference in behavior under dynamic loading is due primarily to the increase in stirrup contribution which might not be accompanied by a comparable increase in the flexural capacity of the cross section reduced by propagation of the diagonal tension crack. Thus, shear-compression failures can occur in the high shear zone when the ratio of moment to moment resistance becomes greater in the region of high shear than in the region of high moment.

9. In beams with web reinforcement, the critical diagonal tension crack upon yielding in shear might be a different crack from the one which was critical upon shear cracking.

10. The location of the critical section is predictable using the method given in Appendix A of the report.[23]

11. The location of the critical section does not change much with change in loading rate and stirrup spacing.

12. The shear and moment distributions along the span are a function of position and time under dynamic loads. However, the difference between these distributions for static and dynamic conditions was small; therefore the static distributions can be used in designing beams of normal proportions to withstand dynamic loads.

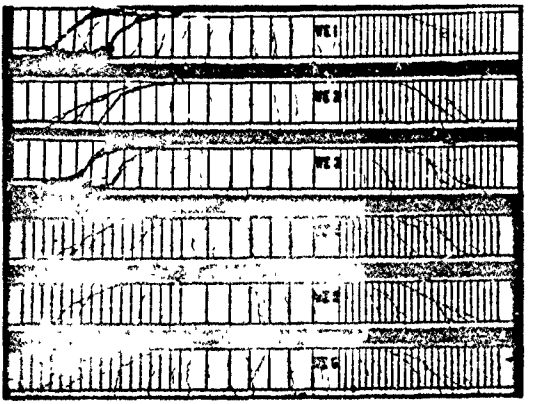

Figure 8 Post test photograph of dynamically loaded beams WE1 through WE6.

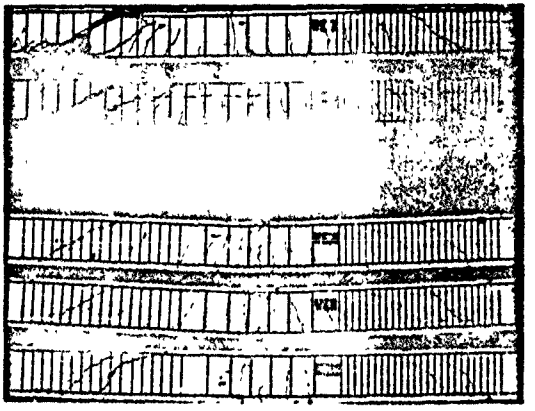

Figure 9 Post test photograph of statically loaded beams WE7 through WE11 and dynamically loaded beam WE12

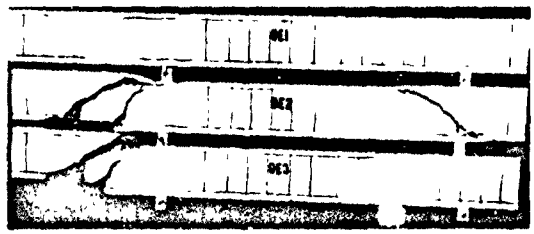

Figure 10 Post-test photograph of statically loaded beams OE1 and OE3 and dynamically loaded beam OE2.

13 The usable ultimate shear resistance was predicted satisfactorily by the ACI-ASCE Committee 326 formula as modified by Keenan and Seabold The capacity reduction factor, ϕ, value of 0 85 is adequate for dynamic and static loadings.

14. Stirrups were effective having areas less than areas required by the ACI Building Code.[13]

15 The chart developed from the modal analysis was adequate for predicting the maximum shearing force at the supports.

It was emphasized in the report that the strain rates needed for determining the dynamic increase coefficients, C_1 and C_2, were measured during the test in the beams, *the rates were not predicted.*

Series H and Series L Beam Tests

To study the effectiveness of different types of welded-wire fabric reinforcement in thin-webbed I-beams, two groups of five beams each were tested One group, designated Series L, was reinforced with a relatively light fabric, the other group, designated Series H, was reinforced with heavier fabric The proportions and static material properties of the I-beams are given in Table 2 For each of the groups of beams, one beam was subjected to a uniformly distributed static load and four beams were subjected to a uniformly distributed dynamic load The dynamic loads were essentially step pulses with short rise times and long durations. The magnitude of the step pulse varied within each group of beam tests.

The tests were reported in NCEL Technical Report R 534, Dynamic Shear Resistance of Thin-Webbed Reinforced Concrete Beams.[26] The results of dynamic and static tension tests on the welded-wire fabric are given in Appendix A of that report, and Appendix B presents the development of theory for dynamic diagonal tension resistance. The theory is not limited to I beams.

The longitudinal tension steel yielded at midspan in all of the beams. After that, three beams failed in shear, two failed in flexure, and there was insufficient load to fail the other five beams. Figures 11 and 12 are post-test photographs of the beams. The cracks that can be seen in Figure 11 indicate that the Series H beams, containing the heavier web reinforcement, were flexure sensitive. On the other hand, the cracks shown in Figure 12 indicate that the Series L beams, containing the lighter web reinforcement, were shear sensitive. The resistance upon shear cracking was approximately as predicted by the theory, but the ultimate shearing resistance was underestimated. The heavier welded wire fabric was effective in carrying shearing forces after shear cracking, but the effectiveness of the lighter fabric was doubtful. In the beams with lighter fabric, shear resistance after cracking in shear might have been due largely to the flanges, especially the longitudinal reinforcement.

In general, the I-beams behaved similarly to the rectangular beams of Series A through Series E, and the conclusions were about the same. There were three conclusions which deserve special notice here.

1. It is not necessary to limit the yield strength of web reinforcement to 60,000 psi as specified in the ACI Building Code.[13]
2. The $10\sqrt{f'_c}$ limitation on ultimate usable shear strength should be maintained and no dynamic increase allowed.
3. The theory successfully provided the means of estimating the diagonal tension stress rate needed for determining the dynamic increase coefficient, C_1, for concrete in tension.

A method was not developed for estimating the strain rates in web reinforcement, rates which are needed for determining the dynamic increase coefficient, C_2, for tension in stirrups.

The I-beam tests were funded by NAVFAC under Work Unit Y-F011-05-04-002.

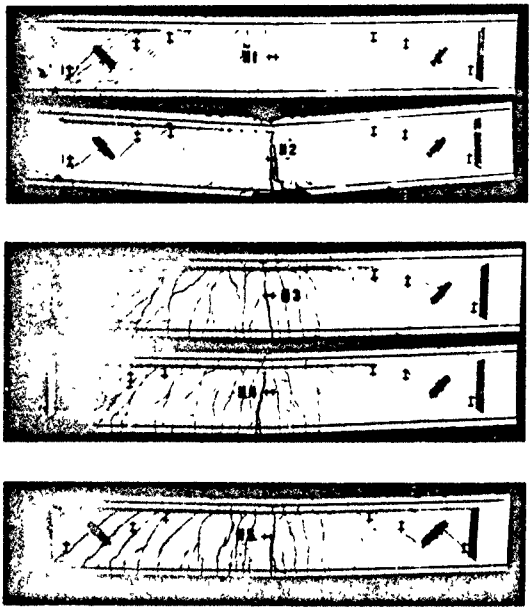

Figure 11 Post-test photograph of Series H beams.

THEORY

Concept of Ductility Along the Span

It was pointed out in the Background and Definitions that there are several types of design criteria, and some of these might be superimposed over others Ductility through underreinforcing is considered the primary one Next, allowable strain criteria must be superimposed, and last, limitations on motion parameters such as deflection must be superimposed The

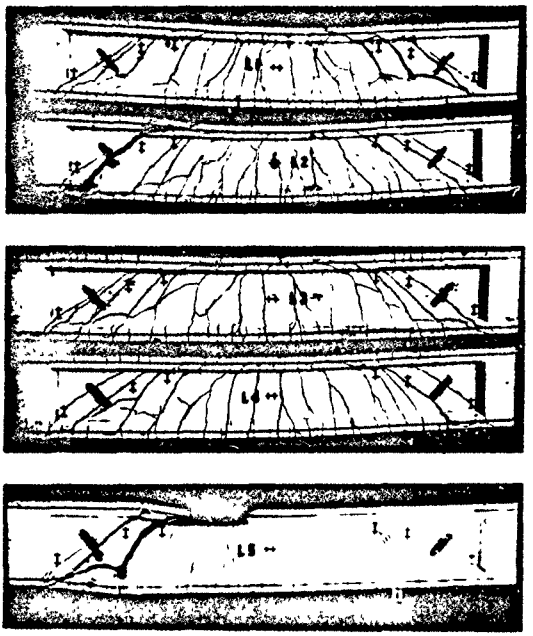

Figure 12. Post-test photograph of Series L beams.

concepts of ductile yielding and ductile failure were extended to shear as well as flexure and to dynamic as well as static loadings, and specific limits were expressed in terms of strain. Now, the concept of underreinforcing must be extended to all points along the beam, not just to the critical flexural section.

First, consider just the static flexural behavior of a uniformly loaded prismatic beam on simple supports. The critical section in flexure is at mid-span. For that section, the compressive strain in the remote fiber of the

concrete can be plotted with respect to the tensile strain in the longitudinal tension reinforcement as shown in Figure 13. The limiting strains (ϵ_{cy}, ϵ_{cu}, ϵ_{sy}, and ϵ_{su}) defining yielding and failure of the two materials divide the plot into six zones. Zones 1 and 2 represent the elastic region, and zones 5 and 6 represent the inelastic region. Zones 3 and 4 are transition zones where one material is elastic and the other is not, for practical purposes, these are also considered inelastic zones. If the beam is underreinforced, the concrete–steel strain relationship will plot as shown in the figure linearly through zone 2 as the load is slowly increased. Ductile yielding occurs when the yield strain of the steel, ϵ_{sy}, is reached and the plotted line passes into zone 4. The line curves in zone 4 because the neutral axis changes in the beam with increase in load. The sequence of events leading to failure has three alternatives as shown by the solid line and two dashed lines. Failure can occur by crushing of the concrete or by failure of the steel either with or without yielding of the concrete. If the beam was overreinforced, the function would plot in zones 1 and 3 and maybe into zones 5 and 6. Ideally, the function of a balanced beam would plot up the boundary of zones 1 and 2 to the balance point which is one point common to all zones.

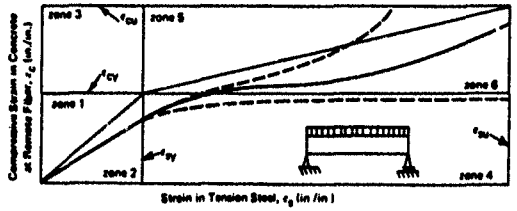

Figure 13. Plot showing ductile, flexural behavior at midspan.

Next, consider the same conditions, but at the shear-compression zone instead of at midspan. The plot in Figure 14 is similar to the one in Figure 13 except that it is for the shear compression zone. If the beam is underreinforced, the function plots linearly in zone 2 as the load is slowly increased until shear cracking occurs at point 1 in the plot. The line changes slope upon cracking and continues to change slowly as the load increases. At point 2, the stirrups begin to yield, and the line curves more rapidly upward as the crack progresses upward in the beam and the area of concrete acting in compression is greatly reduced. If stability of the section is maintained, the concrete will yield (point 3), perhaps the steel will yield (point 4), and failure will occur by crushing of the concrete (point 5).

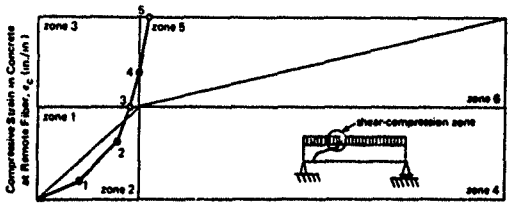

Figure 14. Plot showing ductile, shear behavior and brittle, flexural behavior at the shear-compression zone.

The line in Figure 14 is but one example In another instance, the numbered events (points in the plot) might occur in different zones, in a different sequence, and some of them might not occur at all Failure can occur prematurely if the beam becomes unstable For example, it could fail in diagonal tension at event 1 if the stirrups and dowel resistance are insufficient, in diagonal tension retarded by dowel action at event 2 or 4, or in shear-compression at any time when the gradient of the function approaches infinity. The sequence of events indicates ductility in shear, and the relationship of the line to the balance point indicates ductility in flexure, both at the shear-compression zone. If the functions of Figures 13 and 14 were on the same plot, direct comparisons could be made between sections (locations) as well as between types of behavior (shear and flexure). Families of curves representing various sections along the span can be generated to study the effect of shear behavior on flexural ductility along the span and to determine where the critical sections are. In addition, plots for the static and dynamic cases can be overlaid for comparison

The concept is illustrated in the hypothetical example plotted in Figure 15. One line represents the midspan location, and the other represents the shear-compression zone The numbered events are

1. Shear cracking
2. Yielding of the tension steel at midspan
3. Yielding of stirrups
4. Yielding of the concrete at midspan
5. Yielding of the concrete at the shear-compression zone
6. Failure of the concrete at midspan

Events are numbered on both curves so that the critical points on one curve can be compared with corresponding points on the other This order of events appears to satisfy the failure and design criteria discussed in the Introduction This beam could be utilized in the elastic and inelastic regions of response, and if failure did occur, it would be at midspan in the ductile flexure mode If the load caused the steel at midspan to approach yielding (event 2), shear cracks would exist, but the stirrups would be elastic and flexural response at both sections would be ductile and elastic (zone 2) If the load were increased until a stirrup approached yielding (event 3), the shear and flexural responses at the shear-compression zone remain ductile and elastic, but the tension steel at midspan has yielded (zone 4) This might be good criteria for the allowable load carrying capacity of military structures which must continue functioning after a load exceeding normal service loads has been applied For greater economy (and less safety), the load could be permitted to increase until the concrete at the remote fiber at midspan approaches yielding (event 4) Over this interval the stirrups have yielded and the shear-compression zone has become overreinforced (zone 1) If underreinforcing is to be maintained over the entire span length, this beam is unsatisfactory for a load-carrying capacity corresponding to event 4 The design could be improved by adding sufficient web reinforcement to cause the line in the figure to pass through the balance point thus bringing point 4 back into zone 2. (See the dashed line in the figure) This should not be done by inclining the web reinforcement, which has the effect of lengthening line segment 1b-3 (which is good) and increasing the slope of that segment (which is bad) Inclining stirrups might force events 3 and 4 into zone 3, causing extreme brittle behavior and perhaps shear failure. Designing beams to respond in zones 5 and 6 is not considered practical. However, it is desireable to proportion beams with the largest possible energy absorbing capacities when they are to function in atomic shelters where economy is important, collapse is to be avoided, and large deflections can be permitted The full energy-absorbing capacity of both materials at midspan can be utilized if event 6 can be made to coincide with point A in the figure This most easily can be accomplished in the design by selecting a suitable value of the steel ratio, p Experience has shown that p values of about 0 02 provide maximum energy-absorbing capacity Larger values tend to cause failure through zone 5, and smaller ones through zones 6 or 4

The plot for a dynamically loaded beam would contain the same six zones, but the boundaries of the zones would be the dynamic rather than static limit strains In general, this difference, by changing the position of the balance point, makes it more difficult to maintain ductile behavior in flexure at the shear compression zone.

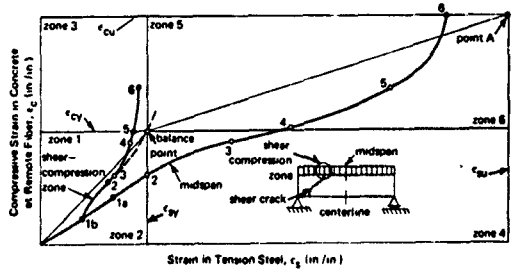

Figure 15 Plot showing ductility at midspan and shear-compression zone

General Approach to Design

Beams for use in atomic defense protective construction usually must be designed to carry static service loads without yielding and dynamic overloads without exceeding designated strains or motions The beams should be designed to behave similarly to the example in Figure 15, and event 2 should be used as the criteria with regard to static loads. With regard to dynamic loads, event 3 might be used for command posts, event 4 for personnel shelters, event 5 for equipment shelters, and event 6 for unoccupied structures Such beams could be designed using this general approach

1 Design for static service loads in flexure at midspan proportioning for maximum strain energy capacity in case of overload and in shear at the critical section and shear compression zone proportioning for adequate flexural ductility in case of overload

2 Analyze for dynamic overloads for flexure at midspan, for shear at the critical section, and for shear and flexure at the shear-compression zone.

3 If necessary, revise the design and repeat the analysis.

If the design is inadequate in shear only, these changes singly or in combination would be best

1 Decrease the stirrup spacing, s

2 Increase the stirrup area, A_v

3 Increase the stirrup yield strength, f_{vy}

The first is best for small adjustments, the second for larger adjustments, and the third for the largest Increasing the concrete strength, f'_c, increases the shear resistance, but it influences the flexural resistance too Increasing the steel ratio, p, to increase shear resistance should be used only as a last resort, because it has a large effect on the flexural resistance and the energy absorbing capacity, an effect which might not be advantageous

If the design is slightly inadequate in flexure, appropriate changes should be made and the analysis repeated If the design is grossly inadequate in flexure, the beam should be designed for the dynamic loads using approximate methods and then analyzed using more precise methods In either case, a preliminary design must be done first, and then analyzed

If the preliminary design is not evolved by normal static design procedures, the flexural aspects of the design can be accomplished by employing dynamic design aids in the form of charts, graphs, and tabulated data Such aids are available in References 2, 4, and 5. The charts in NCEL Technical Report R-121, Design Charts for R/C Beams Subjected to Blast Loads[27] are probably the most rapid means available. In conjunction with these methods, the shear aspects of the design can be accomplished by employing the chart in Figure 4 to determine the maximum shear at the supports and Equations 10 and 11 to determine the minimum amount of web reinforcement.

General Approach to Analysis

Equivalent Dynamic System. Beams have an infinite number of degrees of freedom, mathematical analysis is possible for structural systems having only limited degrees of freedom, and solutions become exceedingly tedious with only a few degrees. It is recognized that practical solutions can be obtained easiest by modeling the actual structural system with a single-degree-of-freedom system called an equivalent dynamic system The solutions obtained by using equivalent dynamic systems, then, are approximate and not exact

The kinetic energy, strain energy, and work done by external loads for the equivalent system are equivalent at all times to the corresponding total energies for the actual system The displacement, velocity, and acceleration of the equivalent system are at all times equal to those motions at one preselected section along the span of the actual system. Midspan is the section selected for modeling in this theory for reinforced concrete beams.

Methods for Solving Equations of Motion. General methods that can be used for solving equations of motion are classical methods, graphical methods, and numerical integration The advantages and disadvantages of each method are discussed in Appendix B of Reference 4 Single versus

multi degrees of freedom systems and equivalent dynamic systems also are discussed there Numerical integration of a single degree-of freedom equivalent dynamic system is the general method selected for this theory for reinforced concrete beams. The advantages of the method are discussed in Reference 28

Flexure-Shear-Bond Integrated Analysis. If numerical integration is used, the analysis of flexure, shear, and bond, and checks for deflection, velocity, and acceleration need not be divorced They can be combined into one integrated analysis that follows the behavior of the reinforced concrete beam through the elastic and inelastic ranges in flexure and the uncracked and cracked ranges in shear For each increment of time, Δt, deflections, accelerations, velocities, and strains can be compared with allowable, yield, or ultimate values at midspan, the critical section, the shear compression zone, and the face of the support to predict events representing changes in behavior in flexure, shear, and bond All of the events referred to in the concept of ductility along the span (Figure 15) can be predicted in any sequence or zone

Linear Acceleration Extrapolation Method

Motion at Midspan. The linear acceleration extrapolation method was the specific method of numerical integration used in the computer code that generated data which were compared with measured data of the Series F tests The procedure had a constant time interval and was self starting These characteristics make the method a good one for computer programming The recursion formulas are

$$\ddot{y}_{n+1} = \frac{P_{n+1} - R_{n+1}}{m K_{Lm}} \qquad (12)$$

$$\dot{y}_{n+1} = \dot{y}_n + \frac{1}{2}\ddot{y}_n \Delta t + \frac{1}{2}\ddot{y}_{n+1}\Delta t \qquad (13)$$

$$y_{n+1} = y_n + \dot{y}_n \Delta t + \frac{1}{3}\ddot{y}_n (\Delta t)^2 + \frac{1}{6}\ddot{y}_{n+1}(\Delta t)^2 \qquad (14)$$

where $\ddot{y}$ = acceleration (in /sec^2)

$\dot{y}$ = velocity (in /sec)

y = deflection (in)

P = load between supports (lb)

R = flexural resistance (lb)

K_{Lm} = load mass factor

m = mass (lb sec^2/in.)

Δt = time increment (sec)

n = cycle number in numerical integration

In this theory, the effects of damping are included, in part, in the resisting function, R, which is a function of velocity as well as displacement.

Shear at Support. At any given time the shear at the support can be expressed as the sum of resisting and forcing functions

$$V_s = C_r R + C_p P \qquad (15)$$

where V_s = shear at the support (lb)

C_r = resistance coefficient

C_p = load coefficient

Factors and Coefficients. Values of the factors and coefficients for the equivalent dynamic system at midspan of beams on simple supports under uniformly distributed loading are

Coefficient or Factor	Value	
	Elastic Region of Response	Inelastic Region of Response
Load-mass factor, K_{Lm}	0.78	0.66
Resistance coefficient, C_r	0.39	0.38
Load coefficient, C_p	0.11	0.12

Dynamic Stress Rate of Concrete in Diagonal Tension

Fuss[26] derived an equation for estimating the stress rate of concrete in diagonal tension in reinforced concrete beams on simple supports and subjected to uniformly distributed dynamic loads

$$\dot{f}_t = 2.5 \frac{w_o (L - 2x_c) Q}{I_g b' T_n} \qquad (16)$$

where f_t = stress rate of concrete in diagonal tension (psi/sec)

w_o = peak uniform load (lb/in.)

L = span length (in.)

x_c = distance from the support to the critical section for shear (in.)

Q = statical moment of the cross section (in^3)

I_g = gross moment of inertia (in^4)

b' = web width (in.)

T_n = natural period of vibration (sec)

In the case of rectangular beams,

$$\frac{Q}{b' I_g} = \frac{3}{2bh}$$

where b = beam width (in.)

h = total depth of the beam (in.)

and therefore,

$$\dot{f}_t = \frac{15}{4} \left[\frac{w_o (L - 2x_c)}{bh T_n} \right] \qquad (17)$$

Dynamic Strain Rates in the Materials

Approach. The derivations of equations for predicting the approximate strain rates in the materials are summarized here. The approach used in the derivations is to relate the strain rates of the materials at the critical sections

for flexure, diagonal tension, and shear compression to the velocity at midspan, which is equal to the velocity of the equivalent dynamic single degree of freedom system

Assumptions. The following assumptions were made to simplify the equations (1) The dynamic deflected shape is the same as the static deflected shape, (2) the strains and strain rates in the materials, including stirrups, are proportional to the distances from the point of rotation at the shear compression region, and (3) the point of rotation in the shear compression region is at the bottom edge of the compression steel at a distance, x_u, from the support See the diagrams in Figure 16

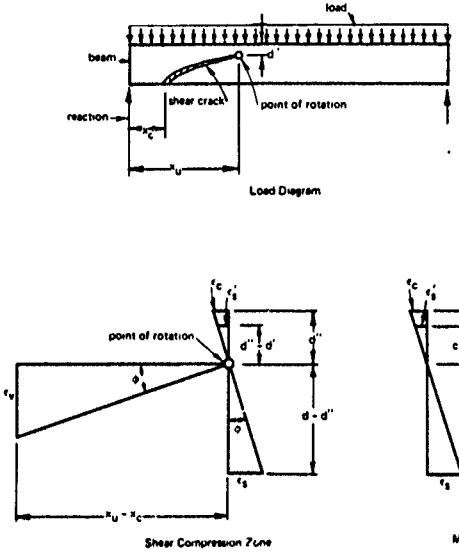

Figure 16 Diagrams of load and strain

Strain Rates in Stirrups. From the strain diagram for the shear-compression zone (Figure 16), it can be seen that

$$\phi \approx \tan\phi = \frac{\epsilon_v}{x_u - x_c} \quad \text{for small values of } \phi$$

where ϕ = unit curvature (rad/in)

ϵ_v = strain in stirrup (in./in)

x_u = distance from the support to the point of rotation (in)

Therefore, the strain in a stirrup at x_c is

$$\epsilon_v = (x_u - x_c)\tan\phi \approx (x_u - x_c)\phi$$

Let

$$K_1 = \frac{y}{y_{\mathfrak{C}}} = \frac{\dot{y}}{\dot{y}_{\mathfrak{C}}}$$

$$K_2 = \frac{\phi}{y} = \frac{\dot{\phi}}{\dot{y}}$$

$$K_3 = x_u - x_c$$

where K_1 = deflection ratio (in /in.)

K_2 = curvature ratio (rad/in ^{2})

K_3 = distance over which stirrups are active (in)

y = deflection at x_u (in.)

$y_{\mathfrak{C}}$ = deflection at midspan (in)

$\dot{y}$ = velocity at x_u (in./sec)

$\dot{y}_{\mathfrak{C}}$ = velocity at midspan (in /sec)

ϕ = unit curvature at x_u (rad/in.)

$\dot{\phi}$ = rate of change of unit curvature at x_u with respect to time (rad/in /sec)

Then, the strain rate in the outboard stirrup affected by the diagonal tension crack can be expressed as follows

$$\dot{\epsilon}_v = -K_1 K_2 K_3 \dot{\gamma}_{\ell} \tag{18}$$

where $\dot{\epsilon}_v$ is the strain rate in the stirrup in in /in /sec In the equation, the ratios K_1 and K_2 provide the transformations from deflection rate at mid span to deflection rate at the shear compression zone to curvature rate at the shear-compression zone, and then the radial distance K_3, provides the final transformation to strain rate at the critical section In the case of beams on simple supports and subjected to uniformly distributed load,

$$K_1 = \frac{16 x_u}{5 L^4} (x_u^3 - 2 L x_u^2 + L^3)$$

$$K_2 = \frac{12 (x_u - L)}{x_u^3 - 2 L x_u^2 + L^3}$$

Thus, $$\dot{\epsilon}_v = \frac{192 x_u}{5 L^4} (L - x_u)(x_u - x_c) \dot{\gamma}_{\ell} \tag{19}$$

In making calculations beyond yielding of a single stirrup, it is convenient to assume that the strain rate of the group of stirrups affected by the shear crack is one half the strain rate of the outboard stirrup

$$\dot{\epsilon}_{v(avg)} = \frac{\dot{\epsilon}_v}{2} \tag{20}$$

Strain Rates at the Shear Compression Zone. The strain rates in the materials at the shear compression zone can be expressed in a similar fashion as follows

$$\dot{\epsilon}_c = -K_1 K_2 \dot{\gamma}_{\ell} d'' \tag{21}$$

$$\dot{\epsilon}_s' = -K_1 K_2 \dot{\gamma}_{\ell} r \tag{22}$$

$$\dot{\epsilon}_s = -K_1 K_2 \dot{\gamma}_{\ell} (d - d'') \tag{23}$$

where $\dot{\epsilon}_c$ = strain rate in concrete in compression at remote fiber (in /in /sec)

$\dot{\epsilon}'_s$ = strain rate in compression steel (in /in /sec)

$\dot{\epsilon}_s$ = strain rate in tension steel (in /in /sec)

d'' = distance from the remote fiber to the point of rotation (in)

r = radius of compression bar (in)

d = effective depth of the beam (in)

In these equations, the radial distances d'', r, and (d - d'') provide the final transformations from curvature rate to strain rates at the shear compression zone In the case of beams on simple supports and subjected to uniformly distributed load,

$$-K_1 K_2 = \frac{192 x_u}{5 L^4} (L - x_u) \tag{24}$$

Strain Rates at Midspan. The strain rates in the materials at midspan can be expressed in a similar fashion by letting

$$K_4 = \frac{\phi_{\mathfrak{C}}}{\gamma_{\mathfrak{C}}}$$

where K_4 = curvature ratio at midspan (rad/in ^{2})

$\phi_{\mathfrak{C}}$ = unit curvature at midspan (rad/in.)

Then,

$$\dot{\epsilon}_c = -K_4 \dot{\gamma}_{\mathfrak{C}} c \tag{25}$$

$$\dot{\epsilon}'_s = -K_4 \dot{\gamma}_{\mathfrak{C}} (c - d') \tag{26}$$

$$\dot{\epsilon}_s = -K_4 \dot{\gamma}_{\mathfrak{C}} (d - c) \tag{27}$$

where c = distance from the neutral axis to the remote fiber (in)

d' = distance from the remote fiber to the centroid of the compression steel (in)

In the case of beams on simple supports and subjected to uniformly distributed load,

$$-K_4 = \frac{48}{5L^2} \tag{28}$$

Dynamic Yield Strength of Reinforcing Steel

If the elastic strain rates and static yield strengths are known, the following equation can be used to determine the dynamic yield strengths of stirrups and longitudinal reinforcing steels

$$\frac{\sigma_{dy}}{\sigma_y} = 1 + \frac{13{,}700}{\sigma_y} - \frac{94.9 \times 10^6}{\sigma_y^2} + \left(\frac{3{,}000}{\sigma_y} + \frac{423 \times 10^6}{\sigma_y^2}\right)\log(10\dot{\epsilon}) \tag{29}$$

where σ_{dy} = dynamic yield stress (psi)

σ_y = static yield stress (psi)

$\dot{\epsilon}$ = strain rate (in /in /sec)

and $$1 \leq \frac{\sigma_{dy}}{\sigma_y} \leq 2$$

The upper limit is recommended because experimental data above that limit is sparse. The lower limit is recommended because the equation gives low values in the case of small static yield strengths at very slow strain rates

Data to corroborate the equation may be found in References 14, 22, and 23 and in Appendix A of this report. Values of σ_{dy}/σ_y are plotted in Figure 17

The dynamic increase coefficient for stirrups, C_2, can be computed from Equation 29 since $\sigma_{dy}/\sigma_y = C_2$ in the case of stirrups

Dynamic Compressive Strength of Concrete

If the strain rate and static compressive strength are known, the following equation can be used to determine the dynamic compressive strength of portland cement concrete.

$$\frac{f'_{dc}}{f'_c} = 1.17 + 0.173\dot{\epsilon} + 0.06\log(10\dot{\epsilon}) \tag{30}$$

where f'_{dc} = dynamic compressive strength of the concrete at 28 days (psi)

f'_c = static compressive strength of the concrete at 28 days (psi)

and $$1 \leq \frac{f'_{dc}}{f'_c} \leq 2$$

The upper limit is recommended because experimental data above that limit is sparse. The lower limit has little practical importance with regard to beam behavior since the ratio, f'_{dc}/f'_c, is greater than one for all strain rates greater than 0.0001 in./in./sec. However, this limit is very important to computer programmers because the ratio approaches minus infinity as the strain rate approaches zero if a finite limit is not given.

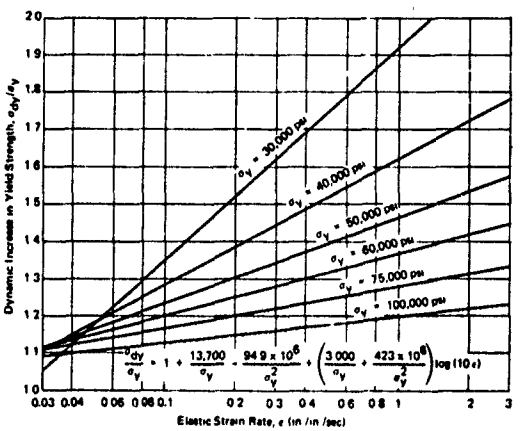

Figure 17 Plot of dynamic increase in yield strength versus elastic strain rate for reinforcing steel

Values of f'_{dc}/f'_c are plotted in Figure 18. Data to corroborate the equation may be found in Reference 24. Over most of the range of strain rates considered, the U. S. Air Force[4] and U. S. Army[29] currently recommend dynamic increases in compressive strength which are slightly larger than those given by the equation here.

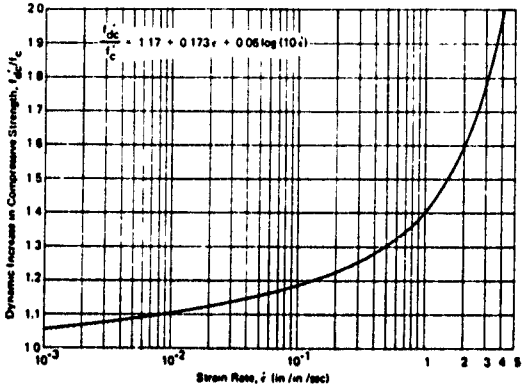

Figure 18. Plot of dynamic increase in compressive strength versus strain rate for portland cement concrete

Dynamic Tensile Strength of Concrete

If the tensile stress rate and static tensile strength are known, the following equation can be used to determine the dynamic increase in tensile strength of portland cement concrete.

$$C_t = \frac{f'_{dt}}{f'_t} = 0.951 + (1.33 \times 10^{-6})\dot{f}_t + 0.0693 \log \dot{f}_t \qquad (31)$$

where C_t = dynamic increase coefficient for concrete in tension

f'_{dt} = dynamic tensile strength of the concrete at 28 days (psi)

f'_t = static tensile splitting strength of the concrete at 28 days (psi)

$\dot{f}_t$ = stress rate of concrete in tension (psi/sec)

and $1 \leq C_1 \leq 1.74$

The upper and lower limits are recommended for the same reasons as those in the equation for dynamic compressive strength

Values of C_1 are plotted in Figure 19 Data to corroborate the equation may be found in References 14, 17, and 24 In tests by Cowell,[24] it was found that the dynamic increase in tensile strength was considerably less for specimens cured 49 days with respect to those cured the customary 28 days. Of course, during that same time interval, the static tensile strength increased slightly Since the reduction in dynamic increase predominates over increase in static strength for a time after 28 days, the equation given above was developed to give values of C_1 slightly lower than values obtained from tests on specimens cured 28 days This adjustment permits the use of conventional 28 day test data in the formula, otherwise, tests after a longer curing time would be required.

Shear Resistance

Location of the Critical Section. The following equation was used for computing the distance from the support to the diagonal tension critical section

$$x_c = \frac{x_c^4 + x_c^3(4\gamma - 2L) + x_c^2(L^2 - 2z^2 - 6\gamma L) + z^4 - 0.5\gamma L^3}{2z^2 L - 3\gamma L^2} \qquad (32)$$

where $\gamma = 2{,}500\,p\,d/1.9\,C_1\sqrt{f'_c}$

z = overhang (in)

This equation is derived in Appendix A of Reference 23 for the conditions including overhang as shown in the diagram below

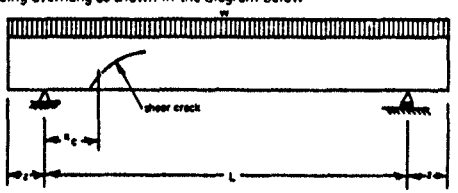

Conditions of Loading and Restraint

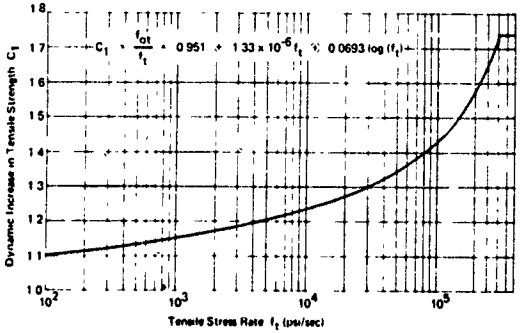

Figure 19 Plot of dynamic increase in tensile strength versus tensile stress rate for portland cement concrete

Shear-Moment Ratio at the Critical Section. If the location of the critical section is known, the shear moment ratio at the critical section can be computed as

$$\frac{V}{M} = \frac{L - 2x_c}{Lx_c - x_c^2 - z^2} \tag{33}$$

where V = shear (lb)

M = moment (in-lb)

Dynamic Shear Strength at the Critical Section With the dynamic increase coefficients, C_1 and C_2, known and the shear moment ratio, V/M, known, Equations 5, 10, and 11 can be used to calculate the dynamic shear strength at the critical section Since all the stirrups in the test beams were vertical, the angle, α, was 90 degrees and the quantity $(\sin\alpha + \cos\alpha)$ was equal to one Since the equations were being used to analyze test specimens, the capacity reduction factor, ϕ, was also taken as one Therefore, the equations for diagonal cracking strength v_c, and usable ultimate shear strength, v_u, were simplified as follows

For $p < 0.012$,

$$v_c = (0.8 + 100p)C_1\sqrt{f_c'} \tag{34}$$

where p = reinforcement ratio

v_c = shear strength contributed by the concrete (psi), diagonal tension cracking strength (psi)

For $p \geq 0.012$,

$$v_c = 1.9 C_1 \sqrt{f'_c} + 2{,}500 \frac{pVd}{M} \leq 3.5 C_1 \sqrt{f'_c} \qquad (35)$$

For $A_v < 0.0015bs$,

$$v_u = v_c \qquad (36)$$

where A_v = stirrup area parallel to the beam axis (in^2)

s = stirrup spacing center to center, parallel to the beam axis (in.)

v_u = usable ultimate shear strength (psi)

For $A_v \geq 0.0015bs$,

$$v_u = v_c + C_2 \frac{A_v f_{vy}}{bs} \leq 8 \sqrt{f'_c} \qquad (37)$$

where C_2 = dynamic increase coefficient for steel in tension

f_{vy} = static yield strength of stirrups (psi)

Dynamic Shear Resistance at the Support. If the location of the critical section is known and the shear distribution along the span is linear, the shear resistance at the support corresponding to the diagonal tension cracking strength and usable ultimate shear strength can be expressed as

$$V_{sc} = \frac{v_c bd}{1 - \frac{2x_c}{L}} \qquad (38)$$

$$V_{su} = \frac{v_u bd}{1 - \frac{2x_c}{L}} \qquad (39)$$

where V_{sc} = shear resistance at the support corresponding to the diagonal tension cracking resistance (lb)

V_{su} = shear resistance at the support corresponding to the usable ultimate shear resistance (lb)

For each cycle of the calculation prior to shear cracking, the resistance at the support corresponding to the diagonal tension cracking resistance was compared with the shear at the support obtained from Equation 15. If at any time the value of V_s exceeded V_{sc}, the output of the computer indicated that shear cracking had occurred, and all further computations were made using formulas for a beam cracked in shear. This change in behavior is represented by event 1 in Figure 15. For each cycle of the calculation after shear cracking, the resistance at the support corresponding to the usable ultimate shear resistance was compared with the shear, V_s. If at any time the value of V_s exceeded V_{su}, the output indicated that the usable ultimate shear strength had been exceeded, and in subsequent cycles no further comparisons of these values were made. This event corresponds to yielding of the stirrups (event 3 in the figure) or to dowel failure depending on which one occurs first.

Bending Resistance at the Shear-Compression Zone. For predicting events in shear behavior other than those already discussed, a different hypothesis is offered. After a diagonal tension crack has formed and propagated into the upper portion of the beam near the under side of the compression reinforcement, the prediction of behavior at the shear-compression zone becomes primarily a bending (rotation) problem rather than a shear problem. The center of rotation might be a considerable distance from the support at a point where vertical shearing forces are not largest, but the maximum resistance of the cross section in bending is greatly reduced by the shear crack. Failures in this zone occur when the ultimate bending resistance is exceeded.

A section through the shear compression zone at the head of the shear crack might remain stable after yielding of the compressive concrete and after yielding of stirrups, but not after yielding of the longitudinal tension steel. It appears that yielding of the longitudinal tension steel in a region of high shear near a support triggers dowel failure by the formation of a mechanism that is not very well understood. Therefore, in a stable section, the stirrups may be elastic or yielded, the concrete in compression may be elastic or yielded, but the longitudinal tension steel must be elastic. Combinations of these material conditions have been designated case I through case IV as follows:

Case	Material Conditions		
	Stirrups	Compressive Concrete	Longitudinal Tension Steel
I	elastic	elastic	elastic
II	partly yielded	elastic	elastic
III	partly yielded	yielded	elastic
IV	elastic	yielded	elastic

The free-body diagram for case I is shown in Figure 20. The point of rotation, point O in the figure, is at the bottom of the compression reinforcement at a distance, x_u, from the support. Also, a small overhang, z, is shown at the support, and the outboard stirrup affected by the shear crack is assumed to be at the critical section, x_c. Vectors in the diagram represent the distributed load, the reaction, the horizontal forces in longitudinal reinforcement, the horizontal stress distribution in the compressive concrete, and the vertical force distribution in uniformly spaced stirrups. The inertia of the concrete mass of the free body relative to the adjacent material of the main portion of the beam is very small compared to the reaction at the support at times when failure is likely to occur, therefore, the inertia is neglected. The free-body diagrams for the other cases are different only in concrete stress distribution and/or stirrup force distribution where trapezoidal shapes are used in lieu of triangular shapes.

For each of the cases described above, equations were derived for computing (1) the distance from the support to the point of rotation, x_u, (2) the ratio of the maximum resisting moment to the resisting moment, M_R/M, and (3) the stresses in those materials that are assumed to be unyielded. The equations for cases I and II apply over the range of possible rotations within the stated conditions, those for cases III and IV are different in that they apply specifically to the rotation at which time the compressive concrete strain is at its ultimate value (0.006 in./in.). The three computed items are important because (1) the point of rotation coincides with the point where the ratio is least and, therefore, indicates where failure is most likely to occur, (2) if the ratio is greater than unity, the section is stable, and (3) the stresses must be compared with corresponding dynamic yield stresses to determine the validity of the case used. With regard to the third item, if any one of the computed stresses is greater than the corresponding dynamic yield stress, the case used does not apply. If the dynamic yield stress of the longitudinal reinforcement is exceeded, one must assume that the beam is failed by dowel failure. If any of the others are exceeded, one must try another case.

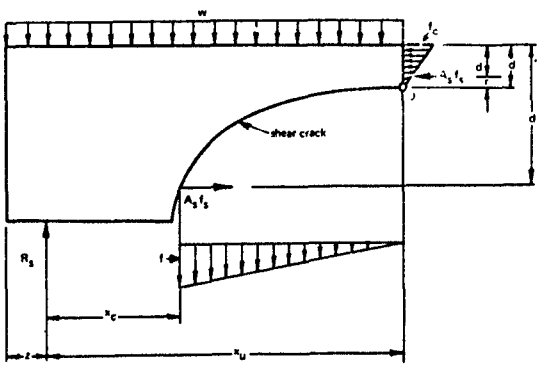

Figure 20 Free-body diagram for case I

When the computer code was used, calculations for the bending resistance at the shear-compression zone were initiated upon shear cracking and were continued for each cycle of the numerical procedure It was supposed that propagation to point O is instantaneous, but no assumption was made of the horizontal location of point O The subroutine for case I was loaded and used first. Equations 40 through 44 apply to case I. The distance from the support to the point of rotation was determined by iterative solution of x_u in the following equation

$$+ x_u^4[\beta(L - 2x_c)]$$

$$+ x_u^3[\beta(6x_c^2 - 2Lx_c - 2z^2)]$$

$$+ x_u^2[\alpha(3) + \beta(6x_c z^2 - 3x_c^3)]$$

$$+ 2x_u[\alpha(-L - x_c) + \beta(Lx_c^3 + x_c^4 - 3x_c^2 z^2)]$$

$$+ [\alpha(Lx_c + z^2) + \beta(-Lx_c^4 + 2x_c^3 z^2)] = 0 \qquad (40e)$$

where $$\alpha = A_s f_v (d - d'') \left(\frac{E_s}{E_v}\right) \left[\frac{2d' - r}{3 + \frac{9 n r A_s'}{b(d'')^2}} + d - d'\right] \quad (40b)$$

$$\beta = \frac{A_v f_v}{3s} \quad (40c)$$

and A_s = area of tension steel (in ^{2})

f_v = stress in stirrup (psi)

E_s = modulus of elasticity of steel (psi)

E_v = modulus of elasticity of stirrups (psi)

$n = E_s/E_c$, modulus of elasticity ratio

E_c = modulus of elasticity of concrete in compression (psi)

A_s' = area of compression steel (in ^{2})

The stresses in the remote fiber and the longitudinal tension reinforcement can be expressed in terms of the stress in the outboard stirrup (the stirrup at x_c) as follows

$$f_c = \left(\frac{d - d''}{x_u - x_c}\right)\left(\frac{E_s}{E_v}\right)\left(\frac{2 A_s f_v}{b d'' + \frac{3 n r A_s'}{d''}}\right) \quad (41)$$

$$f_s = \left(\frac{d - d''}{x_u - x_c}\right)\left(\frac{E_s}{E_v}\right) f_v \quad (42)$$

where f_c = stress in concrete (psi)

f_s = stress in tension steel (psi)

When the subroutine for case I was loaded, the arbitrary assumption was made that stress in a stirrup at x_c governs shear yielding. The initial value of stress was taken equal to the dynamic yield strength ($f_v = f_{dvy}$), and the distance, x_u, was obtained from Equation 40. This value of x_u is the predicted location of the point of rotation at the time of yielding if stirrup yielding governs. Next, the stress in the remote fiber was computed from Equation 41. If the concrete stress was less than its dynamic yield strength ($f_c < f_{dcy}$), the initial assumption was maintained and the procedure continued. Otherwise, the initial assumption is invalid because the concrete yields

before the stirrups. If the initial assumption was proved wrong, the concrete was assumed equal to its dynamic yield strength ($f_c = f_{dcy}$), the corresponding stirrup stress f_v, was computed from Equation 41, and Equation 40 was solved again to obtain the value of x_u, which is the prediction of the location of the point of rotation at the time of yielding *if* concrete yielding governs. The entire procedure was done again using Equation 42 to check the validity of the assumption regarding which material yields first and to revise the assumption and the values of f_v and x_u if necessary. After the material governing shear yielding was known and the correct values of f_v and x_u were obtained, the *maximum* resisting moment, for the case being considered, was calculated as follows:

$$M_R = \frac{\alpha}{x_u - x_c} + \beta(x_u - x_c)^2 \qquad (44)$$

where M_R = maximum resisting moment (in-lb)

and where α and β are the values obtained from Equations 40b and 40c. The moment at the same time and position was calculated as

$$M = \frac{P_n}{2L}(L x_u - x_u^2 - z^2) \qquad (45)$$

If the ratio of the maximum resisting moment to the moment, M_R/M, was less than unity, the computer output indicated that the beam was yielded in shear, the case I subroutine was abandoned, and either another subroutine was loaded or bending resistance calculations for the shear compression zone were terminated.

The subroutine for case II was loaded if yielding of a stirrup governed the final cycle of case I. Equations 46 through 49 apply to case II. The distance from the support to the point of rotation was determined by iterative solution of x_u in the following equation:

$$+ x_u^2(L - 2x_c) + 2x_u\left(x_c^2 - z^2 + \frac{\gamma}{\delta} - \zeta\right)$$

$$+ \left(2z^2 x_c - L x_c^2 - \frac{\gamma L}{\delta} + \zeta L\right) = 0 \qquad (46a)$$

where

$$\gamma = A_v f_v \left[\frac{2d' - r}{3 + \frac{9nrA_s'}{b(d')^2}} + d - d'\right] \qquad (46b)$$

$$\delta = \frac{A_v f_{dvv}}{2s} \tag{46c}$$

$$\zeta = \frac{1}{3}\left[\frac{E_s f_{dv}}{E_v f_s}\ (d - d'')\right]^2 \tag{46d}$$

and f_{dvv} = dynamic yield strength of stirrups (psi)

The stress in the remote fiber can be expressed in terms of the stress in the longitudinal tension steel as follows

$$f_c = \frac{2A_s f_s}{bd'' + \frac{3nrA_s'}{d''}} \tag{47}$$

When the subroutine for case II was loaded, the arbitrary assumption was made that stress in the longitudinal tension steel governs the upper boundary of case II. The initial value of stress was taken equal to the dynamic yield strength ($f_s = f_{dy}$), and the stress in the remote fiber was obtained from Equation 47. If the concrete stress was less than its dynamic yield strength ($f_c < f_{dcy}$), the initial assumption was maintained, and the distance, x_u, was determined by solving Equation 46. Otherwise, the initial assumption is invalid because the concrete yields before the steel. If the initial assumption was proved wrong, the concrete stress was set equal to its dynamic yield strength ($f_c = f_{dcy}$), the corresponding steel stress, f_s, was computed from Equation 47, and then Equation 46 was solved to obtain the value of x_u. After the governing material was known, and the correct values of f_s and x_u were obtained, the *maximum* resisting moment was calculated as

$$M_R = \gamma + \delta[(x_u - x_c)^2 - \zeta] \tag{48}$$

where γ, δ, and ζ are the values obtained from Equations 46b, 46c, and 46d. The moment at the same time and position was obtained by the use of Equation 45. If the ratio of the maximum resisting moment to the moment, M_R/M, was less than unity, the case II subroutine was abandoned, and either another subroutine was loaded or bending resistance calculations for the shear compression zone were terminated. An unessential but nonetheless interesting, value computed during each cycle of case II was the number of yielded stirrups, N

$$N = \frac{1}{s}\left[x_u - x_c - \frac{E_s f_{dvv}}{E_v f_s}\ (d - d'')\right] \tag{49}$$

The subroutine for case III was loaded if yielding of the concrete governed the final cycle of case II or if the stirrup stress exceeded its dynamic yield value in the final cycle of case IV. Equations 50 through 52 apply to case III. The distance from the support to the point of rotation was determined by iterative solution of x_u in the following equation

$$+ x_u^2(L - 2x_c) + 2x_u\left(x_c^2 - z^2 + \frac{\phi}{\delta} - \theta\right)$$

$$+ \left(2z^2 x_c - L x_c^2 - \frac{\phi L}{\delta} + \theta L\right) = 0 \qquad (50a)$$

where $$\phi = 0.006 \frac{r}{d''} E_s A_s'(d - d') + f_{dc}' b d''(0.75d - 0.291 d'') \qquad (50b)$$

$$\theta = \frac{1}{3}\left[\frac{E_s A_s f_{dvy}(d - d'')}{E_v\left(0.75 f_{dc}' b d'' + 0.006 \frac{r}{d''} E_s A_s'\right)}\right]^2 \qquad (50c)$$

and the value of δ is obtained from Equation 46c. The *maximum* resisting moment was calculated as

$$M_R = \phi + \delta[(x_u - x_c)^2 - \theta] \qquad (51)$$

The moment at the same time and position was obtained from Equation 45 The number of yielded stirrups is

$$N = \frac{1}{s}\left[x_u - x_c - \frac{E_s A_s f_{dvy}(d - d'')}{E_v\left(0.75 f_{dc}' b d'' + 0.006 \frac{r}{d''} E_s A_s'\right)}\right] \qquad (52)$$

If the ratio of the maximum resisting moment to the moment, M_R/M, was less than unity, the computer output indicated that the beam was failed in shear compression, and bending resistance calculations for the shear-compression zone were terminated.

The subroutine for case IV was loaded if yielding of the compressive concrete governed the final cycle of case I. Equations 53 through 55 apply to case IV The distance from the support to the point of rotation was determined by iterative solution of x_u in the following equation:

$$+ x_u^4[-\lambda] + x_u^3[2\lambda L]$$

$$+ x_u^2[3\lambda(x_c^2 - L x_c - z^2)]$$

$$+ 2x_u[\lambda(3z^2 x_c - x_c^3) + \eta]$$

$$+ [\lambda(L x_c^3 - 3z^2 x_c^2) - \eta L] = 0 \qquad (53a)$$

where $$\eta = f'_{dc} b d''(0.75d - 0.291d'')$$

$$+ 0.006 \frac{r}{d'''} E_s A'_s(d - d') \qquad (53b)$$

$$\lambda = \frac{A_v E_v}{A_s E_s}\left[\frac{0.75 f'_{dc} b d'' + 0.006 \frac{r}{d'''} E_s A'_s}{3s(d - d'')}\right] \qquad (53c)$$

The stress in the stirrup at x_c is:

$$f_v = \frac{x_u - x_c}{d - d''}\left(\frac{E_v}{E_s}\right)\left(\frac{0.75 f'_{dc} b d'' + 0.006 \frac{r}{d'''} E_s A'_s}{A_s}\right) \qquad (54)$$

If the computed stirrup stress, f_v, was greater than the dynamic yield stress, f_{dvy}, the subroutine for case IV was abandoned and replaced with the one for case III. If the computed stirrup stress was less than the dynamic yield stress ($f_v < f_{dvy}$), the subroutine for case IV was maintained, and the *maximum* resisting moment was determined from this formula:

$$M_R = \eta + \lambda(x_u - x_c)^3 \qquad (55)$$

The moment, M, was determined by using Equation 45. If the ratio, M_R/M, was less than unity, the computer output indicated that the beam was failed in shear-compression, and bending resistance calculations for the shear-compression zone were terminated.

Bond Resistance

When the computer code was used, bond calculations were made for each cycle of the numerical integration. They were made in accordance with those articles in the ACI Building Code[13] which pertain to bond and anchorage in ultimate strength design. *Dynamic increase in bond strength was not considered.* For instance, for tension bars, other than top bars, with sizes and deformations conforming to ASTM Specification A305:

$$u_u = \frac{9.5\sqrt{f'_c}}{D} \leq 800 \text{ psi} \tag{56}$$

where u_u = ultimate bond stress (psi)

D = nominal diameter of bar (in.)

At the critical section for bond,

$$V_b = \phi \Sigma_o jd\, u_u \tag{57}$$

where V_b = maximum allowable shear at the critical section for bond (lb)

ϕ = capacity reduction factor

Σ_o = sum of perimeters of effective bars (in.)

jd = moment arm between centroids of compressive and tensile forces (in.)

Since the equations were being used to analyze test specimens, the capacity reduction factor, ϕ, was taken as unity. Therefore, Equation 57 was simplified as follows

$$V_b = \Sigma_o jd\, u_u \tag{58}$$

All of the beams analyzed were bolted to bearing plates which were simply supported. Therefore, the critical section for bond was assumed to be at the edge of the bearing plate at a distance x_b from the simple support. Thus, the shear resistance at the support corresponding to the ultimate bond strength was expressed as follows.

$$V_{ub} = \frac{V_b}{1 - \frac{2x_b}{L}} \tag{59}$$

where V_{sb} = shear resistance at the support corresponding to the ultimate bond resistance (lb)

x_u = distance from the support to the critical section for bond (in.)

For each cycle of the calculation, the resistance at the support corresponding to the ultimate bond resistance was compared with the shear at the support obtained from Equation 15. If at any time the value of V_s exceeded V_{sb}, the output of the computer indicated bond failure and bond calculations were discontinued.

Flexural Resistance

General. The flexural resistance, R, in Equation 12 can be computed for each cycle of the calculation taking into account the changing modulus of elasticity of the concrete, which causes a slightly nonlinear resistance–deflection relationship in the elastic region, and the changing strengths of materials, which cause a very definite nonlinear resistance–deflection relationship in the inelastic region. Damping of the system due to the changing strengths of materials occurs in the calculations as the flexural resistance is influenced by the speed of the beam.

The strain rates and dynamic strengths of materials at midspan have been discussed previously and applicable formulas have been given as Equations 25 through 30.

Moment Capacity. The provisions of article 1602 of the ACI Building Code[13] were used to determine the ultimate design, dynamic resisting moment, M_{du}, by simply substituting the dynamic yield stresses in place of the static yield stresses and permitting reinforcement ratios, $p = p'$, up to the balanced condition, p_b. Article 1602 pertains to flexural computations in ultimate strength design for rectangular beams with compression reinforcement. The stress block proportion is approximated by

$$k_1 = 0.85 \qquad f'_{dc} \leq 4{,}000 \text{ psi} \tag{60a}$$

$$k_1 = 0.85 - 0.05\left(\frac{f'_{dc} - 4{,}000}{1{,}000}\right) \qquad f'_{dc} > 4{,}000 \text{ psi} \tag{60b}$$

where k_1 is the stress block proportion. The reinforcement ratio that would produce balanced conditions is predicted by

$$p_b = \frac{0.85 k_1 f'_{dc}}{f_{dy}}\left(\frac{87{,}000}{87{,}000 + f_{dy}}\right) \tag{61}$$

where p_b = reinforcement ratio that produces balanced conditions

f_{dy} = dynamic yield strength of tension steel (psi)

The beam is overreinforced when

$$\frac{p - p'}{p_b} > 1 \qquad (62a)$$

where p' is the compression reinforcement ratio. The beam is underreinforced when

$$\frac{p - p'}{p_b} < 1 \qquad (62b)$$

The beam is underreinforced but does not conform to ACI 1602(d) when

$$0.75 < \frac{p - p'}{p_b} < 1 \qquad (62c)$$

Although yielding of the compression reinforcement does not constitute yielding of the beam, such yielding does influence the moment carrying capacity enough to be considered here. Therefore, different formulas were used to obtain the dynamic resisting moment for the cases of yielded and unyielded compression reinforcement at the time of yielding of the beam. The reinforcement ratio that would produce yielding of the compression reinforcement concurrent with yielding of the tension reinforcement for the current velocity of the beam is predicted by

$$p_1 = 0.85 k_1 \frac{f'_{dc} d'}{f_{dy} d} \left(\frac{87{,}000}{87{,}000 - f'_{dy}} \right) \qquad (63)$$

where p_1 = reinforcement ratio that produces yielding of the compression reinforcement concurrent with yielding of the tension reinforcement

f'_{dy} = dynamic yield strength of compression steel (psi)

If $p - p' \geq p_1$, the compression steel is assumed to be yielded and the dynamic resisting moment can be determined from

$$M_{du} = (A_s f_{dy} - A_s' f_{dy}')\left(d - \frac{a}{2}\right) + A_s' f_{dy}'(d - d') \qquad (64)$$

where $$a = \frac{A_s f_{dy} - A_s' f_{dy}'}{0.85 f_{dc}' b}$$

and M_{du} = ultimate design, dynamic resisting moment (in -lb)

a = ultimate design, stress block depth (in.)

If $p - p' < p_t$, the compression steel is assumed to be elastic and the dynamic resisting moment is

$$M_{du} = 0.85 f_{dc}' a b\left(d - \frac{a}{2}\right) + A_s' E_s \epsilon_{cy}\left(1 - \frac{k_1 d'}{a}\right)(d - d') \qquad (65)$$

where $$a = \left[(A_s f_{dy} - A_s' E_s \epsilon_{cy}) \pm \sqrt{(A_s f_{dy} - A_s' E_s \epsilon_{cy})^2 + 3.4 f_{dc}' b A_s' E_s \epsilon_{cy} k_1 d'}\right] \Big/ 1.7 f_{dc}' b$$

and ϵ_{cy} = yield strain of concrete (in /in)

Neutral Axis. The location of the neutral axis at the time of flexural yielding based on the current velocity of the beam is expressed as

$$c = \frac{a}{k_1} \qquad (66)$$

Modulus of Elasticity. When simplified methods of analysis and design were used, the modulus of elasticity of the concrete for the static case as given in Equation 7 was used. When the computer code was used, the dynamic compressive strength of the concrete was used in lieu of the static strength as follows

$$E_c = \rho^{1.5} 33 \sqrt{f_{dc}'} \qquad (67)$$

where E_c = modulus of elasticity of concrete in compression (psi)

ρ = density of the concrete (lb/ft^3)

f_{dc}' = dynamic compressive strength of the concrete at 28 days (psi)

Moment of Inertia. The moment of inertia, assuming a cracked section, is expressed as

$$I_c = \frac{bc^3}{3} + nA_s(d - c)^2 + (n - 1)A'_s(c - d')^2 \qquad (68)$$

where I_c = moment of inertia of a cracked section (in^4)

Stiffness The ratio of the resistance and the deflection traditionally has been considered to be a constant, called the spring constant, and proportional to the product of the modulus of elasticity and the moment of inertia, called the stiffness, and inversely proportional to the third power of the span length. Thus,

$$k = \frac{EI}{L^3}$$

where k = spring constant (lb/in.)

E = modulus of elasticity (psi)

I = moment of inertia ($in.^4$)

For uniformly loaded beams on simple supports,

$$k = \frac{384}{5}\left(\frac{EI}{L^3}\right)$$

Actually, the moment of inertia changes with deflection, which in turn changes with time, as the flexural critical section passes through the uncracked, cracked, and hinging states of behavior. Also, the stiffness changes slightly with time as the modulus of elasticity of the concrete changes with beam velocity. Therefore, the spring constant is not a constant at all, but a variable.

The spring constant for the cracked regime, k_c, was computed from the modulus of elasticity of the concrete and the moment of inertia for a cracked section

$$k_c = \frac{384}{5}\left(\frac{E_c I_c}{L^3}\right) \qquad (69)$$

where k_c is the spring constant of a cracked section in lb/in. Then, an approximation of the spring constant, which can be used through all regimes (uncracked, cracked, and hinging), was made using the method recommended by Nosseir.[18] In Nosseir's method, the spring constant, k, is obtained from the spring constant for the cracked regime and the span-depth ratio of the beam.

$$k = \left[0.13\left(\frac{L}{d}\right) - 0.0058\left(\frac{L}{d}\right)^2\right] k_c \qquad (70)$$

Data from this empirical formula compared well with measured data within the limits: $4 < L/d < 12$. Corroboration outside those limits was not attempted. Data within those limits to corroborate the equation can be found in Reference 18 and in Appendix B of this report. Appendix B also contains comparisons between Nosseir's method and other methods.

For each cycle of the calculation prior to shear cracking, the natural period of vibration was determined from the mass and the spring constant by application of the following formula:

$$T_n = 2\pi \sqrt{K_{Lm} \frac{m}{k}} \qquad (70a)$$

The natural period was not used in flexural resistance calculations, but was used in Equation 17 to estimate the dynamic stress rate of the concrete in diagonal tension.

Resistance. The flexural resistance is limited by the moment carrying capacity. For uniformly loaded beams on simple supports, the maximum resistance is computed as

$$R_m = \frac{8 M_{du}}{L} \qquad (71)$$

where R_m is the maximum flexural resistance in pounds. Otherwise, the resistance can be expressed as the product of the spring constant and the deflection. Thus,

$$R = ky \leq R_m \qquad (72)$$

Upon the first occasion of R_m governing in Equation 72, the computer output indicated flexural yielding.

Inelastic Hinge. For each cycle of the calculation after flexural yielding, an analysis was made of the inelastic hinge to estimate, for the current velocity of the beam, how much deflection would correspond to flexural failure assuming that failure occurs when the compressive strain in the remote fiber reaches the ultimate strain, ϵ_{cu} (0.006 in./in.). The following general procedure was used:

1. From the assumed stress and strain distributions over the cross section, the neutral axis was found at the section where the dynamic yield moment, M_{du}, exists (boundary of hinging action) and at midspan (center of hinging action).

2. The ratio of the strain in the remote fiber and the distance to the neutral axis was used to represent the curvature of the beam at the center of hinging. The ratio of tension steel strain and its distance from the neutral axis was used at the edge of hinging.

3. A linear curvature distribution from zero at the support through the points indicated above was used to obtain a curvature diagram.

4. The deflection was computed by summing moments of areas in the curvature diagram.

The computer did not make use of a diagram, of course, but executed comparable arithmetic steps. The estimated deflection was compared with the deflection obtained from the recursion formulas, Equations 12 through 14. The computer output indicated flexural failure upon the first occasion when the deflection exceeded the deflection corresponding to flexural failure.

Keenan[30] has used a similar approach assuming linear curvature outside the hinging length and fourth degree curvature, opening downward, within the hinging length. Nordell[31,32] has refined the approach considerably using rigorous methods to predict the shape of the stress block within the hinge and the shape of the curvature diagram across the hinging length.

The equations used to analyze hinging in the Series F beams are given in Appendix C.

Computer Programs

Computer programs were written for the static and dynamic analyses of rectangular reinforced concrete beams with compression reinforcement and stirrups.

Output data from the program for static analysis included the load carrying capacity, deflection, and location of the critical section corresponding to flexural yielding, shear cracking, usable ultimate shear, shear yielding, shear failure, and allowable bond. It also included the modulus of elasticity of the concrete in compression and the effectiveness of the stirrups.

The program for dynamic analysis was written to include the characteristics of the load in the input data. The response history was included in the output. Figure 21 contains sample output giving the title of the program, the identification of the beam, a list of input data, and a list of output data The conditions of loading and restraint were input as a code number and then output in the written form shown in the figure as a check against error. The peak load was input in thousands of pounds per foot if it was a uniformly distributed load or in thousands of pounds if it was a concentrated load. When this data was listed, it was also given in terms of the total load on the beam. If the load duration was omitted, infinite duration was used by the computer and the word "infinity" was output as shown in the figure.

The precision versus cost of the solution was controlled by appropriate input of a time increment and an acceleration tolerance. These values were listed in exponential format; for instance, the time increment shown in the figure is 2.5×10^{-1} msec or 0 00025 second. The precision decreases as the overhang length increases because the overhang is neglected in many of the formulas. Therefore, some judgment must be used in specifying overhang length. A maximum overhang of L/10 is considered reasonable for normal engineering accuracy. If this computer program were to be used to analyze a beam with long overhangs, it might be wise to run the program twice, first for simple supports with overhang and second for fixed supports, to insure that both satisfy the design criteria.

If the half-width of the support is omitted, bond calculations will be made at the center of the support instead of at the face of the support or the edge of the bearing plate Stirrup spacings are in the direction of the beam axis, and the inclination factor is $\sin \alpha + \cos \alpha$ where α is the angle of inclination of the stirrups. Different static yield stresses for compression steel and tension steel may be specified as shown. The proportions and weights of the beam were provided in the output data for comparing the properties of one beam with another and for estimating the weight and cost of the beam. The main portion of the output data was a table giving the predicted behavior. The times listed in the first column were established by the time increment given in the input, and the calculation was terminated when the deflection reached maximum because most of the equations in the theory

do not apply when the velocity is negative. Other columns in the table contain values for the motion at midspan, total load, resistance, shear at the support, and the reaction at the support. Notes were given in the table to indicate events which change the behavior of the beam and to provide supplementary information such as position of the critical section, number of stirrups yielded, location of the shear-compression zone, and effectiveness of stirrups. The sample data in the figure predicted inelastic response (flexural yielding) and failure. Furthermore, it indicated when and where yielding would occur in shear compression

SERIES F TESTS

Objectives

The first objective of the Series F tests was to study the concept of ductility along the span with emphasis on the difference between static and dynamic behavior. The design procedures which resulted from the Series E tests[23] were used to design the test specimens, and the theory given in this report was used to analyze them. It was desired to achieve nearly equal probability of failure in shear or flexure in dynamic tests, and to achieve nearly balanced conditions between ductile and brittle behavior in both the shear and flexure modes. Furthermore, the ductility in bending in the shear compression zone was studied to see if underreinforced conditions could be maintained there.

The second objective was to use the theory to predict the occurrence of (1) shear cracking, (2) yielding of the tension steel at midspan, (3) yielding of stirrups, (4) yielding of the concrete at midspan, (5) yielding of the concrete at the shear compression zone, and (6) mode of failure. The predictions included time and location of occurrence in dynamic tests, and load and location of occurrence in static tests.

The third objective was to substantiate the equations in the theory for predicting dynamic shear strength over a range of concrete strength, f'_c, using predicted values of the dynamic increase coefficient, C_1, and over a range of stirrup spacing, s, using predicted values of the dynamic increase coefficient, C_2.

Test Specimens

Description. Twelve specimens were fabricated with a span of 138 inches (11 feet 6 inches) between supports and an overhang of 6 inches at each end giving a total length of 150 inches (12 feet 6 inches). All had

rectangular cross sections of 7 inch width, 15 69 inch effective depth, and 18 inch total depth. The distance from the top surface to the center of the compression steel was 1.44 inches All beams were doubly reinforced with two no. 9 deformed bars in tension and two no. 7 bars in compression All had vertical box-type stirrups made from 6 gage wire hooked to the compression steel. The ends of each beam were supported on and bolted to 10 inch long by 1 inch thick bearing plates which were free to translate horizontally and to rotate.

The beams designated WF1 through WF4 had 3 inch spacing, center to center, between stirrups in the critical region, and those designated WF5 through WF12 had 5 inch spacing there Details are shown in Figures 22, 23, and 24

The beams were intended to fail in shear near the east end or in flexure at midspan, therefore, the stirreps were spaced closer together near the west end The departure from symmetry in the design was not large enough to cause unsymmetrical flexural response, but large enough to preclude shear failure near the west end

Material Properties. Tests on concrete control cylinders and steel coupons to determine the static and dynamic properties of the materials are discussed, and the results are given in Appendix A Also, the static material properties are summarized in Table 1.

The concrete was made from Type I portland cement, 3/4-inch maximum size aggregate, and sand. Two mixes were used. The average static compressive strength at about 28 days was 5,770 psi for the higher strength and 3,480 psi for the lower strength concrete. The average tensile splitting strength was 550 psi for the higher strength and 430 psi for the lower strength concrete. The higher strength concrete was used in specimens WF1 through WF8

The longitudinal reinforcing bars satisfied the strength requirements of ASTM Specification A432 and the deformation requirements of ASTM Specification A305 56T The average static upper yield stress was 69,000 psi for the no 9 bars, used in tension, and 70,000 psi for the no 7 bars, used in compression

The stirrups were made from annealed plain wire which was received in 6 foot straight lengths. The average static yield stress was 30,000 psi. The wire had a linear stress–strain relationship to a well defined proportional limit at about 23,000 psi and had a tangent modulus of elasticity of about 29,200,000 psi

INPUT DATA

CONDITIONS OF LOADING AND RESTRAINT

SIMPLE SUPPORTS AND UNIFORM LOAD

DYNAMIC LOAD

PEAK UNIFORM LOAD (KIP/FT)	PEAK TOTAL LOAD (KIP)	LOAD DURATION (MSEC)	RISE TIME (MSEC)	TIME OF ARRIVAL (MSEC)
7.000	91.1	INFINITY	2.00	0.00

PRECISION OF COMPUTATIONS

TIME INCREMENT (MSEC)	ACCELERATION TOLERANCE (IN/SEC/SEC)
4.590E-01	1.000E+00

CONCRETE DIMENSIONS AND PROPERTIES

COMPRESSIVE STRENGTH (KSI)	DENSITY (LB/CU FT)	BREADTH (IN)	HEIGHT (IN)	LENGTH OF SPAN (IN)	LENGTH OF OVERHANG (IN)	HALF-WIDTH OF SUPPORT (IN)
5.00	150.	7.00	18.00	138.00	6.00	5.00

STIRRUP DIMENSIONS AND PROPERTIES

YIELD STRENGTH (KSI)	AREA (SQ.IN.)	SPACING (IN)	INCLINATION FACTOR	MODULUS OF ELASTICITY (KSI)
30.0	.0307	5.00	1.00	29000.

COMPRESSION STEEL DIMENSIONS AND PROPERTIES

YIELD STRENGTH (KSI)	AREA (SQ.IN.)	EFFECTIVE DEPTH (IN)	BAR DIAMETER (IN)
69.2	1.24	1.44	.875

TENSION STEEL DIMENSIONS AND PROPERTIES

YIELD STRENGTH (KSI)	AREA (SQ.IN.)	EFFECTIVE DEPTH (IN)	MODULUS OF ELASTICITY (KSI)	BAR DIAMETER (IN)	TOTAL PERIMETER (IN)
69.5	2.86	15.69	29000.	1.128	7.98

OUTPUT DATA

PROPORTIONS AND WEIGHTS

L/D RATIO	TENSION STEEL RATIO	COMPRESSION STEEL RATIO	BEAM WEIGHT (KIP)	UNIFORM MASS (SLUGS)	CONCENTRATED MASS (SLUGS)
8.79	.0182	.0134	1.6	46.9	0.0

Figure 21. Sample computer output.

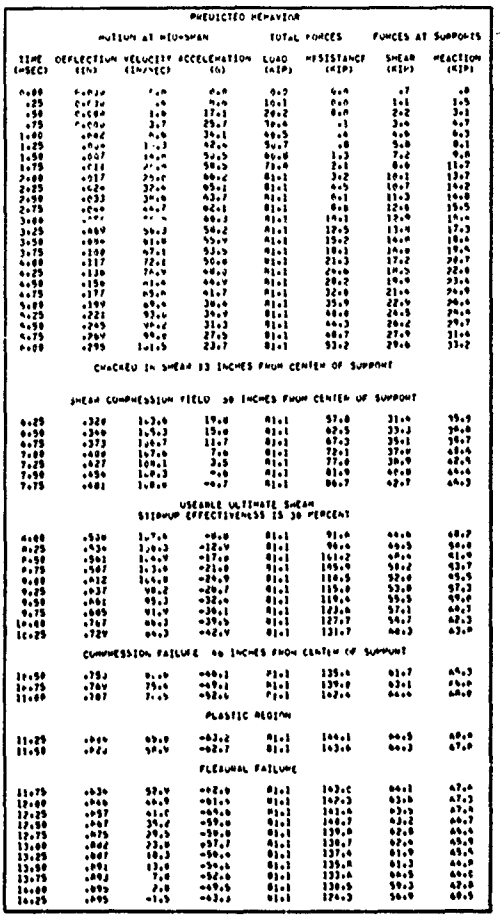

PREDICTED BEHAVIOR

TIME (MSEC)	DEFLECTION (IN)	MOTION AT MIDSPAN VELOCITY (IN/SEC)	ACCELERATION (G)	TOTAL FORCES LOAD (KIP)	RESISTANCE (KIP)	FORCES AT SUPPORTS SHEAR (KIP)	REACTION (KIP)
0.00	0.000	0.0	0.0	0.0	0.0	.7	.8
.25	0.013	.4	0.0	10.1	0.0	1.1	1.5
.50	0.050	1.0	17.1	20.2	0.0	2.2	3.1
.75	0.109	3.7	29.7	30.4	.1	3.4	4.7
1.00	.192	8.8	39.1	40.5	.4	4.6	6.3
1.25	.301	17.3	42.4	50.7	.8	5.8	8.1
1.50	.437	30.5	52.5	60.8	1.3	7.2	9.8
1.75	.611	49.4	58.9	71.0	2.1	8.9	11.7
2.00	.817	73.6	66.2	81.1	3.2	10.1	13.7
2.25	1.026	97.4	65.1	81.1	4.5	10.7	14.2
2.50	1.233	120.9	63.7	81.1	6.1	11.3	14.8
2.75	1.440	144.7	62.4	81.1	8.0	12.0	15.5
3.00	1.647	168.3	60.9	81.1	10.1	12.9	16.4
3.25	1.859	192.2	59.4	81.1	12.5	13.9	17.3
3.50	2.076	216.8	55.9	81.1	15.2	14.9	18.4
3.75	2.299	241.8	53.5	81.1	18.1	15.9	19.4
4.00	2.527	267.1	50.8	81.1	21.3	17.2	20.7
4.25	2.760	292.9	48.2	81.1	24.8	18.5	22.0
4.50	2.998	319.1	46.9	81.1	28.2	19.9	23.4
4.75	3.241	345.6	45.7	81.1	32.0	21.4	24.9
5.00	3.489	372.4	44.1	81.1	35.9	22.9	26.4
5.25	3.742	399.5	39.9	81.1	40.0	24.5	28.0
5.50	4.000	426.9	31.3	81.1	44.3	26.2	29.7
5.75	4.263	454.6	27.5	81.1	48.7	27.9	31.4
6.00	4.531	482.5	23.7	81.1	53.2	29.6	33.2

CRACKED IN SHEAR 13 INCHES FROM CENTER OF SUPPORT

SHEAR COMPRESSION FIELD 30 INCHES FROM CENTER OF SUPPORT

6.25	4.804	510.6	19.8	81.1	57.8	31.4	35.0
6.50	5.081	538.9	19.8	81.1	62.5	33.2	36.8
6.75	5.363	567.3	19.7	81.1	67.3	35.1	38.7
7.00	5.650	595.8	19.6	81.1	72.1	37.0	40.6
7.25	5.942	624.4	19.5	81.1	77.0	38.9	42.5
7.50	6.239	653.1	19.3	81.1	81.9	40.8	44.4
7.75	6.541	681.9	19.2	81.1	86.7	42.7	46.3

USEABLE ULTIMATE SHEAR
STIRRUP EFFECTIVENESS IS 30 PERCENT

8.00	6.848	710.8	18.8	81.1	91.6	44.6	48.2
8.25	7.160	739.8	18.4	81.1	96.4	46.5	50.0
8.50	7.477	768.9	17.9	81.1	101.2	48.4	51.9
8.75	7.799	798.1	17.4	81.1	106.0	50.2	53.7
9.00	8.126	827.4	16.9	81.1	110.5	52.0	55.5
9.25	8.458	856.8	16.4	81.1	115.0	53.8	57.3
9.50	8.795	886.3	15.8	81.1	119.4	55.5	59.0
9.75	9.137	915.9	15.2	81.1	123.8	57.1	60.7
10.00	9.484	945.6	14.6	81.1	127.7	58.7	62.3
10.25	9.836	975.4	13.9	81.1	131.7	60.3	63.9

COMPRESSION FAILURE 48 INCHES FROM CENTER OF SUPPORT

10.50	10.193	1005.3	13.2	81.1	135.4	61.7	65.3
10.75	10.555	1035.3	12.5	81.1	139.0	63.1	66.8
11.00	10.922	1065.4	11.8	81.1	142.4	64.4	68.0

PLASTIC REGION

11.25	11.294	1095.6	11.0	81.1	144.1	64.5	68.0
11.50	11.672	1125.9	10.2	81.1	145.8	64.3	67.8

FLEXURAL FAILURE

11.75	12.056	1156.3	9.4	81.1	143.6	64.1	67.6
12.00	12.446	1186.8	8.6	81.1	142.3	63.8	67.3
12.25	12.842	1217.4	7.8	81.1	141.0	63.5	67.0
12.50	13.243	1248.1	6.9	81.1	139.7	63.2	66.7
12.75	13.650	1278.9	6.0	81.1	138.3	62.8	66.4
13.00	14.062	1309.8	5.1	81.1	136.7	62.4	65.9
13.25	14.480	1340.8	4.2	81.1	135.0	61.9	65.4
13.50	14.903	1371.8	3.3	81.1	133.4	61.3	64.8
13.75	15.332	1402.9	2.3	81.1	133.4	60.5	64.0
14.00	15.766	1434.1	1.3	81.1	130.5	59.3	62.8
14.25	16.205	1465.4	.3	81.1	126.3	56.9	60.5

Figure 21. Continued

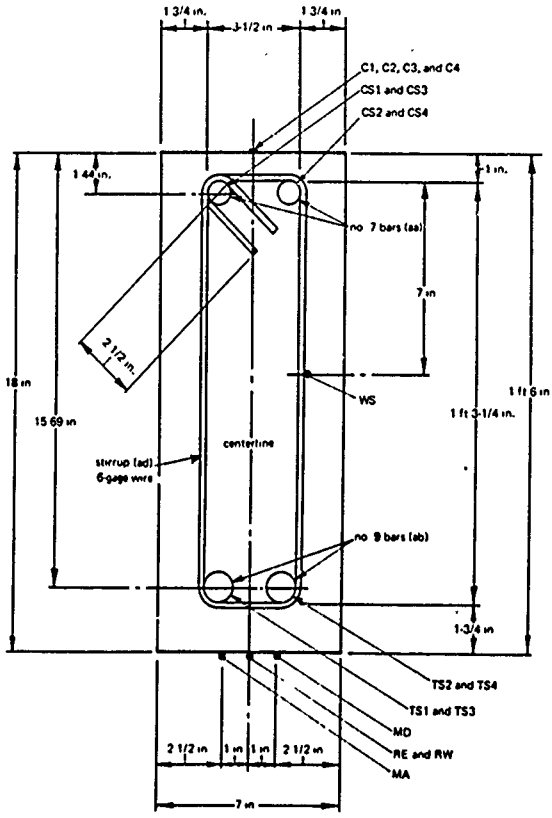

Section A A
Scale 3 in. = 1 ft 0 in

Figure 22. Cross section of Series F beams.

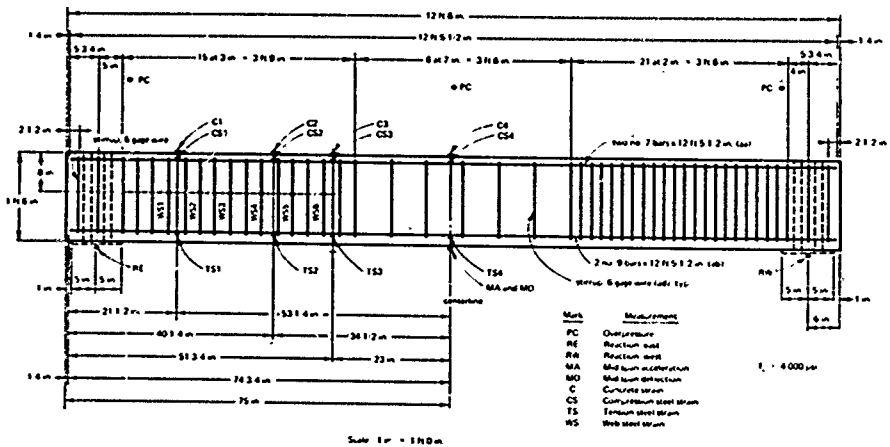

Figure 23. Details and instrumentation of beams WF1 through WF4.

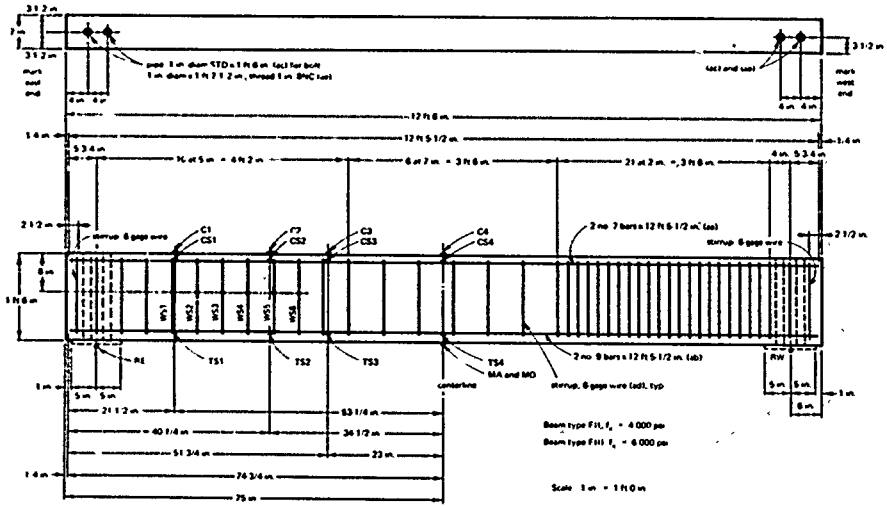

Figure 24. Details and instrumentation of beams WF5 through WF12.

Equipment

Loading Machine. The beams were tested in the NCEL blast simulator which is capable of applying a uniformly distributed static or dynamic load. Dynamic loads are applied by generating expanding gases in the simulator from the detonation of Primacord by means of two blasting caps. The rise time is controlled by the holes in the firing tube, the peak pressure by the amount of Primacord, and the decay time by opening valves which vent the gases to the atmosphere. A system of baffle plates in the pressure chamber assists in obtaining uniform distribution. Static loads are applied by admitting compressed air into the simulator by means of a compressor. A neoprene seal was placed on top of the beam between the walls of the blast simulator to contain the pressure.

The design capacity of the blast simulator is 185 psi and the width between the walls is 8.1 inches. Therefore, the maximum uniform load that can be applied is about 18 kip/ft.

The blast simulator has been discussed in detail by Shaw and Allgood.[33] Since that discussion, the blast simulator has been modified to accept deeper beams, and the operating procedures have been changed to retard carbon deposits.

Supports. The supports at each end of the beam provided a 10-inch-long bearing plate which was free to translate horizontally and to rotate. The beam was bolted to the bearing plate and the beam had a 6-inch overhang measured from the center of the bolt pattern to the end of the beam. Each of the two supports contained a 60-kip capacity load cell.

A cut-away isometric drawing of the support configuration appears in earlier reports.[14,23]

Measurements

Instrumentation. Measurements were taken to study the applied load, shear at the supports, effectiveness of the stirrups, flexural behavior along the span, and motion at midspan. The locations of the measurements are shown in Figures 22, 23, and 24. The data was gathered, recorded, reduced, and presented by the NCEL Data Tape System which is the subject of a separate report.[34]

Overpressure. The applied load (overpressure) was measured about 20 inches above the top surface of the beam at three locations along the span. Pressure transducer PC2 was positioned directly above the center of the span, PC1 4 inches from the center of the east support, and PC3 4 inches from the center of the west support. Measurement PC3 was omitted in the dynamic tests.

Reaction. The reactions at the supports (forces) were measured by load cells RE and RW located in the supports. These force measurements, corrected for the effects of the 6-inch overhang, were used to determine the shearing force at the supports.

Acceleration. In the dynamic tests only, accelerometer MA was attached to the underside of the beam at midspan to measure the motion of the beam. The values obtained were integrated once to obtain velocity and twice to obtain deflection.

Deflection. Linear potentiometer MD was located at midspan to measure deflection. The fixed part was attached to the steel cover over the blast simulator pit under the beam, and the movable part was spring loaded against the underside of the beam. Also, a rotating drum in conjunction with paper and pencil was used to corroborate measurement MD. The spring-loaded pencil was attached to an insert in the side of the beam 6 inches up from the bottom at midspan, and recorded on paper taped to the rotating drum which was attached to the bottom edge of the blast simulator wall and powered by an electric motor. In the static tests only, a scale (100 parts to the inch) oriented in the vertical direction was attached with masking tape to the side of the beam at midspan, and a surveyor's transit with the telescope in a fixed position was used to read the deflection.

Strain. Stirrup strains, WS1 through WS6, were measured with one electronic strain gage at each location, bonded to the wire in the vertical direction, and positioned 6 inches from the top of the beam. The stirrup strain measurements were used to detect cracking in shear, trace crack propagation, and indicate yielding of the stirrups. Strains C1 through C4 were measured with electronic strain gages bonded to the top surface of the concrete in the longitudinal direction, one gage at each of the four locations. Strains CS1 through CS4 and TS1 through TS4 in the longitudinal steel were measured with two electronic strain gages at each location placed diametrically opposite each other on the bar and wired to form opposite arms of a Wheatstone bridge circuit. The longitudinal strain measurements were taken at four locations (1) a distance from the support equal to the effective depth, d, (2) the quarter point, L/4, (3) the third point, L/3, and (4) the midpoint, L/2. These measurements were used mainly to study the ductility along the span and to indicate yielding and failure at the shear compression zone and at midspan.

Procedure

Fabricating Reinforcing Steel Cages. One cage for each beam was made from the longitudinal reinforcement and the stirrups using the following procedure:

1. Samples of the 6-gage wire were tested to determine the material properties.
2. The wire, received in straight lengths, was formed into box-shaped stirrups by cutting it to the required length and bending it around a pin.
3. Six wire stirrups were selected and one strain gage was applied to each, the gage being oriented along the axis of the wire and positioned 7 inches from the top of the stirrup.
4. The longitudinal steel (no. 9 and no. 7 bars) was labeled for identification and cut to the required length.
5. Selected coupons of the longitudinal steel were tested to determine the material properties.
6. At two locations on each of the four bars, the deformations were filed off by hand to prepare the surfaces for receiving strain gages.
7. Two strain gages were attached to each filed location; these gages were oriented along the axis of the bar and placed diametrically opposite each other. The pairs of gages CS1 and CS3 were on one bar, and CS2 and CS4 were on its companion The same arrangement was used for TS1 through TS4.
8. The longitudinal steel bars were placed on a wooden form which positioned them and held them firmly in place.
9. The stirrups were positioned and then tied with wire to the longitudinal steel.
10. Lifting eyes were made from no. 2 bars and were tied to the longitudinal steel at each end of the beam
11. In the final step, the wooden form was removed.

Casting. Thirteen cubic feet of concrete per batch was made at the casting site in a diesel powered mixer of 16-ft^3 capacity. The weights of the ingredients were carefully measured. A small quantity of water was added if necessary to obtain the specified slump. One batch was sufficient to cast one beam and six associated control cylinders.

The reinforcing steel cage was positioned in the steel form by means of small hydrostone cubes wired to the longitudinal bars as spacers against the form sides. Steel sleeves were installed to create the holes for the tiedown bolts at the supports. The lead wires from the strain gages were inserted outward through small holes drilled into the side of the form. Finally, a metal insert was positioned for holding the pencil which would record deflection.

The beam and six test cylinders were cast by shoveling the concrete into the forms and vibrating it with an electric probe-type vibrator. Finally, the top surfaces of the beam and cylinders were troweled smooth.

Curing. The beam and associated cylinders were removed from the forms about 2 days after casting and cured under wet burlap until about 2 days before testing. The burlap was watered once a day, 5 days a week.

Preparing Specimens. The following steps were taken to prepare each beam for testing:

1. The beam was set out to dry for 2 days.
2. Strain gages C1 through C4 were bonded to the top face of the beam.
3. The sides of the beam were whitewashed to emphasize the crack pattern which would form during the test.
4. The sides of the beam were lined with black paint to indicate the location of the stirrups and longitudinal reinforcement.
5. The beam was positioned and bolted on the supports, the assembly was placed on wheeled jacks, the lifting eyes were cut off, and the entire assembly was wheeled into position in the blast simulator.
6. The wheeled jacks under the supports were removed, and the supports were anchored to the concrete foundation.
7. A strip of neoprene was placed over the top of the beam to seal the pressure chamber of the blast simulator.
8. The rotating drum and pencil were installed.
9. For dynamic tests only, transducer MA was fastened. For static tests only, the scale for visually measuring midspan deflection was taped to the beam.
10. Finally, all electrical connections were made and the beam was ready for testing as shown in Figure 25.

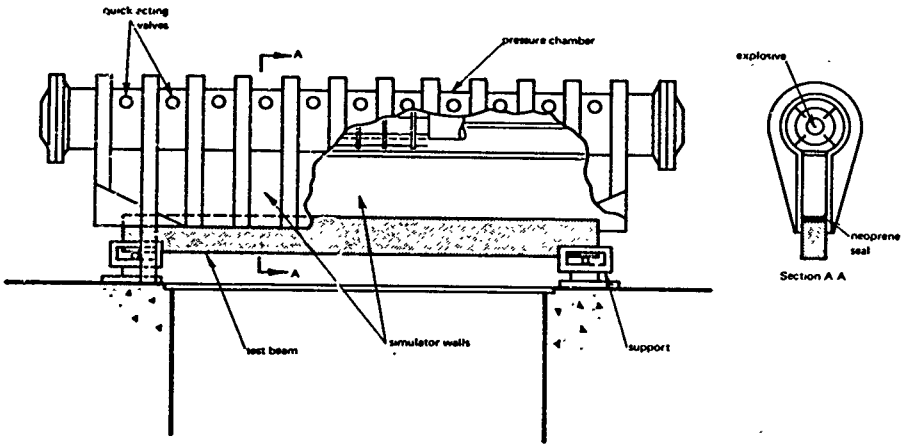

Figure 25. Schematic of beams in NCEL blast simulator.

Testing. The varied parameters in the experiment plan were load, concrete strength, and stirrup spacing as indicated in Table 3. Two concrete mixes and two stirrup spacings were used, six beams were loaded dynamically and six statically. The beams can be classified into three groups. group I had the higher concrete strength and closer stirrup spacing, group II had the higher strength and greater spacing, and group III had the lower strength and greater spacing. Within each group, two beams were loaded statically and two dynam ically. The beams in group II were designed to be underreinforced at midspan in the elastic range (zone 2 in the theory) and to have a large energy-absorbing capacity in the inelastic range (zones 4, 5, and 6). Furthermore, they were designed to be balanced with regard to yielding in flexure and yielding in shear. In the design, the usable ultimate shear was used to approximate yielding in shear. Closer spacing of stirrups was provided in group I to insure yielding in flexure and to study the influence of stirrups on ductility in the shear-compression zone. Lower concrete strength was provided in group III to insure shear failures and to study brittle behavior (zones 1 and 3). The ages of the beams at the time of testing were.

Group	Beam No.	Age (days)
I	WF1	28
	WF2	36
	WF3	29
	WF4	35
II	WF5	29
	WF6	29
	WF7	31
	WF8	30
III	WF9	30
	WF10	31
	WF11	29
	WF12	31

In the static tests, a uniformly distributed load on the beam was gradually and continuously increased to the point of beam collapse or to the point when the neoprene seal failed to contain the additional pressure. The uniform load was applied by admitting air pressure into the blast simulator from an air compressor. The amount of overpressure was monitored visually with an Emery pressure gage of 375-psi capacity. Measurements of load, reaction, deflection, and strain were recorded with the NCEL Data Tape System at each 5-psi increment of overpressure until an overpressure

of 30 psi was attained; then an increment of 2 psi was used until an overpressure of 90 psi was attained; and then an increment of 1 psi was used. At each increment, midspan deflection was recorded on the rotating drum, and transit readings of midspan deflection were recorded by hand, as was the overpressure indicated by the Emery pressure gage.

Table 3. Experiment Plan for Series F Tests

Constant test parameters:

L = 138 in	A_s = 2.00 in^2	A_v = 0.0567 in.^{2}
b = 7.00 in	A'_s = 2.20 in^2	E_y = 29.2 x 10^6 psi
h = 18.0 in.	p = 0.0182	f_{vy} = 30,000 psi
z = 6.00 in.	p' = 0.0109	α = 90 deg
d = 15.69 in.	E_s = 29.0 x 10^6 psi	L/d = 8.79
d' = 1.44 in.	f_y = 69,000 psi	b/d = 0.446

Beam No	Load Type[a]	Group No	Nominal Concrete Strength, f'_c (psi)	Stirrup Spacing, s (in.)
WF1 WF2	static	I	5,000	3
WF3 WF4	dynamic			
WF5 WF6	static	II	5,000	5
WF7 WF8	dynamic			
WF9 WF10	static	III	3,000	5
WF11 WF12	dynamic			

[a] Static test loads are to be increased slowly from zero to collapse. Dynamic test loads are to have rise times of 2 msec and are to be of long duration with a peak overpressure of 76 psi in the blast simulator.

In the dynamic tests, first the firing tube of the blast simulator was loaded with the amount of Primacord required to obtain the desired peak overpressure, and the sequence and delay time of the simulator valves were set to obtain the desired overpressure decay rate. A blasting cap was then inserted in each end of the firing tube and wired to the master control circuit. Finally, a switch was closed to start an electromechanical programmer which in turn (1) started the recording equipment, (2) placed a time reference on the records, (3) placed a calibration step pulse on the records, (4) ignited the explosive charge, (5) controlled the opening of the blast simulator valves, and (6) stopped the recording equipment. Continuous measurements of load, reaction, acceleration, deflection, and strain were recorded on magnetic tape. The rotating drum was switched on and off by hand, and continuous measurements of deflection were recorded on the paper.

After the test, the beam was inspected and removed from the blast simulator. The transducers were removed, the cracks lined with black ink for contrast, and the beam was photographed (Figures 26 through 29).

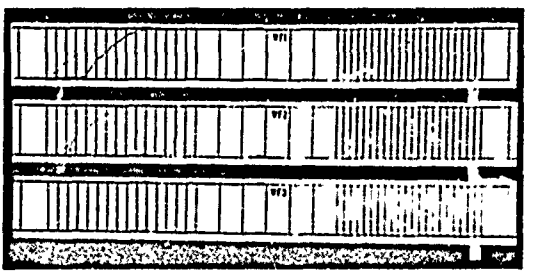

Figure 26. Post test photograph of statically loaded beams WF1 and WF2 and dynamically loaded beam WF3.

Findings and Conclusions

Accuracy of the Results. The accuracy and precision of experiments should be consistent with those of the theory and those required in designs Maximum errors in experiment data must be equal to or slightly less than those of the theory in order to prove or disprove the accuracy of the theory, but additional accuracy and precision are unwarranted and usually not desirable in the interest of experiment economy. In a similar manner, differences in agreement between experiment and theory should be equal to or slightly

less than the allowable error in the designs, and any terms in the theory giving contributions less than the allowable error should be omitted in the interest of economy in design procedure. Accuracy of test results can be governed by (1) accuracy of measurements and precision of data reduction, (2) controls over specimens, and (3) controls over testing.

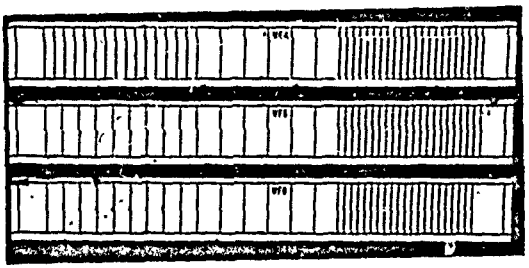

Figure 27. Post test photograph of statically loaded beams WF5 and WF6 and dynamically loaded beam WF4.

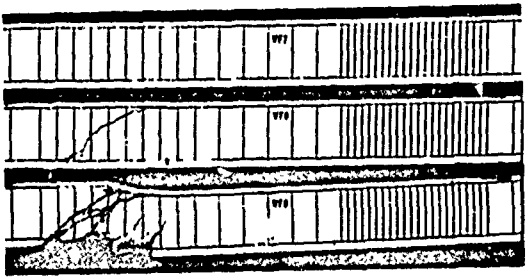

Figure 28. Post test photograph of dynamically loaded beams WF7 and WF8 and statically loaded beam WF9.

The accuracy of measurements and the precision of data reduction are shown in Table 4. Sliderule accuracy in computing calibration factors and precision resistances during pre-test calibration governed the accuracy of each channel of electronic instrumentation. Therefore, in each case, the

estimated error is ±2% of full scale. The system accuracy, including noise level, and transducer accuracies were much better. The precision with which the analog-to digital converter digitized the data was 1 part in 999 parts at band edge. Thus, in the case of force measurements where band edge was set at 80 kips, the estimated error is ±0.1% at 80 kips or ±0 08 kip. The scales used in conjunction with the telescope and the rotating drum were both 100 parts per inch, but additional error is estimated for play in the spring-loaded pencil which recorded on paper taped to the rotating drum. Measurement of time on a given channel was very accurate ($1/10^5$), but the coordination between various channels had a constant maximum error of ± 1/2 msec which gives only fair comparisons between values on one dynamic test record and another when values change rapidly with time.

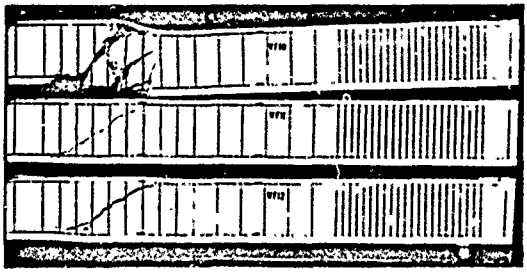

Figure 29. Post test photograph of dynamically loaded beams WF11 and WF12 and statically loaded beam WF10.

The controls over specimens are listed in Table 5. These controls represent ability, in the laboratory, to fabricate the beams as intended. The estimated errors associated with dimensions, proportions, and weight are all within 4.2% except the effective depth to the compression reinforcement, d', which is 8.7% This least accurate dimension is of little importance in the theory for shear up to the point of usable ultimate shear, and then it is very important in computing bending resistance in the shear compression zone. The flexural resistance in the theory is more dependent on the moment arm, d - d', which has a maximum error of only about 1%. The material used as stirrups was purchased by special order to guarantee accuracy, and tests showed no more than 5% error in yield strength On the other hand, tests on longitudinal reinforcing steel coupons and concrete control cylinders revealed strengths above the nominal strengths up to 26 and 28%, respectively.

For that reason, the strengths obtained in the tests on materials were used as input to the theory instead of the nominal strengths in order to achieve consistent accuracy. If the average values from the tests are substituted in place of the nominal strengths, the errors are as follows.

Parameter	Average Measured Value (psi)	Maximum Error (psi)	Maximum Percent Error (%)
f_y	69,000	+2,900	+4 2
f'_y	70,000	+5,600	+8 0
f'_c	5,767 3,478	-747 -458	-12.9 -13 2
E_c	$4\,54 \times 10^6$ $3\,52 \times 10^6$	$-0\,38 \times 10^6$ $-0\,29 \times 10^6$	-8 4 -8 2

The poorest control, then, over specimens was in concrete strength with a maximum error of 13 2% obtained from tests on 36 cylinders, and concrete strength is a dominant parameter throughout the theory Therefore, in comparing results of various tests in the experiment plan, better than 13% agreement in stress dependent parameters cannot be anticipated. This is consistent with required design accuracy if a capacity reduction factor, ϕ, of 0 85 is used

The controls over testing are listed in Table 6 These are also consistent with other sources of error except for the control over rise time in dynamic tests. Impulse is the only dominant parameter directly dependent on rise time, so computed impulse errors based on overpressure and rise time are given at 10 msec and 15 msec, the boundaries of the time interval over which most critical events were predicted The impulse error in percent decreases with time after the rise time and was only 8 2% at 10 msec The errors associated with controls over static tests were all less than 2%.

Table 4. Accuracy of Measurements and Precision of Data Reduction

Parameter	Accuracy of Measurements		Precision of Data Reduction		Maximum Total Error
	Error	Percent Error	Error	Percent Error	
Overpressure (fluid)	±3.0 psi	2% at 150 psi	±0.20 psi	0.1% at 200 psi	±3.2 psi
Force (reaction)	±1.2 kips	2% at 60 kips	±0.08 kip	0.1% at 80 kips	±1.3 kips
Acceleration (motion)	±4.0 g	2% at 200 g	±0.25 g	0.1% at 250 g	±4.2 g
Distance (deflection)					
Linear potentiometer	±0.08 in.	2% at 4 in.	±0.002 in.	0.1% at 2 in.	±0.08 in.
Rotating drum	±0.03 in.	[a]	0	0	±0.03 in.
Scale	±0.01 in	[a]	0	0	±0.01 in.
Strain	±0.00012 in./in.	2% at 0.006 in./in	±0.000003 in./in.	0.1% at 0.008 in./in.	±0.00013 in./in
Time					
Discrete channel	$1/10^5$	0.001%	$\Delta t = 0.00025$ sec	0.00001%	$\Delta t = 0.00025$ sec
Between channels	±0.0005 sec	[a]	0	0	±0.0005 sec

[a] Not applicable

Table 5 Controls Over Specimens

Parameter	Value	Error	Percent Error (%)
	Dimensions		
L	138 in.	±1/8 in.	±0.1
b	7 in	±1/16 in	±0.9
h	18 in.	±1/16 in	±0.3
z	6 in.	±1/16 in.	±1.0
d	15.69 in.	±1/16 in.	±0.4
d'	1.44 in.	±1/8 in	±8.7
s	3 in	±1/8 in	±4.2
	5 in.	±1/8 in	±2.5
α	90°	±0.50°	±0.6
bd	109.8 in.^{2}	±1.4 in.^{2}	±1.3
A_s	2.00 in.^{2}	±0.01 in.^{2}	±0.5
A'_s	1.20 in.^{2}	±0.01 in.^{2}	±0.8
A_v	0.0567 in.^{2}	±0.00017 in.^{2}	±0.3
	Proportions		
L/d	8.79	±0.044	±0.5
p	0.0182	±0.00033	±1.8
p'	0.0109	±0.00023	±2.1
A_v/bs	0.00270	±0.00015	±5.4
	0.00162	±0.00006	±3.7
	Weight		
ρ	150 lb/ft^3	±4 lb/ft^3	±2.7
W	1,641 lb	±66 lb	±4.0
	Material Properties		
f_y	60,000 psi	+11,900 psi	+19.8
f'_y	60,000 psi	+15,600 psi	+26.0
f_{vy}	30,000 psi	+800 psi	+2.7
		-1,500 psi	-5.0
f'_c	5,000 psi	+1,330 psi	+26.6
	3,000 psi	+830 psi	+27.7
E_s	29 x 10^6 psi	±1 x 10^5 psi	±3.4
E_v	29 x 10^6 psi	±1 x 10^6 psi	±3.4
E_c[a]	4.2 x 10^6 psi	±0.8 x 10^6 psi	±19.0
	3.3 x 10^6 psi	±0.6 x 10^6 psi	±18.0

[a] $E_c = \rho^{1.5} 33\sqrt{f'_c}$

Table 6. Controls Over Testing

Parameter	Value	Error	Percent Error (%)
Static Loads			
Overpressure	100 psi[d]	±1 psi	1.0
Load width	8.1 in.	±0.05 in.	0.6
Uniform load	810 lb/in.	±13.2 lb/in	1.6
Load length	150 in.	±1/4 in	0.2
Total load[b]	121.5 kips	±2.18 kips	1.8
Total load[c]	123.1 kips	±2.25 kips	1.8
Dynamic Loads			
Overpressure	76 psi[d]	±4 psi	5.3
Load width	8.1 in.	±0.05 in.	0.6
Uniform load	615.1 lb/in.	±36.4 lb/in.	5.9
Load length	150 in.	±1/4 in.	0.2
Total load[b]	92.3 kips	±5.62 kips	6.1
Rise time	2 msec	±0.5 msec	25.0
Impulse at 10 msec[e]	684 psi-msec	±56 psi-msec	8.2
Impulse at 15 msec[e]	1,064 psi-msec	±76 psi-msec	7.1

[a] Approximate overpressure required to cause yielding of the longitudinal tension steel at midspan

[b] Includes load on overhang, but excludes beam weight.

[c] Includes load on overhang and beam weight.

[d] Approximate overpressure required to cause flexural failure in group II, neglecting shear.

[e] Most of the critical events were expected to occur during the time interval between 10 and 15 msec.

Summation of vertical forces in static tests was used to confirm the accuracy of results in regard to forces The poorest agreement between total load and total reaction was in test WF6, and the results at 10-psi increments of load for that test are listed in Table 7. The largest difference of 4.3 kips was within the maximum difference anticipated (4 8 kips), and it was less than 4% of the corresponding load The poorest agreement between the east and west reactions was in test WF1, and the results at 10 psi increments of load for that test are listed in Table 8. The agreement between total load and total reaction is very good, and the difference between the half load and the reactions is consistently equal in magnitude and opposite in sign. These data show that friction in the rollers of the support can provide enough resisting moment to shift 3 kips from one support to the other. This lack of control over testing is believed to be less in dynamic tests where sudden loading should help to free the rollers

Loads and Reactions. In two static tests, the beams (WF9 and WF10) were loaded until they collapsed in shear as can be seen in the post-test photographs (Figures 28 and 29). In the other four static tests (WF1, WF2, WF5, and WF6), the neoprene seal failed to contain sufficient pressure to permit loading to the point of collapse, but the advanced stages of shear cracking evident in the photographs (Figures 26 and 27) indicate that collapse was nearly achieved. The maximum loads applied were

Beam No	Overpressure in the Simulator (psi)	Total Load Between Supports (kips)	Remarks
WF1	105	117	Leak in neoprene seal
WF2	100	112	Leak in neoprene seal
WF5	101	113	Leak in neoprene seal
WF6	102	114	Leak in neoprene seal
WF9	93	104	Shear collapse
WF10	96	107	Shear collapse

Agreement between the predicted and measured reactions over the full range of static loads was excellent. Typical data is shown in Figure 30, which is a plot of predicted and measured reactions with respect to load for static test WF6 This test had the best agreement between east and west reactions and the poorest agreement between the average reaction and the predicted reaction. A static overpressure in the blast simulator of 90 psi

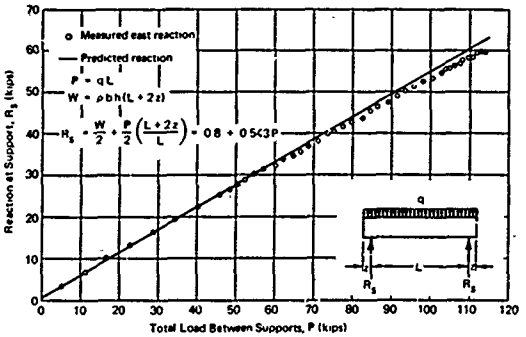

Figure 30. Reaction at support, beam WF6.

corresponded to a total load between supports of 100 6 kips, a load on the two overhangs of 10.2 kips, and the predicted reactions at the supports for that load were 55.4 kips. The measured values were:

Beam No.	Reaction, R_s (kips)		
	East	West	Average
WF1	59 5	52 0	55 8
WF2	56.3	51.4	53 8
WF5	58 4	52.1	55 2
WF6	53 3	53 4	53 4
WF9	55.1	54 3	54.7
WF10	56 9	55 1	56 0

A bad lot of Primacord was responsible for the underloading of the beams in the first three dynamic tests (WF3, WF4, and WF7). The other beams were loaded as intended. Because of this lack of control over peak overpressure, the load measured in the tests was used as input to the theory instead of the nominal load to achieve consistent accuracy (Table 6). This deviation from the experiment plan (Table 3) made peak overpressure a variable rather than a constant in Series F; it limited the comparisons that could be made between tests with regard to stirrup spacing and concrete

strength, but at the same time made possible some comparisons with regard to peak overpressure None of the dynamically tested beams collapsed, but all did yield at midspan, and the advanced stages of shear cracking in WF8, WF11, and WF12 (Figures 28 and 29) indicate that collapse was nearly achieved.

Figure 31 contains a plot of load with respect to time for dynamic test WF8, Data points in the figure labeled "load measured" were obtained by multiplying the average of the two overpressure measurements by the span length (138 inches) and the distance between the simulator skirts (8.1 inches). The perturbation during the rise of the load at about 40 kips is due to the poor time coordination (± 1/2 msec) of the two overpressure records. It is not due to irregularities of the load or poor response of the transducers, because the overpressure records were "clean" and "responsive" when studied independently. The dashed line in the figure labeled "load predicted" is an equivalent load with a linear rise of 2 msec and a constant peak value. The peak value was obtained by equating the impulses of the measured and equivalent loads out to the measured time of maximum deflection. The equivalent load was then used as input to the theory. All dynamic loads had characteristics similar to the one in the figure. The loads applied were:

Beam No	Total Load Between Supports (kips)		
	First Maximum	First Minimum After First Maximum	Equivalent Maximum
WF3	66 8	56.1	65.3
WF4	67.7	62.5	63.4
WF7	71 6	59 9	62.6
WF8	86.1	78 5	81.1
WF11	80.4	73 9	77.8
WF12		70 3	76.7

Table 7. Static Load and Reactions for Beam WF6

Nominal Overpressure (psi)	Overpressure (psi)					Reactions (kips)		Total Forces (kips)		
	PC1	PC2	PC3	Average	Maximum Difference[a]	RE	RW	Reactions	Loads[b]	Difference[c]
10	10.3	10.1	9.9	10.1	±0.2	6.9	6.5	13.4	13.9	0.5
20	21.3	19.9	20.5	20.6	±0.7	13.3	12.7	26.0	26.6	0.6
30	31.8	30.1	30.7	30.9	±0.9	19.7	18.8	38.5	39.1	0.6
40	42.0	40.2	41.2	41.1	±0.9	25.6	24.7	50.3	51.5	1.2
50	50.2	48.2	49.1	49.2	±1.0	30.2	29.2	59.4	61.4	2.0
60	61.2	58.6	59.9	59.9	±1.3	35.9	35.3	71.2	74.4	3.2
70	70.9	67.6	69.6	69.4	-1.8	41.8	40.8	82.6	85.9	3.3
80	81.5	77.9	80.2	79.9	-2.0	47.6	47.1	94.7	98.7	4.0
90	91.9	87.8	90.2	90.0	-2.2	53.3	53.4	106.7	111.0	4.3
100	102.5	97.3	100.5	100.1	-2.8	59.5	59.6	119.1	123.2	4.1

[a] Maximum difference between a measurement and the average measurement. The maximum difference anticipated was ±3.2 psi (accuracy of data).

[b] The weight of the beam (1.6 kips) plus the product of the area of the load (1,215 in.^{2}) and the average overpressure

[c] Anticipated maximum difference at 100 psi.

Total Load	±2.18 kips (control over testing)
Weight	±0.07 kips (control over specimens)
East Reaction	±1.3 kips (accuracy of data)
West Reaction	±1.3 kips (accuracy of data)
Total Error	±4.85 kips (total maximum difference at 100 psi)

Table 8. Static Reactions for Beam WF1

Nominal Overpressure (psi)	Reaction (kips)			Total Load[a] (kips)	Total Load Minus Total Reaction[b] (kips)	Half Total Load (kips)	Difference Between Half Load and Reaction,[c] (kips)	
	East	West	Total				East	West
10	8.1	4 5	12 6	13 8	+1.2	6 9	+1 2	-2 4
20	15.1	11 4	26 5	25 9	-0 6	13 0	+2.1	-1.6
30	21.3	17 3	38 6	38 0	-0 6	19 0	+2 3	-1.7
40	27 8	22 4	50 2	50 0	-0 2	25 0	+2 8	-2 6
50	33 8	27.6	61 4	62 4	+1.0	31 2	+2 6	-3 6
60	39 9	34 0	73 9	74 5	+0 6	37.2	+2.7	-3 2
70	45 8	39 8	85 6	86 6	+1 0	43.3	+2 5	-3 5
80	52 6	46 2	98 8	98 8	±0 0	49 4	+3 2	-3 2
90	59 5	52 0	111 5	111 0	-0 5	55 5	+4 0	-3 5
100	63 9	58 3	122 2	123.1	+0 9	61.5	+2 4	-3 2

[a] The weight of the beam (1 6 kips) plus the product of the area of the load (1,215 in.^{2}) and the nominal overpressure.

[b] The maximum difference anticipated was ±4 8 kips as calculated in note c of Table 7.

[c] Accuracy of data, ±1 3 kips.

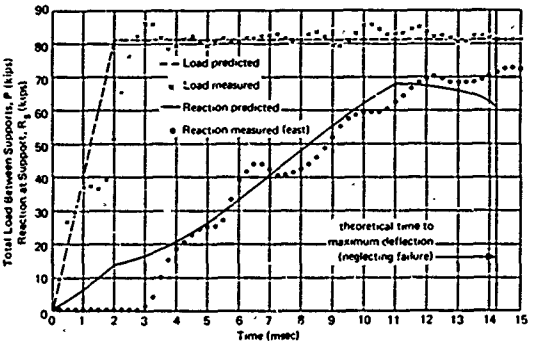

Figure 31. Load and reaction versus time, beam WF8.

Figure 31 also contains a plot of the reaction at the east support with respect to time for dynamic test WF8. The line in the figure labeled "reaction predicted" is the locus of points obtained from the computer code using the equivalent load and measured material strengths as input. The dynamic reaction at the support was computed after each time increment by simply adding the weight of the overhang and the load on the overhang to the shear at the support as obtained from Equation 15 in the theory.

$$R_s = V_s + \rho bhz + \frac{Pz}{L} \qquad (73)$$

where R_s is the reaction at support in pounds. The data points labeled "reaction measured" were measured by the load cell in the east support. Some of the disagreement between measured and computed values is due to unsymmetrical modes and other modes of vibration not accounted for in the theory. If the average values of the east and west reactions are plotted, these effects are partly filtered and agreement is slightly improved as shown in Figure 32. Most of the apparent disagreement is experimental data inaccuracy due to the poor time coordination between records (± 1/2 msec), and a little is due to error in measuring the reactions (± 1.3 kips). Thus, errors in the horizontal direction in the plot appear greater than in the vertical direction, and errors appear greater when the reaction is changing rapidly with

time. The limits of these maximum errors are also shown in the figure. With 1/2 msec subtracted from and 1.3 kips added to each measured data point agreement is almost perfect except for the first few milliseconds and at times near to the time of maximum deflection. During the earlier times, the disagreement is due to poor control over rise time and thus the impulse and to the first few modes of vibration above the fundamental mode. During the later times, the disagreement is probably due to accumulated error in the numerical integration and less accurate theory in the inelastic region of response. The best agreement occurred in test WF7 (Figure 33) where there was no disagreement outside the limits of experimental accuracy for times from 6.5 msec to the theoretical time of maximum deflection (13.7 msec).

The agreement between predicted and measured reactions at 10 msec was important because the usable ultimate shear was predicted to exist about that time, the earliest time predicted was 7.75 msec for test WF12, and the latest was 11.75 msec for test WF4. The reactions at the supports at 10 msec in the various tests were:

Beam No.	Reaction at Support, R_s (kips)				Percent Difference Between Average Measured Values and Predicted Values (%)
	East	West	Average	Predicted	
WF3	49.9	46.7	48.3	50.8	+5.2
WF4	51.1	46.1	48.6	49.1	+1.0
WF7	50.0	48.7	49.4	48.4	-2.0
WF8	59.2	57.9	58.6	62.3	+6.3
WF11	60.6	58.5	59.6	58.3	-2.2
WF12	60.5	59.7	60.1	60.3	+0.3

The random nature of the percent differences between tests indicate the disagreement is due to experimental error and/or higher modes and not to the predictions. These data show that the theory predicted the shear at the support very well at the time of usable ultimate shear. The largest difference between the east reaction and the predicted reaction at 10 msec was 5.2% and occurred in Beam WF8 (Figure 31).

Deflection at Midspan in Static Tests. Comparisons between static test data obtained from the linear potentiometer and those obtained from the scale were used to confirm the accuracy of results in regard to deflections. The poorest agreement occurred in tests WF2 and WF9, and the results at

10 psi increments of load for these tests are listed in Table 9. The largest difference of 0.07 inch was within the maximum difference anticipated (0.09 inch), and it was about 10% of the corresponding deflection. The largest difference in test WF9 was less than that of WF2, but the percent difference at low overpressure was very large. For instance, at a load of 50 psi, the difference was 0.05 inch, 16.7% of the corresponding deflection (0.30 inch). And agreement was even worse at lower deflections. These data indicate that maximum deflections were measured by the transducer with suitable accuracy, but deflections less than 0.30 inch might not have been adequately measured.

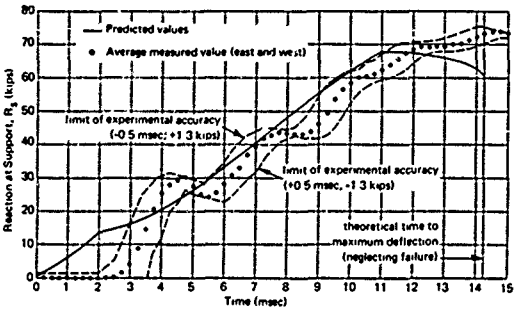

Figure 32. Average reaction versus time, beam WF8.

Figure 34 shows the agreement between predicted and measured values of deflection at midspan with respect to load for static test WF6. This test was chosen as an example not because it had the best or worst agreement, but because it was the same test used as an example in discussing reactions at the supports. The agreement in the other static tests was about the same. The data points labeled "measured deflection" were measured with the transducer, and the line labeled "predicted deflection" was obtained from the theory using Nosseir's method of predicting the spring constant. This excellent straight-line fit to curved data confirms the superiority of Nosseir's method.

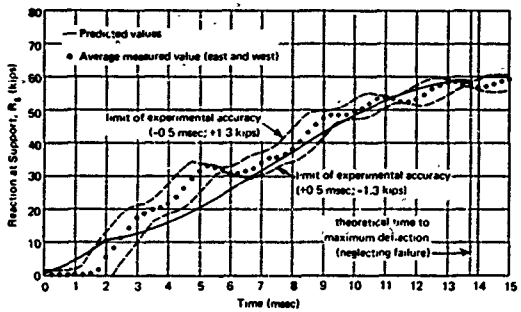

Figure 33. Average reaction versus time, beam WF7.

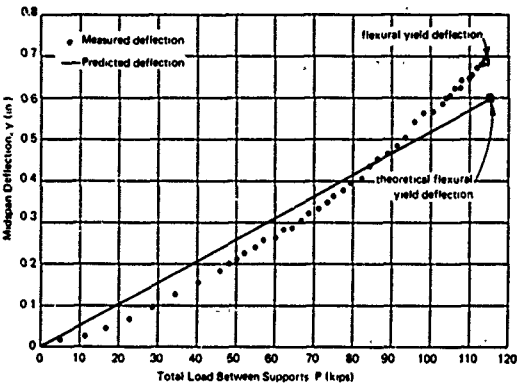

Figure 34. Deflection at midspan, beam WF6.

Table 9. Static Deflections for Beams WF2 and WF9

Nominal Overpressure (psi)	Total Load Between Supports (kips)	Midspan Deflection, y (in.)					
		Beam WF2			Beam WF9		
		Scale	Transducer	Difference[a]	Scale	Transducer	Difference[a]
10	11.2	0.04	0.03	-0.01	0.04	0.00	-0.04
20	22.4	0.08	0.07	-0.01	0.09	0.04	-0.05
30	33.5	0.14	0.13	-0.01	0.15	0.11	-0.04
40	44.7	0.20	0.19	-0.01	0.23	0.18	-0.05
50	55.9	0.25	0.24	-0.01	0.30	0.25	-0.05
60	67.1	0.34	0.31	-0.03	0.38	0.33	-0.05
70	78.3	0.40	0.39	-0.01	0.46	0.41	-0.05
80	89.4	0.46	0.44	-0.02	0.56	0.51	-0.05
90	100.6	0.55	0.50	-0.05	0.68	0.62	-0.06
100	111.8	0.65	0.58	-0.07	[b]	[b]	[b]

[a] Anticipated maximum difference at 100 psi.

Scale ±0.01
Transducer ±0.08
Total Error ±0.09

[b] Beam collapsed in shear at 94 psi.

Motions at Midspan in Dynamic Tests. The most accurate measurements of maximum deflection at midspan in dynamic tests were made with the rotating drum with pencil and paper (±0.03 inch), but the drum did not record the time to maximum. The deflection–time histories with the most accurate times to maximum deflection were obtained by continuous and time-coordinated measurements with the linear potentiometer (±0.5 msec, ±0.08 inch), and histories were also obtained indirectly by twice integrating the acceleration measurements using 1/4-msec increments. The maximum error accumulated with the square of time in the integrations (±0.5 msec, ±0.0016 in./msec^2). The integrated accelerations were the more accurate from 0 to about 7 msec, and then the directly measured deflections were the more accurate.

The maximum deflections and times to maximum are listed in Table 10. Beam WF8 was in group II, was loaded with just slightly more than the desired dynamic load, yielded in flexure, and deflected well into the inelastic regime. The shear crack was well developed as can be seen in Figure 28, the beam did not collapse, and there was no disagreement between measured and predicted maximum deflections. Beam WF11 was in group III, the group with lower concrete strength, was loaded with the desired amount of load, also yielded in flexure, and also deflected well into the inelastic regime. It behaved similarly with a well developed shear crack (Figure 29), no collapse, and no disagreement between measured and predicted maximum deflections. Beam WF12 was a companion to WF11 and received about the same amount of load. Its behavior was different in one respect; the shear crack opened enough to cause a large shear deformation (Figure 29). Therefore, the measured maximum deflection was about 20% larger than the predicted maximum due to the shear deformation contribution which is not accounted for in the theory. Any beam designed to function this near to shear collapse would certainly not have strict deflection criteria, so this error in predicting maximum deflection is considered consistent with allowable errors in designs. Beam WF7 was a companion to WF8, but it received less load than intended. It barely yielded at midspan, and although the shear crack propagated to the level of the compression reinforcement, it did not open far (Figure 28). The residual deflection was small, and the predictions overestimated the maximum deflection by about 17%. Beams WF3 and WF4 were in group I, which had the closer stirrup spacing and higher concrete strength. They were underloaded, as was WF7, and they also just barely yielded in flexure at midspan. Here, too, shear cracks developed fully, but shear deformations were small (Figure 26). Residual deflections were also small, and predictions overestimated the maximum deflection by about 24% in WF4 and 32% in WF3.

Table 10. Maximum Deflections at Midspan in Dynamic Tests

Beam No.	Maximum Deflection				Time to Maximum Deflection			
	Measured[a] (in.)	Predicted (in.)	Difference		Measured[b] (msec)	Predicted (msec)	Difference	
			Inch	Percent			msec	Percent
WF3	0.53	0.70	+0.17	+32.1	15.00	13.50	-1.50	-10.0
WF4	0.55	0.68	+0.13	+23.6	15.75	13.75	-2.00	-12.7
WF7	0.58	0.68	+0.10	+17.2	16.00	13.75	-2.25	-14.1
WF8	0.90	0.90	0.00	0.0	16.50	14.25	-2.25	-13.6
WF11	0.90	0.90	0.00	0.0	17.50	14.25	-3.25	-18.6
WF12	1.02[c]	0.82	-0.20	-19.6	18.00	14.00	-4.00	-22.2

[a] Measured with the rotating drum, data accuracy. ±0.03 in.

[b] Measured with the linear potentiometer, data accuracy. ±0.5 msec.

[c] Shear deformation was a major contribution.

These data show that in predicting maximum deflections the theory is conservative in the elastic regime, accurate through a large part of the inelastic regime, and unconservative near shear failure when the shear component of deflection becomes large. The conservatism in the elastic regime is due mainly to damping, most of which is not included in the theory; the conservative error due to damping is then compensated for at a later time by the unconservative error due to the changing deflected shape of the beam. The change in shape is due to hinging both at midspan and the shear-compression zone. These data show that when deflection criteria are used in design, the beams can be designed to respond to 100% of the allowable deflection.

Predicted times to maximum deflection were earlier than measured values in all of the dynamic tests. However, the errors exceeded 15% only in the two tests of group III where the beams responded into the inelastic regime near to the point of collapse in shear. Besides, time would seldom, if ever, be used as design criteria.

The maximum accelerations and velocities are listed in Table 11. The theory consistently underestimated the maximum acceleration and overestimated the maximum velocity. The initial high peaks in the acceleration data were expected and are due to high modes of vibration in the beam and also in the transducer. Since they are of short duration, they have only a small influence on velocity and deflection. However, when acceleration criteria are used in design, the peak accelerations in the beams should be considered; therefore, the beams should not be designed to respond above 50% of the allowable acceleration. The maximum velocity, which occurs later when the acceleration is zero, is less than predicted mainly because of damping components not included in the theory, and partly due to conservative approximations of spring constant. These conservative approximations occur at early times in dynamic response just as they do under small amounts of load in static response (shown in Figure 34). Thus, when velocity criteria are used in design, the beams can be designed to respond to 100% of the allowable velocity.

Sample deflection, acceleration, and velocity data are plotted in Figures 35, 36, and 37, respectively. Again, WF8 is used as the example so that the reader can associate the plots with those for load and reaction (Figures 31 and 32).

The predicted deflection is plotted in Figure 35 along with measured data points obtained directly from linear potentiometer measurements and indirectly from twice integrating accelerometer measurements. The moving part of the potentiometer, which was spring loaded to prevent damage to the instrument, bounced away from the beam upon initial loading for 5 msec and then regained contact. This caused an anomaly of no consequence since the integrated acceleration data was the more accurate during the first 7 msec anyway.

Table 11. Maximum Accelerations and Velocities at Midspan in Dynamic Tests

Beam No.	Maximum Acceleration				Maximum Velocity			
	Measured[a] (g)	Predicted (g)	Difference		Measured[c] (in./sec)	Predicted (in./sec)	Difference	
			g[b]	Percent			in./sec	Percent
WF3	59.0	53.2	-5.8	-9.8	51.2 ± 11.6	85.6	+34.4	+67.1
WF4	62.3	51.7	-10.6	-17.0	64.9 ± 13.6	83.7	+18.8	+29.0
WF7	67.6	51.0	-16.6	-24.6	70.2 ± 12.8	82.8	+12.6	+17.9
WF8	79.7	66.2	-13.5	-16.9	96.6 ± 13.2	108.3	+11.7	+12.1
WF11	92.9	63.6	-29.3	-31.5	90.5 ± 12.4	106.5	+16.0	+17.7
WF12	84.0	62.7	-21.3	-25.4	84.6 ± 13.2	100.3	+15.7	+18.6

[a] Absolute maximum, not the first maximum

[b] Anticipated maximum difference: ±4.2g.

[c] Integrated from accelerometer measurements using a time increment of 1/4 msec and no interpolation.

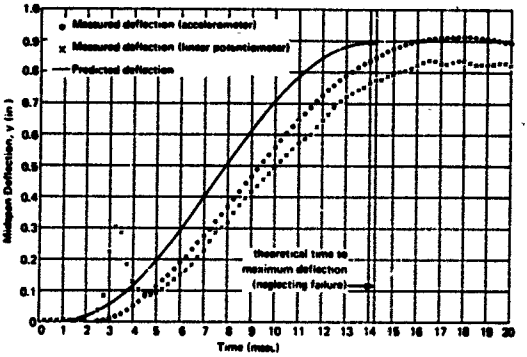

Figure 35. Midspan deflection versus time, beam WF8.

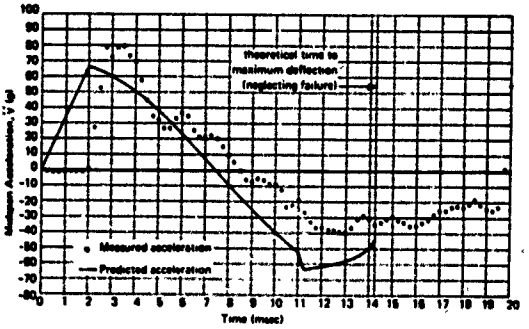

Figure 36. Midspan acceleration versus time, beam WF8.

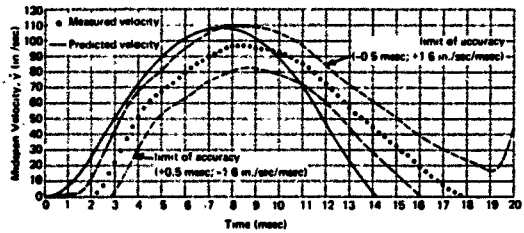

Figure 37. Midspan velocity versus time, beam WF8.

The acceleration data plotted in Figure 36 show that the time lag is nearly constant; the maximum acceleration, zero acceleration, and maximum deceleration were all predicted about 1 msec early. If the data were time adjusted by that amount, agreement would be very good.

The predicted velocity is plotted in Figure 37 along with the data points obtained by integrating the acceleration measurements. The limits of accuracy of the experimental data (± 0.5 msec, ± 1.6 in./sec/msec) are plotted also. The amplitude of the predictions is within experimental accuracy, but the period is a little short, and the maximum value is about 3/4 msec early.

Beams WF3 and WF4 were companions and received about the same amount of load. Inspection of the deflection records obtained from the rotating drum revealed that the beams deflected about the same amount, and inspection of the deflection records for WF3 obtained from all three methods of measuring deflection indicated that the accelerometer gave low values in test WF3. Thus, at least some of the disagreement between measured and predicted velocities in WF3 (Table 11) was due to error in the measurement.

Shear at Support. In the theory, the shearing force and resistance at the support are the basis of comparison in determining the occurrence of certain critical events. Unfortunately, the shearing force could not be measured directly in the experiments. The next best thing was to measure the reaction at the support and correct it for the effects of the overhang. Thus, shear data was obtained by subtracting the load on the overhang and the weight of the overhang from the reaction. Since the overhang was short (6 inches), the inertia of the overhang was neglected, and the correction was no more than 10% of the shear upon occurrence of any critical event. Errors in making this conversion are believed to be less than 1% of the shear.

Shear Cracking. Shear cracking was predicted and did occur in all of the tests. The measured and predicted values of the load and the shear at the support upon shear cracking for each of the static tests are listed in Table 12. In general, the data show that predicted values were within or near to the confidence limits of the experimental data, and the agreement between experiment and theory was within 15%. The only difference exceeding 15% was a conservative difference (18%) between the predicted and measured shear in WF2. Considering all of the data in the table, the maximum unconservative difference was only 4%.

Table 12. Loads and Shears Upon Shear Cracking in Static Tests

Beam No.	Cracking Load, P_c				Cracking Shear at Support, V_{sc}			
	Measured (kips)	Predicted (kips)	Difference		Measured (kips)	Predicted (kips)	Difference	
			Kips	Percent			Kips	Percent
WF1	50 ± 9	52	+2	+4	29 ± 2	27	-2	-7
WF2	61 ± 4	52	-9	-15	33 ± 2	27	-6	-18
WF5	52 ± 6	51	-1	-2	30 ± 2	26	-4	-13
WF6	48 ± 2	50	+2	+4	25 ± 2	26	+1	+4
WF9	46 ± 5	40	-6	-13	22 ± 2	21	-1	-5
WF10	42 ± 3	42	0	0	24 ± 2	22	-2	-8

The measured and predicted values of the time and the shear at the support upon shear cracking for each of the dynamic tests are listed in Table 13. Predicted values of both time and shear were conservative in all of the tests. The differences between measured and predicted shears ranged from 11% in WF3 to 36% in WF12. The conservatism with regard to WF7, WF8, WF11, and WF12 was at least partly due to the upper limit of 1.74 applied to the increase in diagonal tension strength. (See Equation 31.)

The data from the static and dynamic tests indicate that a capacity reduction factor of 0.85 would be adequate in design with regard to shear cracking.

Shear crack formation was detected by the strains in the stirrups, strains which were small prior to cracking and increased rapidly when the beam cracked in shear. The strain in the adjacent stirrup when the shear crack forms was estimated with the assumptions that (1) the diagonal tension

stress trajectory in the concrete was oriented 45 degrees from the axis of the stirrup, (2) the modulus of elasticity of the concrete in tension (E_t) is 3×10^6 psi, and (3) the mid-depth location of the strain gage is sufficiently near to the crack. The elevation of the strain gage is not a problem for two reasons: (1) the crack propagates to mid-depth instantaneously for practical purposes, and (2) upon cracking, the strains become distributed somewhat evenly over the stirrup length instead of being localized. The tests on control cylinders associated with WF2 determined the tensile strength of the concrete (f_t') to be 575 psi; therefore, the strain in the concrete in diagonal tension upon cracking (ϵ_t') in test WF2 was approximately

$$\epsilon_t' = \frac{f_t'}{E_t} = \frac{575}{3 \times 10^6} = 192 \times 10^{-6} \text{ in./in.}$$

and the corresponding strain in the stirrup was approximately

$$\epsilon_v = \epsilon_t' \sin 45^\circ = \frac{192 \times 10^{-6}}{\sqrt{2}} = 136 \times 10^{-6} \text{ in./in.}$$

This can be expressed as percent strain as follows:

$$\epsilon_v = 0.0136\%$$

The strains in the stirrups in static test WF2 are plotted in Figure 38, and the strain at which the shear crack formed (computed above) is also shown in the figure. The measured cracking load data given in Table 12 was obtained from plots like this one, and the confidence limits given with the data were based on estimated accuracy in measuring strain, estimating the strain at which the shear crack forms, and load application. The confidence limits tend to be narrow when the slope of the plotted line is greater. Only two anomalies occurred in the 36 stirrup strain measurements made in the static tests. One of these, strain WS6 in beam WF6, can be seen in Figure 39. This could have been a bad strain gage, but close examination of the data reveals that it could have been a damaged stirrup, perhaps damaged during casting of the beam. In analyzing this data, the shear crack formation was presumed to be detected by strain gage WS3. The other anomaly was similar in character, but much smaller in magnitude.

Strain gage WS5 in dynamic test WF11 did not produce a meaningful record; the other 35 strain gages in dynamic tests produced good records with no anomalies. The strains in the stirrups in dynamic test WF8 are plotted in Figure 40, and the strain at which the shear crack formed is also shown in the figure. The dynamic increase in tensile strength was accounted

for in estimating the strain by (1) assuming the modulus to be 3×10^6 psi, (2) using the slope of the strain–time curve averaged over 1 msec as the strain rate, (3) computing the approximate stress rate from the strain rate and the modulus, (4) entering the plot in Figure 19 with the stress rate and obtaining the dynamic increase coefficient, C_1, and then (5) applying the coefficient to the same method used for static data as described above. Thus,

$$\epsilon_v = C_1 \epsilon_i' \sin 45^\circ = \frac{C_1 \epsilon_i'}{\sqrt{2}} \text{ in./in.}$$

The measured times of cracking given in Table 13 were obtained in this manner.

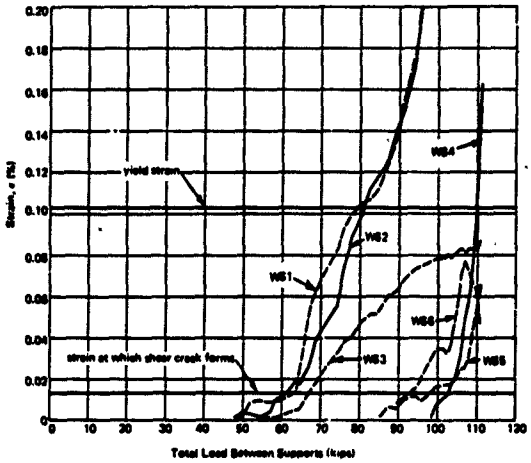

Figure 38. Strain of stirrups, beam WF2.

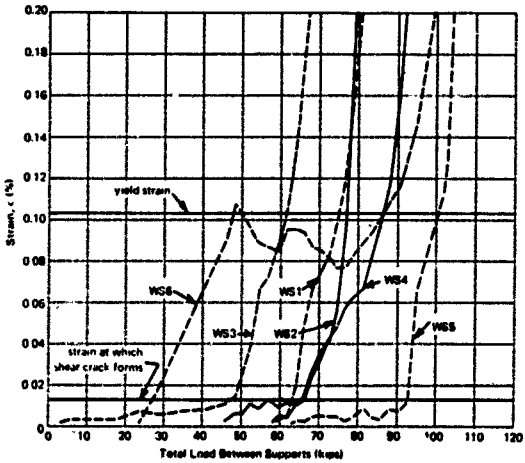

Figure 39. Strain of stirrups, beam WF6.

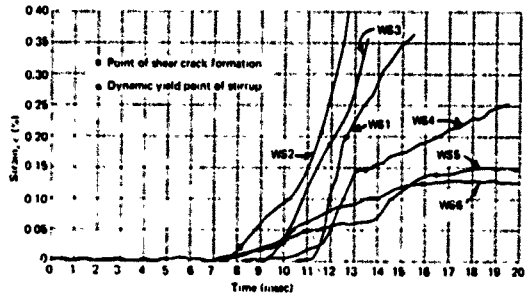

Figure 40. Strain of stirrups, beam WF8.

Table 13. Times and Shears Upon Shear Cracking in Dynamic Tests

Beam No	Time of Shear Cracking				Critical Shear at Support V_{ac}			
	Measured (msec)	Predicted (msec)	Difference		Measured (kips)	Predicted (kips)	Difference	
			msec	Percent			Kips	Percent
WF3	7.50 ± 2.00	7.25	+0.25	+3.3	35.8	31.9	3[illegible]	+10.9
WF4	8.75 ± 1.75	7.50	+1.25	+14.3	40.4	32.3	+8.1	+20.0
WF7	10.50 ± 0.75	7.50	+3.00	+28.6	49.7	31.8	+17.4	+35.4
WF8	8.25 ± 0.75	6.25	+2.00	+24.2	39.5	31.4	+8.1	+20.5
WF11	7.75 ± 0.75	6.00	+1.75	+22.6	41.8	27.6	+14.2	+34.0
WF12	7.25 ± 0.75	5.75	+1.50	+20.7	42.5	27.2	+15.3	+36.0

The strain gages which detected shear cracking in the beams were

Static Test No.	Gage No
WF1	WS2
WF2	WS2
WF5	WS3
WF6	WS3
WF9	WS3
WF10	WS3

Dynamic Test No	Gage No
WF3	WS3
WF4	WS3
WF7	WS3
WF8	WS2
WF11	WS3
WF12	WS4

These data show that the crack initiated at about the same location in all of the tests, and that the initiation point was not very sensitive to changes in loading rate.

The vertical position of the initiation point was assumed to be between the level of the tension reinforcement and the midheight (h/2) of the beam. Therefore, the distances from the center of the support to the main shear crack at both these levels were measured with a tape after testing, and the measurements were compared with the distance to the critical section (x_c) predicted in the theory. The measured and predicted values can be seen in Table 14. The predicted values are between the measured values for four of the six static tests and three of the six dynamic tests. The values outside are not far. The predicted values were also compared with average values of the two measurements. This was done to detect trends in differences between static and dynamic behavior. The accuracy and precision was about 0 ± 5 inches for static tests and -5 ± 3 inches for dynamic tests. The data in

dynamic tests are just as precise as in static tests, but the agreement between experiment and theory is not as accurate, predicting distances 5 inches shorter than measured.

Usable Ultimate Shear. The beams were predicted to respond beyond the usable ultimate shear in all of the tests, and the usable ultimate shear was reached in all except WF3. Beam WF3 was in group I, which had the higher concrete strength and closer stirrup spacing, was tested dynamically, and was underloaded. The stirrups in tension and concrete in compression remained elastic.

The measured and predicted values of the load and the shear at the support upon reaching the usable ultimate shear for each of the static tests are listed in Table 15. Agreement between experiment and theory was within 15% except for WF5 where the predictions were very conservative (37% with regard to shear). Considering all of the data in the table, the maximum unconservative difference was only 6%.

Table 14. Distances From the Supports to the Critical Sections

Test No.	Distance, x_c (in.)				
	Measured			Predicted	Difference
	a	*b*	Average		
Static					
WF1	16	22	19	14	-5
WF2	11	16	14	15	+1
WF5	8	22	15	15	0
WF6	9	24	16	15	-1
WF9	7	16	12	17	+5
WF10	8	19	14	16	+2
Dynamic					
WF3	16	20	18	12	-6
WF4	17	22	20	12	-8
WF7	13	23	18	12	-6
WF8	11	21	16	13	-3
WF11	10	23	17	14	-3
WF12	16	23	20	14	-6

[a] Measured at the level of the tension reinforcement.

[b] Measured at midheight of the beam (h/2).

Table 15. Loads and Shears Upon Reaching Usable Ultimate Shear in Static Tests

Beam No.	Usable Ultimate Load, P_u				Usable Ultimate Shear at Support, V_{us}			
	Measured (kips)	Predicted (kips)	Difference		Measured (kips)	Predicted (kips)	Difference	
			Kips	Percent			Kips	Percent
WF1	82 3	75 0	-7 3	-8.9	44.1	38.3	-5 8	-13.2
WF2	79 4	74 3	-5 1	-6 4	41 7	38 0	-3 7	-8.9
WF5	98 3	64 2	-34 1	-34 7	52 3	32 9	-19 4	-37 1
WF6	61 5	63 5	+2 0	+3 2	30 9	32 6	+1 7	+5.5
WF9	62 9	53 9	-9 0	-14 3	32 5	27 8	-4 7	-14 5
WF10	59 6	53.7	-5.9	-9 9	31 4	28 6	-2 8	-8 9

The measured and predicted values of the time of usable ultimate shear and the usable ultimate shear at the support for each of the dynamic tests are listed in Table 16. The dynamic usable ultimate shear resistance was predicted just as precisely as the dynamic shear cracking resistance, and even a little more accurately. The difference between measured and predicted shears ranged from an unconservative 6% in WF4 to a conservative 29% in WF8

The data from the static and dynamic tests indicate that a capacity reduction factor of 0.85 would be adequate in design with regard to usable ultimate shear.

The usable ultimate shear resistance was governed by yielding of the stirrups in all of the tests, and not to dowel failure Statically tested beams WF9 and WF10 collapsed in shear, but at loads about 40% higher than the usable ultimate. The strains in the stirrups in static test WF2 are plotted in Figure 38, and the yield strain (0.103%) is shown also. In the plot of stirrup strains for dynamic test WF8 (Figure 40), the dynamic yield strain is shown for each of the stirrups. The dynamic increase in stirrup yield strain was accounted for by (1) using the slope of the strain–time curve averaged over 1 msec as the strain rate, (2) entering the plot in Figure 17 with the strain rate and the static yield stress and obtaining the dynamic increase coefficient, C_2, and (3) applying the coefficient to the static strain as follows

$$\epsilon_{dyy} = C_2 \epsilon_{yy} = 0.103 C_2 \%$$

The stram gages which detected usable ultimate shear were

Static Test No	Gage No
WF1	WS1
WF2	WS1
WF5	WS4
WF6	WS3
WF9	WS1
WF10	WS2

Dynamic Test No	Gage No.
WF3	–
WF4	WS3
WF7	WS2
WF8	WS2
WF11	WS3
WF12	WS3

No gage is listed for test WF3 because the stirrups remained elastic in that test. The data in the table, along with the data in a similar table in the discussion about shear cracking, suggest the existence of at least two major shear cracks with the inboard one starting first, shear cracking, and the outboard one dominating at ultimate shear. The two cracks may join in the upper part of the beam as in the case of beam WF6 as can be seen in Figure 27.

Table 16. Times and Shears Upon Reaching Usable Ultimate Shear in Dynamic Tests

Beam No	Time of Usable Ultimate Shear				Usable Ultimate Shear at Support, V_{su}			
	Measured (msec)	Predicted (msec)	Difference		Measured (kips)	Predicted (kips)	Difference	
			msec	Percent			Kips	Percent
WF3	a	10.75	a	a	a	54.8	a	a
WF4	18.50	11.25	-7.25	-39.2	50.5	53.5	+3.0	+5.9
WF7	14.50	9.75	-4.75	-32.8	57.2	44.6	-12.7	-22.2
WF8	11.50	8.00	-3.50	-30.4	63.0	44.6	-18.4	-29.2
WF11	10.00	8.00	-2.00	-20.0	56.9	41.5	-15.4	-27.0
WF12	9.75	7.75	-2.00	-20.5	56.3	41.8	-14.5	-25.8

[a] Stirrups remained elastic

Flexural Yielding. Theoretical data for flexural yielding at midspan were calculated for all of the beams, even though some of the beams were predicted to fail in shear without flexural yielding. The theoretical and measured loads and shears upon flexural yielding in static tests are listed in Table 17. The agreement was excellent. The largest difference between experiment and theory was 7% in regard to load in WF5. The theoretical and measured time of flexural yielding in dynamic tests and the shear at that time are listed in Table 18. These data are less precise than the static data, but on the conservative side. The largest unconservative difference was only 5% in regard to shear in WF12. The theoretical times to flexural yielding were early, as was the case in all the dynamic data, and the shears were very conservative (30% in WF3), as were the velocities and deflection, in the underloaded beams of group I. The reasons for this conservatism were given in the discussion on motions at midspan.

Table 17. Loads and Shears Upon Flexural Yielding at Midspan in Static Tests

Beam No.	Load Which Produced Flexural Yielding at Midspan				Shear at Support Upon Flexural Yielding at Midspan			
	Measured (kips)	Theoretical (kips)	Difference		Measured (kips)	Theoretical (kips)	Difference	
			Kips	Percent			Kips	Percent
WF1	113.6	115.1	+1.5	+1.3	60.3	58.4	+1.9	+3.2
WF2	105.9	110.7	+4.8	+4.5	54.7	56.2	+1.5	+2.7
WF5	107.1	114.8	+7.7	+7.2	56.6	58.2	+1.6	+2.9
WF6	112.2	115.3	+3.1	+2.7	55.0	58.4	+3.4	+6.2
WF9	[a]	112.2	[a]	[a]	[b]	58.9	[b]	[b]
WF10	105.8[c]	110.3	+4.5	+4.3	54.0[d]	58.0	+2.0	+3.7

[a] Collapsed in shear without yielding at midspan under a load of 103.7 kips.

[b] Collapsed in shear without yielding at midspan when the shearing force at the support reached 52.4 kips.

[c] Collapsed in shear under a load of 106.1 kips just shortly after yielding in flexure.

[d] Collapsed in shear when the shearing force at the support reached 54.2 kips just shortly after yielding in flexure.

Table 18. Times and Shears Upon Flexural Yielding at Midspan in Dynamic Tests

Beam No	Time of Flexural Yielding at Midspan				Shear at Support Upon Flexural Yielding at Midspan			
	Measured (msec)	Theoretical (msec)	Difference		Measured (kips)	Theoretical (kips)	Difference	
			msec	Percent			Kips	Percent
WF3	17.50	12.75	-4.75	-27.2	45 8	59 7	+13 9	+30 4
WF4	19 00	13 50	-5 50	-28 9	48 0	58 3	+10 3	+21 5
WF7	14 00	13 75	-0.25	-1.8	53 6	56 2	+2 6	+4 8
WF8	12.75	11.25	-1 50	-11.8	65.1	64.5	-0 6	-0 9
WF11	12 50	11.75	-0 75	-6 0	65.4	62 9	-2 5	-3 8
WF12	13.75	11.75	-2 00	-14 5	68 4	64.7	-3,7	-5 4

Shear Yielding. Shear yielding occurred as predicted by yielding of the stirrups in all of the static tests. Therefore, shear yielding coincided with usable ultimate shear, and the values in Table 15 apply to shear yielding as well as to usable ultimate shear. The strain gages located at the quarter point and third point along the span on the concrete, compression steel, and tension steel indicated that yielding did not occur at those locations. However, the beams were not loaded to collapse in four of the tests, and large strains in the concrete indicate that yielding might have occurred if additional load had been applied.

Shear yielding was predicted to occur by yielding of the shear compression zone in all of the dynamic tests. This did not happen. Shear yielding did not occur at all in WF3 and occurred by yielding of the stirrups in the other tests. Therefore, shear yielding coincided with usable ultimate shear, as it did in the static tests. The shear-compression zone yielded in tests WF8, WF11, and WF12, but a short time after the stirrups yielded.

Theoretical and experimental distances from the center of the support to the shear-compression zone (x_u) are presented in Table 19. The experimental distances were measured at the level of the compression reinforcement. Agreement was poor, and static test agreement was no better than dynamic test agreement. The distances could not be measured accurately because the cracks were nearly horizontal at the level of the compression reinforcement, and local conditions adjacent to the steel bars probably influenced the pattern of cracks.

In summary, shear yielding predictions were accurate in the static case and conservative in the dynamic case. This is consistent with flexural yielding predictions which were also accurate in the static case and slightly conservative in the dynamic case. The conservatism in the dynamic predictions with regard to shear was greater than that with regard to flexure; therefore, the theory contains some safety in insuring the development of the ultimate flexural resistance of beams, and premature shear-compression yielding is not likely.

Flexural Failure. The theoretical time to flexural failure, neglecting shear and bond, was just prior to the theoretical time of maximum deflection for tests WF8, WF11, and WF12. The beams deflected to or beyond the theoretical maximum, did not collapse, and did not fail. Theoretical flexural failure was not reached in the calculations for the other three dynamic tests, and the beams did not fail.

No flexural failures were anticipated in static tests, and none occurred.

Shear Failure. Statically loaded beams WF9 and WF10 failed and collapsed in shear when the stirrups failed to contain the longitudinal tension reinforcement under shears much greater than the usable ultimate shears and just prior to yielding of the concrete at the location of strain gage C2 (quarter

point). Further classification of the failures could not be made because (1) it is not known whether the stirrups ruptured before or after dowel failure, and (2) it is not known whether or not the limit strain of 0.003 in./in. was reached at points between gage locations.

Table 19 Distances From the Supports to the Shear Compression Zones

Test No	Distance, x_u (in.)		
	Measured[a]	Predicted	Difference
Static			
WF1	34	51	+17
WF2	28	51	+23
WF5	35	56	+21
WF6	40	56	+16
WF9	24	57	+33
WF10	27	57	+30
Dynamic			
WF3	[b]	44	[b]
WF4	[b]	45	[b]
WF7	34	50	+16
WF8	40	50	+10
WF11	35	55	+25
WF12	40	56	+16

[a] Measured at the level of the compression reinforcement.

[b] Visible crack did not reach the level of the compression reinforcement.

The predicted failure loads and shears and the maximum measured loads and shears in the static tests are listed in Table 20. The predictions were conservative, the least being 17% in WF9, which failed, and the most being greater than 33% in WF1, which did not fail.

The data for tests WF9 and WF10 indicate the need for a limit to the area of web reinforcement as given in Equation 4a and as applied to Equations 36 and 37. The lower limit ($0.0015 b s$) was 0.0525 in.^{2} and the area, A_v, was 0.0567 in.^{2} (nearly equal to the limit), and shear failures occurred at the threshold of yielding in the shear-compression zone. It is

believed that smaller areas would influence containment of the longitudinal steel more than yielding of the shear-compression zone, thus, the conservatism of the predictions would be reduced, and shear failures would be brittle rather than ductile.

Shear-compression failures were predicted for dynamic test WF7 at the time of maximum deflection and tests WF8, WF11, and WF12 shortly before the time of maximum deflection. The predicted maximum deflections were reached in the tests, and no failures occurred indicating that the predictions with regard to failure were conservative. Shear failures were not anticipated in the other tests, and none occurred

Ductility Along the Span. The beams in group I (Table 3) had the higher concrete strength and closer stirrup spacing. All were loaded to flexural yield, but not far beyond. Strains at midspan plotted through zone 2 and into zone 4 (Figures 41, 42, and 43), indicating underreinforced conditions with strain ratios no more than 50% of the balanced condition. Strains at the third and quarter points plotted completely within zone 2 at about 50% of balance even though shear cracking occurred in all the tests and stirrups yielded in three of them. There was no appreciable change in the ductility (percent of balanced conditions) with change in loading rate as can be seen by comparing the plots in Figures 42 and 43, however, a change in shear crack location in the statically tested beams influenced the strains at the quarter point as can be seen by comparing the plots in Figures 41 and 42. The shear crack was further inboard in WF1 (Table 14 and Figure 26) causing a reduction in concrete strain after the stirrups yielded (Figure 41). The plot for WF3, not shown, was similar to the one for WF4.

The beams in group II had the higher concrete strength and further stirrup spacing. Since they had less web reinforcement, they were expected to be more shear sensitive than group I. In the static tests and dynamic test WF7, the beams were loaded, as in group I, to flexural yield, but not far beyond. Strain at midspan again plotted through zone 2 and into zone 4 (Figures 44 and 45), indicating underreinforced conditions with strain ratios about 50% of the balanced condition. The flexural ductility at the quarter points and third points were disturbed upon yielding of the stirrups (shear yielding) in static test WF6 and dynamic test WF7, but to a lesser degree in the dynamic test as can be seen by comparing the plots. Beam WF6 behaved like WF1 in that the concrete strain was reduced at the quarter point after shear yielding, but WF7 behaved differently in that the concrete strain increased abruptly upon shear yielding. Beam WF6 appeared to be well balanced with regard to shear and flexure and with regard to ductility at the shear-compression zone. The plot for static test WF6 is nearly identical to the hypothetical plot (Figure 15) discussed in presenting the theory.

Table 20. Predicted Failure Loads and Shears and Maximum Measured Loads and Shears in Static Tests

Beam No.	Total Load Between Supports				Shear at Support				Failed
	Maximum Measured (kips)	Predicted Failure (kips)	Difference		Maximum Measured (kips)	Predicted Failure (kips)	Difference		
			Kips	Percent			Kips	Percent	
WF1	117.2	82.3	-34.9	-29.8	62.6	42.0	-20.6	-32.9	no
WF2	111.7	79.1	-32.6	-29.2	57.0	40.4	-16.6	-29.1	no
WF5	112.8	82.9	-29.9	-26.5	59.0	42.2	-16.8	-28.5	no
WF6	114.0	83.6	-30.4	-26.6	54.9	42.6	-12.3	-22.4	no
WF9	103.8	85.8	-18.0	-17.4	52.4	43.7	-8.7	-16.6	yes
WF10	107.2	83.5	-23.7	-22.1	54.2	42.6	-11.6	-21.4	yes

Shear cracking and shear yielding occurred with both the midpoint and third point plotting in zone 2, which indicates ductility in shear at the critical section; then the third point curve approached the balance point, common to all zones, when the beam yielded at midspan by yielding of the tension steel, which indicates balanced conditions at the shear compression zone and ductility at midspan. This is considered the most economical design. The plot for WF5, not shown, was similar to the one for WF6, but indicated slightly greater ductility at all gage locations. The beam barely yielded at midspan in dynamic test WF7; therefore the velocity was nearly zero at the time of yielding, and the dynamic yield strain of the steel was approximately equal to the static yield strain. A much larger dynamic load was applied to WF8; the yield strain of the steel was increased as shown in Figure 46, but the ductility at midspan was changed little, if any. The curve representing the quarter point "jumped up" after shear cracking, reached a maximum at shear yielding, and then went down, ending with the concrete in tension. The curve representing the third point, which is near the shear compression zone, plotted linearly at about 50% of the balanced condition during much of the strain history and then turned rapidly upward passing right through the dynamic balance point into the zone above. The results of the group II tests indicate that flexural ductility can be maintained at the shear-compression zone, and the sequence of events in the concept of ductility along the span can be predicted by the theory.

The beams in group III had the lower concrete strength and greater stirrup spacing, and were included in the experiment plan to insure shear failures, thus providing data which would bracket the threshold of shear failure. The statically tested beams did fail in shear, just prior to yielding at midspan in WF9 and just after yielding at midspan in WF10. See Table 17. By comparing plots (Figures 44 and 47), one can see that reducing the concrete strength had little effect on ductility at midspan, but a large effect on ductility at both the critical section and the shear-compression zone. The lower strength caused earlier cracking and yielding in shear and increased the slopes of the curves for the third and quarter points after shear cracking. In general, this decreased shear-compression ductility through nearly all the strain history. The quarter point in WF9 (Figure 47) became brittle as the curve passed into zone 1. This did not happen in WF10, not shown, but it was approached. Test WF10 was also different in that the yield strain of the steel at midspan was reached just prior to shear failure. By comparing plots of dynamic test data (Figures 46 and 48), one can see that reducing the concrete strength had effects similar to those in the static tests. The load was not sufficient to cause failure in dynamic test WF12 (Figure 48), and behavior was similar to the comparable dynamic test of group II

(Figure 46). The main differences were earlier occurrence of shear events, increased slope with regard to the third point, and brittle behavior in zones 1 and 3 at the shear-compression zone. The plot for WF 11, not shown, was similar to the one for WF 12, except that the curve for the third point did not quite reach the brittle zones.

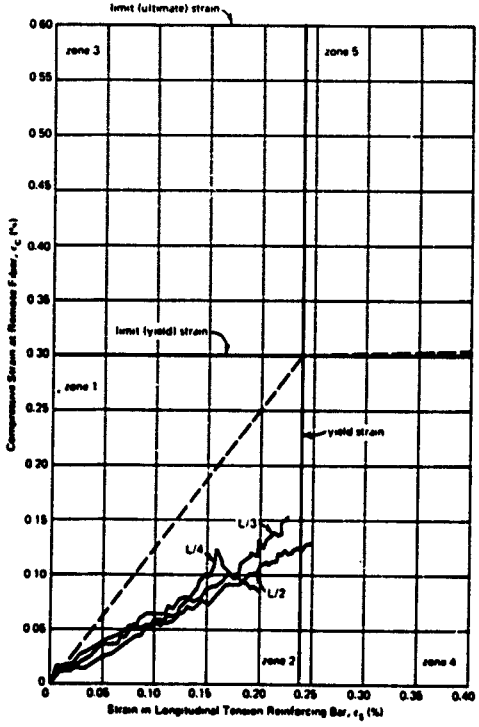

Figure 41. Concrete–steel balance at midpoint, third point, and quarter point of beam WF1.

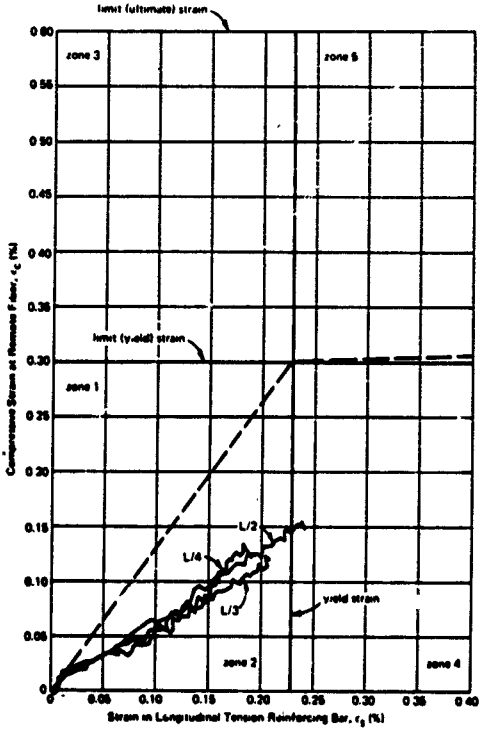

Figure 42. Concrete–steel balance at midpoint, third point, and quarter point of beam WP2.

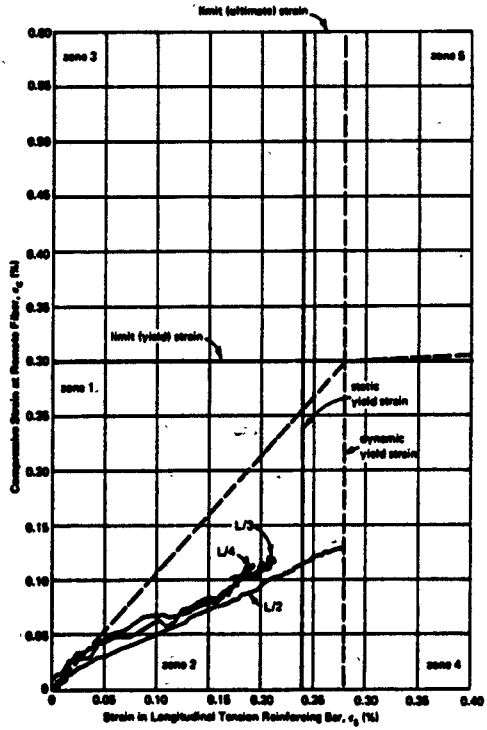

Figure 43. Concrete–steel balance at midpoint, third point, and quarter point of beam WF4.

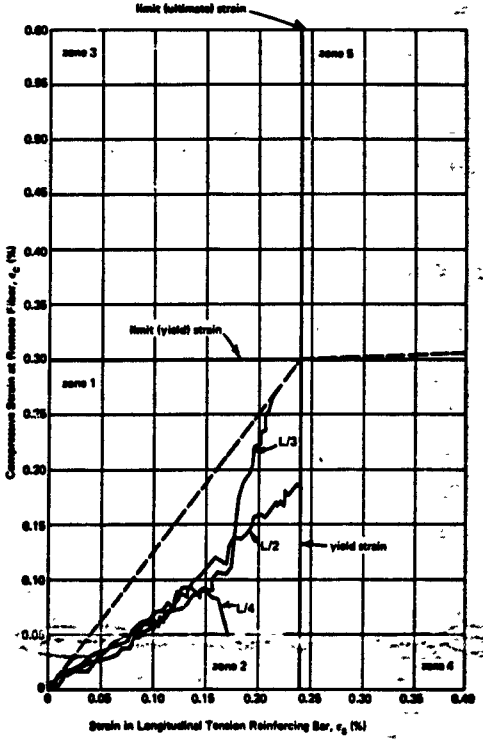

Figure 44. Concrete–steel balance at midpoint, third point, and quarter point of beam WF6.

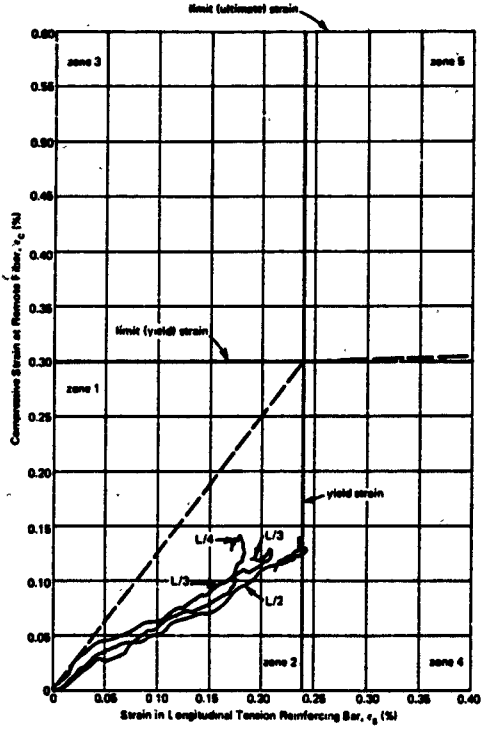

Figure 46. Concrete–steel balance at midpoint, third point, and quarter point of beam WF7.

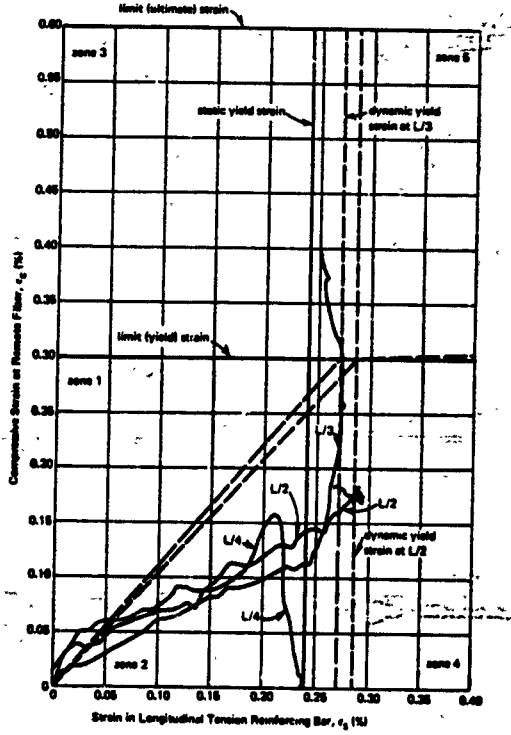

Figure 46. Concrete–steel balance at midpoint, third point, and quarter point of beam WF8.

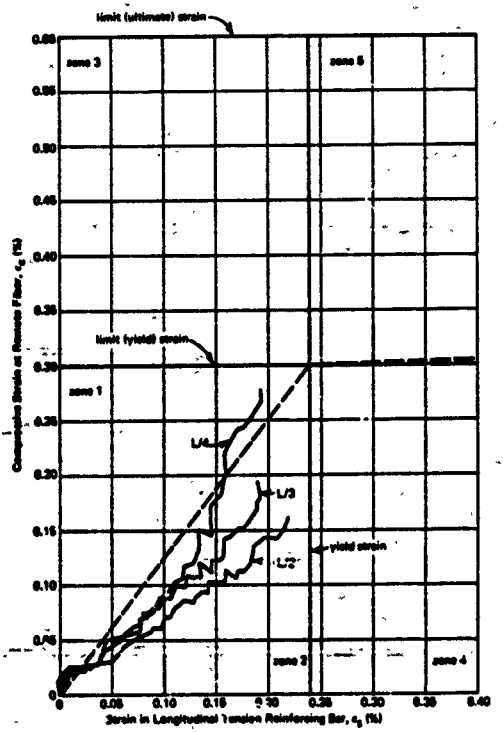

Figure 47. Concrete–steel balance at midpoint, third point, and quarter point of beam WF9.

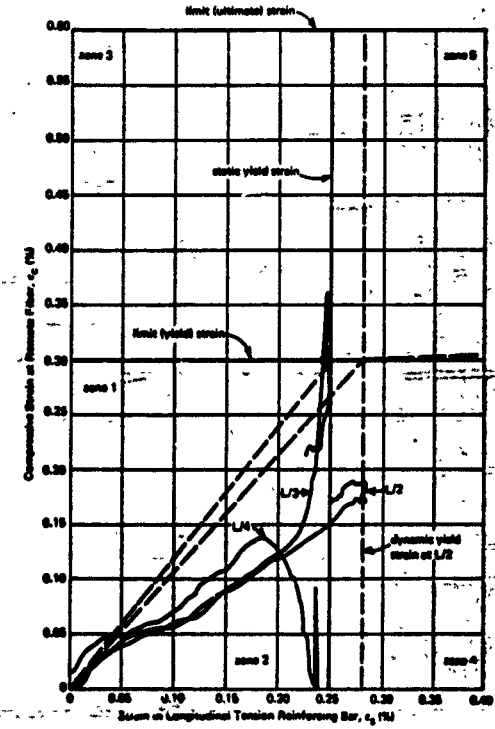

Figure 48. Concrete–steel balance at midpoint, third point, and quarter-point of beam WF12.

Summary. The concept of ductility along the span was studied with emphasis on the difference between static and dynamic behavior. Strains were attained in all six zones, but straining of the midspan tension reinforcement in zone 4 was less extensive than anticipated. Balanced conditions were attained at the shear-compression zone at the time of yielding at midspan in the group II dynamic tests. Yielding in shear and flexure but no failures were obtained in dynamic tests. The differences between static and dynamic histories of strain ratio were rather small indicating that no additional design criteria are needed to insure suitable ductility in flexure at the shear-compression zone in dynamic designs. The threshold of failure due to small areas of web reinforcement was studied, and the minimum area wes found to be most critical at low concrete strength and for the static case. It appears that the minimum area of web reinforcement specified by the ACI Code should be applied in static designs and is adequate for dynamic designs as well.

The theory predicted occurrence of shear cracking, usable ultimate shear, shear yielding, and flexural yielding for the static and dynamic cases well within normal engineering accuracy. Since all unconservative differences between theoretical and experimental shear, at the times of those events, were less than 15%, a capacity reduction factor of 0.85 in design is adequate for static and dynamic designs. Predictions of shear and flexural failure were conservative. Predictions of maximum acceleration were unconservative mainly due to high modes of vibration not included in the theory, and predictions of maximum velocity were conservative mainly due to damping components not included. Predicted deflections were unconservative only when shear yielding caused a large shear deformation by plastic hinging in the shear-compression zone.

Underloading in some of the tests limited the conclusions that can be made with regard to the effects of concrete strength. However, in general, predictions were equally good for the higher and lower strengths. Lowering the strength decreased the ductility in the shear-compression zone and decreased the conservatism of the predictions of shear failure in static tests. The dynamic increase coefficients for concrete, C_1, and stirrups, C_2, were successfully computed from the velocity at midspan and used to predict events in the shear behavior.

CONCLUSIONS

The conclusions in this section are general conclusions which apply to the three-part study. Specific conclusions pertaining to the Series F tests are combined with the findings of those tests and are presented in the previous section. Specific conclusions pertaining to other Series are presented in the section "Summary of Previous Work."

1. The shear, moment, shear strength, and flexural strength all increase under dynamic load with respect to the same load applied statically; both the shear strength contributions from the concrete and web reinforcement increase.

2. The shear and moment at the critical section increase in about the same proportions with respect to the loading rate. Thus, the shear-moment ratio does not change much at the critical section. Differences between static and dynamic values of shear-moment ratio are greater further from the support, under shorter duration loads, in deeper beams, and at relatively early times within the natural period of vibration.

3. The usable ultimate shear strength and the flexural yield strength increase in different proportions. Furthermore, the contributions to the usable ultimate shear strength from the concrete and the web reinforcement increase in different proportions, depending mainly on the material used for stirrups and the rate of strain in the stirrups. Thus, the mass and the characteristics of the dynamic load influence the relative increases in the flexural strength, shear strength from the concrete, and shear strength from stirrups.

4. Web reinforcement provides shear resistance by containing the longitudinal reinforcement, resisting rotation about the shear-compression zone, and resisting diagonal tension forces. If the area of web reinforcement is too small, the web reinforcement may strain excessively and thus fail to contain the longitudinal reinforcement triggering premature dowel failure. If the web reinforcement contribution to shear resistance is very large, shear yielding may occur by yielding at the shear-compression zone without yielding of the web reinforcement. Thus, a maximum limit on usable ultimate shear strength based on concrete strength and independent of the web reinforcement and a minimum limit on the area of web reinforcement are required to insure against premature failures. Under dynamic loading, there is a tendency toward relatively larger contributions from web reinforcement due to the dynamic increase in yield strength; therefore, the minimum limit on area of web reinforcement is less critical, the maximum limit on shear strength is more critical, and the general behavior in shear is less ductile or more brittle.

5. Strains in the stirrups are small until shear cracking occurs at which time there is a pronounced increase in rate of straining in stirrups located near the shear crack. In general, the stirrups act more or less independently, instead of as a group. The loading rate changes the yield strength of the stirrups, but does not change the general characteristics of performance.

6. It is possible for a beam to have enough web reinforcement to force flexural yielding prior to shear yielding in the static case, but not enough to cause that sequence in the dynamic case. The probability of change in sequence is greater when higher strength steel is used as stirrups and when the natural period of vibration is shorter.

7. The dynamic increase in yield strength of reinforcing steels is greater in lower strength steels. Between a curing time of 28 and 49 days, the dynamic increase in compressive strength of portland cement concrete is influenced more by curing time than by static compressive strength. Although the concrete has better than 90% of its compressive strength at 28 days, the dynamic increase in strength is considerably less at a later time.

8. Yielding at midspan retards further increase in shear at the supports in dynamically loaded beams. Many reasons were considered and none conclusively proved.

9. It is possible for a beam to fail in flexure after the usable ultimate shear resistance has been exceeded. In other words, the additional shear resistance beyond yielding in shear might be enough to force flexural failure. The probability is much less under dynamic loading.

10. Diagonal tension failures can occur upon shear cracking if stress redistribution is not accomplished or later when the longitudinal tension reinforcement suffers dowel failure. This applies to the dynamic as well as the static case, with and without web reinforcement. In beams with very small areas of web reinforcement, the dowel failure can be triggered by failure of the web reinforcement to contain the longitudinal tension reinforcement.

11. The location of the critical section does not change much with change in concrete strength, stirrup spacing, and loading rate. The effective depth of the beam can be used as an estimate of the distance from the support to the critical section for static and dynamic design purposes, and the theory can be used to compute the distance in static and dynamic rigorous analysis.

12. Underreinforced conditions can be maintained in bending at the shear-compression zone. All of the events in the concept of ductility along the span can be predicted with regard to sequence and zone of occurrence.

13. A capacity reduction factor of 0.85 is adequate in analysis and design when using the theory to calculate static and dynamic loads, resistances, and shears corresponding to shear cracking, usable ultimate shear, shear yielding, and flexural yielding. The theory provides only conservative estimates of failures in shear and flexure. The theory gives unconservative

values of maximum acceleration and conservative values of maximum velocity. Predictions of maximum deflection are conservative if most of the response history is elastic, fairly accurate if the beam deflects into the inelastic regime, and unconservative only when shear deformations become large

14. The chart developed from the modal analysis is adequate for predicting the maximum shearing force at the supports.

RECOMMENDATIONS FOR DESIGN

Static Load Design Criteria

Reinforced concrete beams should be underreinforced and designed to remain in the elastic regime under normal service loads, with minor cracking in shear and flexure permitted. The yield strength of longitudinal tension reinforcing should be used as the reference in proportioning and sizing members, and the required usable ultimate shear strength used to determine the amount of web reinforcement. Capacity reduction factors, ϕ, for shear and flexure should be applied to provide safety against flaws in fabrication and inaccuracies in design, and load factors for safety against overloading. Actually, shear cracking in the beams will be nonexistent, or very small, with the use of usable ultimate shear as the design reference if the safety factors are used. Theoretically, if a capacity reduction factor of 0.85 were used for both shear and flexure, and a load factor of 1.2 were applied to all design loads, stirrup effectiveness up to about 35% would not result in any shear cracking at full load, and load factors up to 2.4 are commonly used with live loads giving even additional safety, allowing much higher stirrup effectiveness without shear cracking.

As a result of this study, two provisions, different from those of the ACI Code,[13] are recommended for shear and diagonal tension, ultimate strength design. (1) In sections with web reinforcement, the shear stress, v_u, should not exceed $8\phi\sqrt{f'_c}$ in rectangular sections and $10\phi\sqrt{f'_c}$ in T-sections and I-sections. (See ACI Code provision 1705b.) This provision is discussed on pages 29 and 33 of this report. (2) In rectangular beams with reinforcement ratio, p, less than 0.012, the shear stress permitted on an unreinforced web, or the contribution from the concrete in a reinforced web, should not exceed that given by:

$$v_c = \phi(0.8 + 100p)\sqrt{f'_c} \qquad p < 0.012 \qquad (74)$$

(See ACI Code provision 1701d.) This provision is discussed on page 7 of this report.

Dynamic Load Design Criteria

In protective construction against dynamic overloads, load factors should be omitted and yielding, or additional yielding, permitted in case the load is larger than anticipated. General design criteria are variable depending on the amount of protection required and the deflections that can be tolerated. Capacity reduction factors should be used not necessarily to insure against yielding, but to insure that if yielding or failure occur, they will occur in a predictable fashion, in the most desirable mode, and without sudden failure.

Structures should be classified with regard to protection required and deflection that can be tolerated. Three classes are recommended. They are arbitrarily designated A, B, and C.

Class A contains key structures requiring the most protection and least deflection such as command posts and missile launching facilities. These structures must function under repeated dynamic loads, during dynamic loading, and/or without damage to sensitive equipment. Beams should be designed to remain elastic. Thus, the yield strength of longitudinal tension reinforcement, f_{dy}, should be used as the reference in proportioning and sizing members, and the required usable ultimate shear strength, v_u, used to determine the amount of web reinforcement. A capacity reduction factor of 0.85 in shear and unity in flexure should be used to insure against yielding in shear prior to yielding in flexure, if yielding occurs.

Class B contains personnel shelters and shelters of important equipment and supplies where repeated dynamic loads are not expected, large deflections can be tolerated, but insurance against failure must be maintained. Beams should be designed to yield in flexure, but not in shear. Thus, a limit strain, ϵ_{cy}, of 0.003 in./in. representing yielding of the concrete in compression should be used as the flexural criterion, and the required usable ultimate shear strength used as the shear criterion to determine the amount of web reinforcement. A capacity reduction factor of unity should be used in both shear and flexure.

Class C contains unoccupied structures and shelters of less important equipment and supplies where the least protection is required and deflection is not a consideration. In this class, economy outweighs margin of safety against failure. Beams can be designed to respond to the point of failure in flexure, which is defined by a limit strain, ϵ_{cu}, of 0.006 in./in. representing crushing failure of the concrete. They may be designed to respond to the point of yielding of the shear-compression zone with a limit strain, ϵ_{cy}, of 0.003 in./in. if the numerical integration procedure is used to analyze the beams. Conservatism in the theory will insure against yielding in shear prior to failure in flexure. If the numerical integration procedure is not used, the design for shear should be the same as for class B. A capacity reduction factor of unity should be used both in shear and flexure.

The following table is provided for quick reference in selecting general shear and flexure criteria and applicable capacity reduction factors.

Structure Classification	Dynamic Design Criteria		Capacity Reduction Factor, ϕ	
	Flexure	Shear	Flexure	Shear
A	f_{dy}	f_{dvy}	1	0.85
B	ϵ_{cy}	f_{dvy}	1	1
C	ϵ_{cu}	ϵ_{cy}	1	1

Motion Criteria

If the maximum values of motion parameters calculated in the numerical integration procedure are compared with motion criteria, the following "rules of thumb" should be applied.

Calculated maximum deflections should be permitted to 100% of the maximum allowable deflections. Such designs can be expected to be about 15 to 30% safe with regard to deflection if maximum deflection occurs in the elastic range, and zero to 15% safe if maximum deflection occurs a short distance into the inelastic range. It is assumed that deflection criteria will not be used for beams permitted to deflect far into the inelastic range or to yield in shear.

Calculated maximum velocities should be permitted to 100% of the maximum allowable velocities. Such designs can be expected to be conservative due to damping components not included in the theory.

Calculated maximum accelerations should be permitted to only 50% of the maximum allowable accelerations to allow for unpredictable initial peak accelerations of short duration not accounted for in the theory.

Concrete

Proportions. The theory presented herein is intended for slender beams only ($L/d > 7$), but probably could be used with appropriate capacity reduction factors to obtain less accurate solutions for intermediate beams ($5 < L/d < 7$). It is not recommended for deep beams ($L/d < 5$).

Cover. The minimum cover over reinforcing steel specified in the ACI Code for the static case also applies to the dynamic case.

Strength. Static 28-day compressive strengths of concrete within the limits

$$2{,}000 < f'_c < 7{,}000 \text{ psi}$$

are recommended. The application of higher strengths was not investigated and should be the subject of future studies.

The dynamic increase in tensile strength may be expressed as

$$\bar{C}_1 = \frac{f'_{dt}}{f'_t} = 0.951 + 1.33 \times 10^{-6} \dot{f}_t + 0.0693 \log \dot{f}_t \qquad (75)$$

where $\dot{f}_t = \frac{15}{4}\left[\frac{w_o(L - 2x_c)}{bhT_n}\right]$

and $1 < \bar{C}_1 < 1.74$

Contribution to Shear Strength. The maximum concrete contribution to dynamic shear strength, also called the diagonal cracking strength, can be computed from the following formulas, which are discussed in the theory under "Dynamic Shear Strength at the Critical Section." For $p < 0.012$,

$$v_c = \phi(0.8 + 100p)C_1\sqrt{f'_c} \qquad (76)$$

For $p \geq 0.012$,

$$v_c = \phi\left(1.9C_1\sqrt{f'_c} + 2{,}500\frac{pVd}{M}\right) \quad < 3.5\phi C_1\sqrt{f'_c} \qquad (77)$$

where $\frac{V}{M} = \frac{L - 2x_c}{Lx_c - x_c^2 - z^2}$

Longitudinal Reinforcement

Compression Reinforcement. All dynamically loaded reinforced concrete beams should contain compression reinforcement. The compression reinforcement (1) acts in tension during rebound, (2) contains, in conjunction with stirrups, the concrete of the shear-compression zone, (3) provides additional ductility, (4) helps to arrest the shear crack providing a point of rotation in shear-compression, and (5) provides dowel resistance at the shear-compression zone. Recommended limits of compression reinforcement ratio are

$$0.25p < p' < p$$

It is believed that best results are obtained when the compression steel ratio is between 30 and 50% of the tension steel ratio.

Theoretically, there is no reason why the yield stresses of compression and tension steel need be the same; therefore, equations in the theory are written as if they were different to allow flexibility in design. It is believed that economical results can be obtained with the use of two steel strengths, the lower strength used in compression. If two strengths are used, precautions must be taken to prevent confusion during steel fabrication.

Static yield strengths of longitudinal compression steel within the limits

$$40{,}000 < f'_y < 75{,}000 \text{ psi}$$

are recommended.

Tension Reinforcement. Static yield strengths of longitudinal tension steel within the limits

$$40{,}000 < f_y < 75{,}000 \text{ psi}$$

are recommended. Higher strengths may be used, but suitable ductility is difficult to achieve in design at strengths above 75,000 psi.

Recommended tension reinforcement ratios are

$$0.012 < p < 0.035$$

Ratios below 0.012 may be used, but the shear resistance contribution from concrete must be reduced in accordance with Equation 76. The greatest energy absorption of beams under dynamic load occurs with a reinforcement ratio of about 0.02, so that value is a good starting point for initial designing.

Web Reinforcement

Orientation. Inclined stirrups are not recommended. The horizontal components of inclined stirrups tend to overload the shear-compression zone causing brittle behavior and premature shear yielding by yielding of the concrete in compression. Also, inclined stirrups act in the wrong direction during rebound contributing little, or no, resistance to diagonal tension. No more than half of the web reinforcement over a distance along the axis of the beam equal to the effective depth of the beam should be provided by bent-up bars

for the same reasons. If bent-up bars or inclined stirrups are to be used, a dynamic analysis of compression and rotation at the shear-compression zone should be made including the effects of the horizontal components from web reinforcement.

Amount. The required amount of web reinforcement should be computed from the beam width and the difference between the usable ultimate shear strength required and the shear strength contributed by the concrete as follows

$$C_2 \frac{A_v f_{vy}}{s} = \frac{b}{\phi} (v_u - v_c) \qquad (78)$$

Strength. Static yield strengths of stirrups within the limits

$$30{,}000 \leq f_{vy} \leq 75{,}000 \text{ psi}$$

are recommended. Higher strengths may be used, but might not be economical due to small dynamic increase in strength and the tendency toward yielding in the shear-compression zone without yielding of the stirrups. As mentioned earlier, a change in yielding of the beam from the flexure to the shear mode might occur with increase in loading rate when high-strength steel is used for stirrups.

The dynamic increase in stirrup strength should be computed from the static yield strength and the elastic strain rate as shown in Equation 29 of the theory. Equation 29 is restated in specific stirrup notation as follows:

$$C_2 = \frac{f_{dvy}}{f_{vy}} = 1 + \frac{13{,}700}{f_{vy}} - \frac{94.9 \times 10^6}{f_{vy}^2} + \left(\frac{3{,}000}{f_{vy}} + \frac{423 \times 10^6}{f_{vy}^2} \right) \log (10 \dot{\epsilon}_v) \qquad (79)$$

and $$1 \leq C_2 \leq 2$$

Area. The minimum area of web reinforcement

$$A_v > 0.0015 b s$$

specified in the ACI Code for the static case also applies to the dynamic case.

Spacing. Limitations on maximum stirrup spacing in static design also apply to dynamic design. Thus,

$$s < \frac{d}{2} \quad \text{when,} \quad v_u < 6\phi\sqrt{f'_c}$$

$$s < \frac{d}{3} \quad \text{when,} \quad v_u > 6\phi\sqrt{f'_c}$$

Uniform spacing of stirrups is recommended in dynamic designs since the distances to the critical section and shear-compression zone change with characteristics of the load and with time under a given dynamic load. Where web reinforcement is not otherwise required, ties should be provided as they are in static designs, and the distance from the support to the point, x_t, where the amount of web reinforcement changes should be determined by:

$$x_t = \frac{L}{2} - \frac{v_c}{v_u}\left(\frac{L}{2} - d\right) \quad > \frac{L}{3} \qquad (90)$$

Plain wires 1/4 inch in diameter should be the smallest acceptable size for both ties and stirrups.

Design Procedure

Simplified Method. The general approach to design is discussed on page 39. It is stated there that if the preliminary design is not evolved by normal static design procedures, the flexural aspects of the design can be accomplished by employing dynamic design aids in the form of charts, graphs, and tabulated data. It is further stated that such aids are available in References 2, 4, and 5, and that the charts in NCEL Technical Report R-121[27] are probably the most rapid means available. The simplified method given here for the shear aspects is intended to be used in conjunction with those methods.

This method is intended for initial designs to be analyzed later by a more accurate method. When the method is used for that purpose, the capacity reduction factors recommended in the dynamic load design criteria should be used. However, if it is used for final design, the capacity reduction factors for shear should be reduced by 0.10.

It is assumed that the dynamic load is given and the flexural cross section has been designed, and the purpose of this design procedure is to determine the amount of web reinforcement required.

Maximum Shearing Force at the Support. The chart in Figure 4 may be used to determine the maximum shearing force at the support. The following values must be computed before using the chart: (1) the static shear at the support if the peak dynamic load were applied statically (w_o L/2), (2) the ratio of the effective load duration and the natural period of vibration (T/T_n), and (3) the ratio of peak load and dynamic yield resistance (w_o/r_y). The duration, T, of an effective triangular load should be used in lieu of the actual load duration. The dynamic yield resistance, r_y, is expressed as a force per unit length, as is the load, and can be determined from the maximum total dynamic resistance by:

$$r_y = \frac{R_m}{L}$$

Equations for computing R_m and T_n are given in the theory under "Flexural Resistance." See Equations 60 through 71. In using the chart, one enters at the bottom with the ratio of peak load and dynamic resistance, moves upward to the appropriate ratio of duration and natural period, and then to the left where the maximum dynamic shear factor is obtained. The maximum dynamic shear factor is the ratio of the maximum dynamic shear force at the support, V_m, and the static shear at the support if the peak dynamic load were applied statically (w_o L/2).

Maximum Shear Stress at the Critical Section. The maximum shear stress at the critical section can be estimated by:

$$v_m = \frac{V_m}{bd}\left(1. - 2\,\frac{d}{L}\right) \qquad (81)$$

In this simplified method, the required usable ultimate shear strength, v_u, is considered to be equal to the maximum shear stress at the critical section. Thus,

$$v_u = v_m \qquad (82)$$

Maximum Shear Strength Contributed by the Concrete. The maximum shear strength that can be contributed by the concrete, v_c, should be computed by the use of Equation 75 and either Equation 76 or Equation 77, depending on the reinforcement ratio, p, and letting x_c equal d.

Amount of Web Reinforcement Required. If v_c is larger than v_u, stirrups are not required, but ties should be provided at the maximum allowable spacing. If v_c is smaller than v_u, the amount of web reinforcement should be computed

with the use of Equation 78. The dynamic increase coefficient, C_2 in the equation, can be roughly estimated by assuming an elastic strain rate of 0.6 in./in./sec and using Equation 79 or the chart in Figure 17. The resulting approximate dynamic increase coefficients and dynamic yield strengths for various static yield strengths are:

Static Yield Strength, f_{vy} (psi)	Dynamic Increase Coefficient, C_2	Dynamic Yield Strength, $f_{dvy} = C_2 f_{vy}$ (psi)
30,000	1.79	54,000
40,000	1.55	62,000
50,000	1.41	70,000
60,000	1.33	80,000
75,000	1.26	94,000
100,000	1.18	118,000

Analysis Procedure

Procedure Choice. There are two kinds of economy to be considered in designing. One has to do with the cost of materials, fabrication, and erection; the other has to do with the cost of the engineering designing itself. Both kinds of economy should be considered in selecting a procedure for analyzing reinforced concrete beams.

There are three practical procedures from which to choose: (1) computer programming of the numerical integration method discussed in the theory, (2) hand calculation of the numerical integration method, and (3) the simplified method given below. The numerical integration method gives the greater economy of materials and also the most assurance of safety with regard to brittle behavior in the shear-compression zone. It is also the most economical with regard to engineering effort if a large number of beams are to be analyzed. If a computer is available and a number of beams are to be analyzed, the computer programming procedure is, by far, preferred over hand calculation of the numerical integration because the latter method is very time consuming and subject to human error. The simplified method is recommended *only* when a few beams are to be analyzed and economy of materials is outweighed by the time and cost of engineering.

Simplified Method. This simplified method gives only approximate results; therefore, the capacity reduction factor for shear should be reduced by 0.10 when this method is used.

The shear strength contributed by the concrete, v_c, should be obtained from Equations 75 through 77. The distance to the critical section, x_c, can be approximated by setting it equal to the effective depth, d, and values of the natural period of vibration, T_n, can be obtained by the use of Equations 60 through 70.

The usable ultimate shear strength, v_u, then should be computed as follows:

For $A_v < 0.0015bs$,

$$v_u = v_c \tag{83}$$

For $A_v \geq 0.0015bs$,

$$v_u = v_c + \phi C_2 \frac{A_v f_w}{bs} \quad \leq 8\phi\sqrt{f'_c} \tag{84}$$

Values of the dynamic increase coefficient, C_2, can be approximated as indicated on page 141 in the simplified design procedure.

The maximum allowable dynamic shearing force at the support, V_{su}, should be determined next by using Equation 39.

Then the maximum dynamic shearing force at the support, V_m, should be obtained from the chart in Figure 4. A detailed explanation of how to use the chart is given on page 140 in the simplified design procedure.

Finally, the beam is safe in shear if

$$\frac{V_m}{V_{su}} \leq 1$$

ACKNOWLEDGMENTS

William A. Keenan of this Laboratory, author of Part I,[14] performed the modal analysis, developed the chart for determining the maximum shear force, conducted the tests designated Series A through D, and provided guidance during many phases of the work. Dr. Chester P. Siess, Professor of Civil Engineering at the University of Illinois, also provided guidance in development of experiment plans.

Several engineers of this Laboratory participated in the work. Walter L. Cowell, W. Dean Atkins, and Lawrence F. Kahn conducted the static and dynamic testing of materials. The late David S. Fuss derived the theory for predicting dynamic tensile stress rate in diagonal tension and conducted the tests designated Series H and Series L. Dr. Salah B. Nosseir was consulted about the prediction of spring constants, and Dr. William J. Nordell was consulted about plastic hinging in beams.

For the Series F tests, great care and resourcefulness were applied by R. W. Ross, F. H. Billingsley, and L. B. Foster to the fabrication of test specimens and execution of test procedures. All instruments were selected and calibrated, and measurements recorded, by F. E. Nelson.

The theoretical equations and computer calculations were checked by Major Dipl.-Ing. Josef Rottgerkamp, Major Engineer Staff, Army of the Federal Republic of Germany, who wes assigned to the Naval Civil Engineering Laboratory during part of the period of this report.

Appendix A

STRENGTH PROPERTIES OF MATERIALS

INTRODUCTION

To study the strength and behavior of structural elements, it is necessary to determine the strength and behavior of the structural materials from which the elements are made. The objective of the work reported in this appendix was to determine both the static and dynamic strengths of the materials used in the 12 reinforced concrete beams which have been designated the F Series. Strength properties are reported elsewhere[14,23] for the D and E Series.

CONCRETE

Mix

The concrete was made from Type I portland cement, 3/4-inch maximum size San Gabriel aggregate, and San Gabriel sand having a fineness modulus of 2.82. Two mixes were used. The mix proportions for the higher strength concrete were 1.00 (cement) : 2.98 (coarse aggregate) : 2.71 (fine aggregate), by weight, with a water-cement ratio of 0.57 (by weight) or 6.5 gallons per sack. A slump of 3 inches was specified. The mix proportions for the lower strength concrete were 1.00:3.82:3.66 (by weight), with a water-cement ratio of 0.71 (by weight) or 7.98 gallons per sack. A slump of 2 inches was specified.

Static Tests

At the time each beam was cast, six standard 6-inch-diameter by 12-inch-long cylinders were cast from the same batch of concrete. The cylinders were cured under wet burlap along with the beam until 2 days before testing. Three cylinders were used to determine the concrete compressive strength, and three the tensile splitting strength. The results are given in Table A-1. The average static compressive strength at about 28 days was 5,770 psi for the higher strength and 3,480 psi for the lower strength concrete. The average tensile splitting strength was 547 psi for the higher strength and 426 psi for the lower strength concrete.

Table A-1. Static Compressive and Tensile Strength of Concrete

Beam No.	Slump (in.)	Age (days)	Compressive Strength, f'_c (psi)				Tensile Strength, f'_t (psi)			
			Cylinder 1	Cylinder 2	Cylinder 3	Average	Cylinder 4	Cylinder 5	Cylinder 6	Average
Higher Strength Concrete										
WF1	4.5	28	6,210	6,200	6,230	6,210	560	540	530	543
WF2	2.5	36	5,860	5,830	6,330	6,010	550	590	580	573
WF3	2.5	29	6,050	5,720	5,770	5,850	510	530	510	517
WF4	2.5	35	6,320	6,260	6,190	6,260	540	510	610	553
WF5	2.2	29	5,660	5,800	5,660	5,710	570	520	530	540
WF6	2.5	29	5,500	5,430	5,580	5,500	550	550	520	540
WF7	3.0	31	5,610	5,680	5,320	5,540	570	570	600	580
WF8	2.5	30	5,110	5,020	5,060	5,060	550	540	500	530
Avg						5,770				547
Lower Strength Concrete										
WF9	3.5	30	3,020	3,130	3,060	3,070	410	430	430	423
WF10	2.5	31	3,690	3,550	3 180	3,470	420	410	430	420
WF11	2.0	29	3,830	3,750	3,750	3,780	420	490	410	440
WF12	2.5	31	3,590	3,610	3,570	3,590	410	440	410	420
Avg						3,480				426

Dynamic Tests

Seventeen concrete cylinders were cast using the lower strength mix described above. All cylinders were 4 inches in diameter, 8 inches long, and cast from one batch of concrete. The cylinders were tested under various loading rates in accordance with the procedures outlined in ASTM Specification C496-62T, "Splitting Tensile Strength of Moulded Concrete Cylinders." The rate of loading was slow (static) on five cylinders and rapid (dynamic) on 12 cylinders.

The results of the tests are listed in Table A-2 and plotted in Figure A-1. The average static tensile splitting strength was 426 psi, identical to the results of the static tests described above and listed in Table A-1. The average value was used in determining the dynamic increase in tensile splitting strength. The equation in the table and figure was developed by the author from data reported by Cowell[24] and by Lundeen and Saucier.[17] With the exception of two data points, agreement is very good between the experimental data and data computed from the equation.

Cowell[24] performed static and dynamic, tensile splitting, and compressive tests on concrete cured 28 and 49 days. He used the same coarse and fine aggregate as used in the mixes described above, except for Type II portland cement instead of Type I. It is believed that there is no significant difference in the strength properties of Type I and Type II. The static compressive strengths at 28 days for the two mixes used by Cowell were 3,900 psi and 7,420 psi; the tensile strengths were 515 psi and 710 psi.

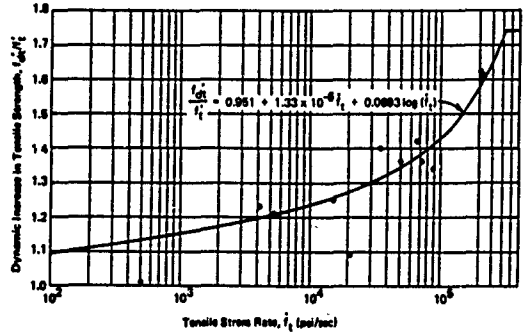

Figure A-1. Results of dynamic tensile splitting tests on concrete with static tensile strength of 426 psi.

Table A-2. Results of Dynamic Tensile Splitting Tests

Static Tests			Dynamic Tests				
Cylinder No.	Tensile Stress Rate, $\dot{f}_t$ (psi/sec)	Tensile Splitting Strength, f'_t (psi)	Cylinder No.	Tensile Stress Rate, $\dot{f}_t$ (psi/sec)	Tensile Splitting Strength, f'_{dt} (psi)	Dynamic Increase in Tensile Splitting Strength, f'_{dt}/f'_t[a]	
						Experiment	Theory[b]
S1	0.4	420	D1	87,800	570	1.34	1.41
S2	0.4	420	D2	71,400	580	1.38	1.38
S3	0.4	415	D3	66,300	600	1.41	1.37
S4	0.6	460	D4	49,200	560	1.36	1.34
S5	0.4	425	D5	34,400	600	1.40	1.31
Avg		426	D6	20,500	480	1.08	1.28
			D7	15,300	530	1.25	1.26
			D8	500	430	1.01	1.14
			D9	4,100	520	1.22	1.21
			D10	5,300	520	1.22	1.22
			D11	210,200	690	1.60	1.60
			D12	200,200	690	1.62	1.58

[a] f'_t = 426 psi (average value from the five static tests).

[b] $f'_{dt}/f'_t = 0.961 + 1.33 \times 10^{-6}\dot{f}_t + 0.0883 \log(\dot{f}_t)$

LONGITUDINAL REINFORCING STEEL

Material

The longitudinal reinforcing steel in each beam consisted of two no. 9 bars in tension and two no. 7 bars in compression. All bars were from the same lot and satisfied the strength requirements of ASTM Specification A432 and the deformation requirements of ASTM Specification A305-56T.

Static Tests

Standard tension tests to determine the upper yield point were made on coupons from one tension and one compression bar from each of the beams, except for beam WF1 where no tension bars were tested. The results

are given in Table A-3. The average upper yield stress was 69,000 psi for no. 9 bars and 70,000 psi for no. 7 bars. Three of the no. 9 bars and three of the no. 7 bars were tested to rupture and complete stress–strain relationships were obtained. The ultimate strengths of those bars are listed in Table A-4. The average ultimate strength was 103,600 psi for no. 9 bars and 100,700 psi for no. 7 bars. The stress–strain plot for tension bar no. 22 is shown in Figure A-2. The stress–strain relationships for all specimens tested had the following characteristics:

1. Linear elastic region
2. Poorly defined proportional limit at about 60,000 psi
3. Well-defined yield point at about 69,000 psi
4. No definition between upper and lower yield points
5. Secant modulus of elasticity about 29,000,000 psi
6. Long linear region before strain hardening at about 0.035 in./in. of strain
7. Ultimate strain about 0.13 in./in.

Dynamic Tests

Tests were performed to determine the dynamic yield strength of no. 9 bars and to relate increase in upper yield strength to strain rate. The bars were different from the ones in the beams in that they came from a different lot of steel and they were machined smooth. Details regarding loading equipment, instrumentation, and procedure are given in Appendix A of Reference 14. Thirteen specimens were tested under various loading rates. The rate of loading was slow (static) on five specimens and rapid (dynamic) on eight specimens.

The results of the tests are listed in Table A-5 and plotted in Figure A-3. The average static upper yield stress was 81,500 psi, considerably higher than for the coupons in the static tests described above and listed in Table A-3. The average value was used in determining the dynamic increase in upper yield strength. The equation in the table and figure was developed by the author from data reported by Cowell,[22] Keenan,[14] and the author[23] from dynamic tests on various steels used as longitudinal steel and stirrups. The line in the figure is the locus of points obtained from the equation using a static upper yield stress of 81,500 psi. Values of the dynamic increase, σ_{dy}/σ_y, computed from the equation are slightly conservative with respect to all data points except one which falls on the line in the figure. Agreement between the slopes of the line and the data points is excellent.

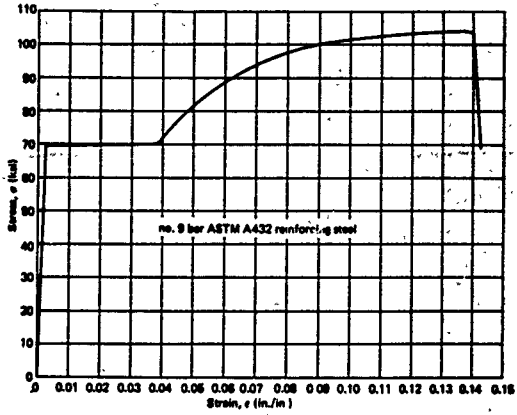

Figure A-2. Typical stress–strain relationship for longitudinal reinforcing steel.

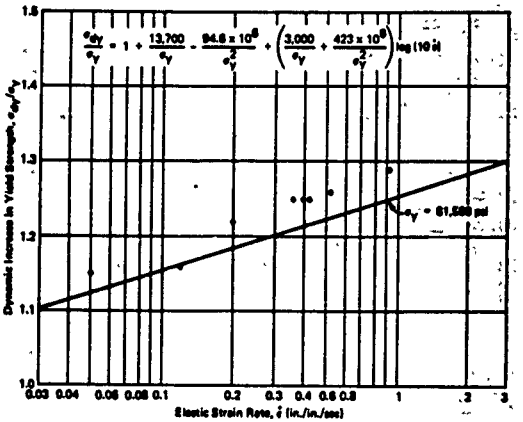

Figure A-3. Results of dynamic tests on longitudinal reinforcing steel with static upper yield strength of 81,500 psi.

Table A-3. Static Yield Strength of Longitudinal Reinforcing Bars

Tension Steel No. 9 Bars			Compression Steel No. 7 Bars		
Bar No.	Beam in Which Used	Upper Yield Stress (ksi)	Bar No.	Beam in Which Used	Upper Yield Stress (ksi)
2	WF1	[a]	32[b]	WF1	68 9
4[b]	WF2	66.5[c]	34[b]	WF2	70.1
6[b]	WF3	67.0	36[b]	WF3	68.1[c]
8	WF4	69 4	38	WF4	69.0
10	WF5	69 2	40	WF5	69 0
12	WF6	69.7	42	WF6	71.2
14	WF7	69.2	44	WF7	70.5
16	WF8	69.5	46	WF8	69 2
18	WF9	69.3	48	WF9	69 4
20	WF10	67.9	50	WF10	69.7
22[b]	WF11	69.5	52	WF11	69.0
24	WF12	71.9[d]	54	WF12	75.9[d]
Avg		69.0	Avg		70 0

[a] Not tested.

[b] Tested to rupture and listed in Table A-4.

[c] Lowest value.

[d] Highest value.

Table A-4. Static Ultimate Strength of Longitudinal Reinforcing Bars

Tension Steel No. 9 Bars			Compression Steel No. 7 Bars		
Bar No.	Beam in Which Used	Ultimate Stress (ksi)	Bar No.	Beam in Which Used	Ultimate Stress (ksi)
4	WF2	102.5[a]	32	WF1	100.7
6	WF3	104 0	34	WF2	101.7[b]
22	WF11	104 2[b]	36	WF3	99 6[a]
Avg		103.6	Avg		100.7

[a] Lowest value.

[b] Highest value.

Table A-5. Results of Dynamic Tests on Longitudinal Reinforcing Steel

Static Tests		Dynamic Tests				
Specimen No.	Upper Yield Stress, σ_y (ksi)	Specimen No.	Elastic Strain Rate $\dot{\epsilon}$ (in./in./sec)	Upper Yield Stress, σ_{dy} (ksi)	Dynamic Increase in Upper Yield Stress, σ_{dy}/σ_y[a]	
					Experiment	Theory[b]
S1	82 5	D1	0.05	93.5	1.15	1.12
S2	81 0	D2	0 12	94 5	1.16	1.16
S3	82.0	D3	0 20	99.0	1.22	1.18
S4	80 5	D4	0 36	102 0	1.25	1.21
S5	81 5	D5	0.40	102.0	1.25	1.21
Avg	81.5	D6	0.41	102.0	1.25	1.22
		D7	0 46	102.5	1.26	1.22
		D8	0.86	105 0	1.29	1.25

[a] σ_y = 81,500 psi (average value from the five static tests).

[b] $$\frac{\sigma_{dy}}{\sigma_y} = 1 + \frac{13{,}700}{\sigma_y} - \frac{94\,9 \times 10^6}{\sigma_y^2} + \left(\frac{3{,}000}{\sigma_y} + \frac{423 \times 10^6}{\sigma_y^2}\right) \log (10\,\dot{\epsilon})$$

STIRRUPS

Material

The stirrups were made from 6-gage annealed plain wire. The wire was received in 6-foot straight lengths.

Static Tests

Four samples of the wire were tested to determine the static strength properties. The specimens were 10 inches long and had one SR-4 foil strain gage (EA-05-500BH) affixed at midlength. Load was applied and measured with a tension testing machine equipped with a recorder, and stress values were computed from the load measured during the test and the diameter of the specimen measured prior to the test. Strain was measured from zero to approximately 0.4% by the single strain gage. Larger strain values were obtained by measuring the elongation of a 5-inch gage length with a scale containing 50 parts to the inch.

The results of the tests are listed in Table A-6 and plotted in Figures A-4 and A-5 The stress–strain relationships for all specimens had the following characteristics:

1. Linear elastic region
2. Well-defined proportional limit at about 23,000 psi
3. Tangent modulus of elasticity about 29,200,000 psi
4. Undefined yield point at about 30,000 psi
5. Very short region between yielding and strain hardening
6. Ultimate strain about 0.20 in /in.

The scatter of data between tests was extremely small; therefore, average values from the four tests were used to plot the stress–strain relationship shown in Figure A-5. The stress–strain relationship of specimen no. 2 from zero strain to 0.32% strain is plotted in Figure A-4 to show the well-defined proportional limit and the undefined, or very poorly defined, yield point. Predictions of beam behavior were computed using the 0.1% offset stress rather than the customary 0.2% offset yield stress. Both are listed in Table A-6. An idealized straight-line stress–strain relationship, shown in the figure, was constructed using the average yield stress (30,000 psi) at 0.1% offset and the average tangent modulus of elasticity (29,200,000 psi).

Table A-6. Static Strength Properties of 6-Gage Wire

Specimen No.	Diameter (in.)	Tangent Modulus of Elasticity (ksi x 10^3)	Proportional Limit (ksi)	Yield Stress (ksi)		Ultimate Strength (ksi)
				Offset 0.1%	Offset 0.2%	
1	0.1897	30.2	24.0	30.6	31.5	44.5
2	0.1903	29.1	22.5	30.0	30 8	45.0
3	0.1900	29.0	22.5	28.5	29.4	44.6
4	0.1900	28.4	22.5	30 8	31.9	45.0
Avg	0.1900	29 2	23.0	30.0	30 9	44 8

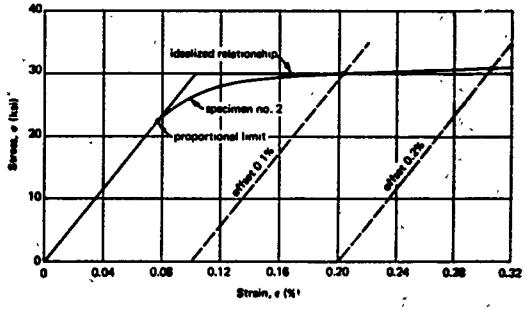

Figure A-4. Stress–strain relationship for 6-gage wire from zero strain to 0.32% strain.

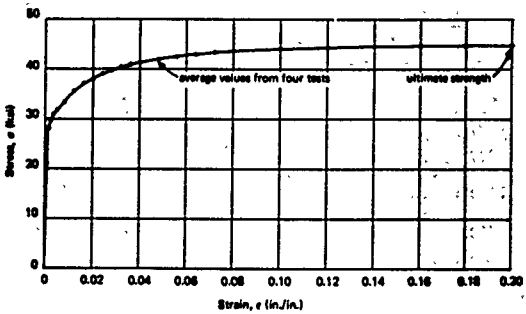

Figure A 5. Stress–strain relationship for 6-gage wire from zero stress to ultimate stress.

Dynamic Tests

Seventeen specimens of the wire, each 10 inches long, were strained in tension with the NCEL dynamic materials testing machine[21] and continuous measurements recorded of tensile strain and force in each specimen. The strain was measured with one SR-4 foil resistance strain gage (EA-05-500BH) placed midway between the ends of the specimen. Force was measured with an NCEL strain gage-type tension link.

The results are listed in Table A-7 and plotted in Figure A-6. The average static yield stress (30,000 psi) from 17 static tests and defined by a 0.1% offset from the tangent modulus of elasticity (as given in Table A-6 and Figure A-4) was used to compute the dynamic increase in yield strength, σ_{dy}/σ_y. The equation in the table and figure is the same equation that was used to predict the dynamic increase in the yield strength of the longitudinal reinforcing steel discussed previously. The line in the figure is the locus of points obtained from the equation using a static yield strength of 30,000 psi. Agreement between the data points and the values computed from the equation is good. Three points are high, three are low, and eleven fall on, or nearly on, the line. The limit $(\sigma_{dy}/\sigma_y) < 2$ is also shown in the figure.

The material had well-defined upper and lower yield points under dynamic load. It was found that the percent dynamic increases in lower yield stress and ultimate yield stress were considerably less than for the upper yield stress. For instance, at an elastic strain rate of 1.0 in./in /sec, the upper yield stress increased 92%; at an inelastic strain rate of 1.0 in./in /sec, the lower yield stress increased 60%; and at an ultimate strain rate of 1.0 in./in./sec, the ultimate stress increased only 19%.

BOND TESTS

Pull-out tests (related to this work) to study the influence of normal pressure on bond between concrete and reinforcing steel were performed by Untrauer, Harris, and Henry[20] at the Iowa Engineering Experiment Station, Iowa State University under NCEL Contract NBy-32222.

Table A-7. Results of Dynamic Tests on 6-Gage Wire

Specimen No.	Diameter (in.)	Elastic Strain Rate, $\dot{\epsilon}$ (in./in./sec)	Upper Yield Stress, σ_{dy} (ksi)	Dynamic Increase in Upper Yield Stress, σ_{dy}/σ_y[a]	
				Experiment	Theory[b]
1	0.190	0.17	44.5	1.48	1.48
2	0.191	0.20	45.5	1.52	1.52
3	0.191	0.21	45.5	1.52	1.54
4	0.190	0.41	53.0	1.77	1.70
5	0.191	0.48	54.0	1.80	1.74
6	0.190	0.51	54.6	1.82	1.76
7	0.191	0.52	53.0	1.77	1.76
8	0.191	0.71	54.5	1.82	1.84
9	0.191	0.92	57.0	1.90	1.90
10	0.191	0.95	53.5	1.78	1.91
11	0.191	0.98	55.0	1.83	1.92
12	0.191	1.03	58.0	1.93	1.93
13	0.191	1.26	59.5	1.98	1.98
14	0.190	1.48	61.5	2.05	2.02[d]
15	0.191	1.5[c]	61.0	2.03	2.02[d]
16	0.191	1.5[c]	61.5	2.05	2.02[d]
17	0.191	1.82	57.5	1.92	2.07[d]

[a] σ_y = 30,000 psi which is the average static yield stress at 0.1% offset.

[b] $\frac{\sigma_{dy}}{\sigma_y} = 1 + \frac{13{,}700}{\sigma_y} - \frac{94.9 \times 10^6}{\sigma_y^2} + \left(\frac{3{,}000}{\sigma_y} + \frac{423 \times 10^6}{\sigma_y^2}\right) \log (10\dot{\epsilon})$

[c] Estimated strain rate.

[d] In the body of this report, the limit $1 \leq \sigma_{dy}/\sigma_y \leq 2$ is recommended.

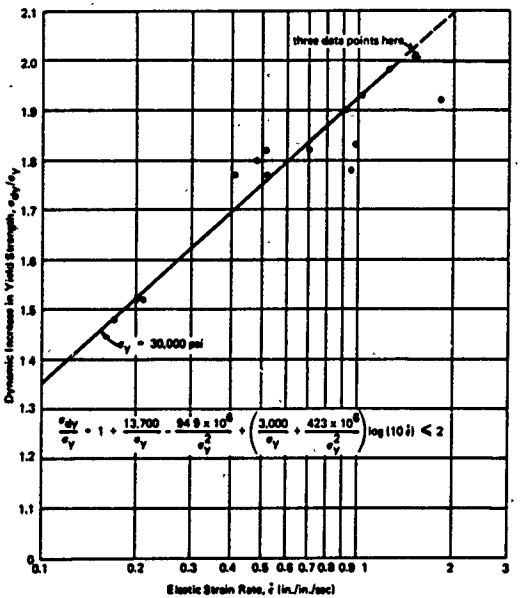

Figure A-6. Results of dynamic tests on 6-gage wire with static yield strength of 30,000 psi.

Appendix B

MOMENT OF INERTIA AND SPRING CONSTANT

INTRODUCTION

The spring constant of an elastic structural element is defined as the quotient of the resistance and the deflection, and the resistance is equal to the load under static loading.

$$k = \frac{R}{y}$$

where k = spring constant (lb/in.)

R = resistance (lb)

y = deflection (in.)

This quotient is related to stiffness and length when applied to bending in beams. The spring constant at midspan of a prismatic beam on simple supports under uniformly distributed loading may be expressed as

$$k = \frac{384\,E\,I}{5\,L^3}$$

where $E\,I$ = stiffness (lb-in.^{2})

E = modulus of elasticity (psi)

I = moment of inertia (in.^{4})

L = span length (in.)

Actually, the spring constant of a reinforced concrete beam does not have a constant value as the deflection of the beam is increased. The value of the spring constant changes with changes in moment of inertia as flexural cracks form and inelastic hinging takes place.

Simplifying assumptions are made to obtain a constant value which best approximates the spring constant over the full range of deflections within the elastic region of response. The primary assumption used in a method presented in the Air Force Design Manual,[4] and other references, is that the moment of inertia is the average of the moments of inertia for the cracked and uncracked sections.

$$I = \frac{I_g + I_c}{2}$$

where I = moment of inertia (in.^{4})

I_g = gross moment of inertia (in.^{4})

I_c = moment of inertia of a cracked section (in.^{4})

The assumption is considered poor because the cracked section influences the spring constant more than the gross section in beams deflected nearly to or beyond the yield deflection. The resulting spring constant predictions are too high. The amount of error also changes with length–depth ratio because of larger shear deformations and fewer flexural cracks associated with lower ratios.

THEORY

Nossair's method[h] is to compute the spring constant from the moment of inertia for the cracked section and then adjust this value using a formula containing the shear span–depth ratio and coefficients based on his measurements. Thus,

$$\frac{k}{k_c} = 0.26\left(\frac{a}{d}\right) - 0.023\left(\frac{a}{d}\right)^2$$

where k = spring constant (lb/in.)

k_c = spring constant of a cracked section (lb/in.)

a = shear span (in.)

d = effective depth of the beam (in.)

The tests were made on simply supported beams under static and dynamic concentrated loads, and the equation was obtained by data point fitting between the limits: $2 < a/d < 6$.

In applying the method to beams under uniformly distributed loads, it is assumed that

$$\frac{a}{d} = \frac{1}{2}\left(\frac{L}{d}\right)$$

$$k_c = \frac{384 E I_c}{5 L^3}$$

Thus,

$$\frac{k}{k_c} = 0.13\left(\frac{L}{d}\right) - 0.0058\left(\frac{L}{d}\right)^2$$

EXPERIMENT

Purpose

In the following computations, Nosseir's method, the Air Force Design Manual method, and a modified version of the Air Force Design Manual method are used to predict the spring constant of the static uniformly loaded beams of test Series E. The tests are reported in Part II,[23] which gives a detailed description, and in Part III, the main part of this report, which gives a summary only. The solutions obtained from each of the three methods are compared with the idealized spring constant obtained from measurements in tests WE10 and WE11.

Specimens

The test specimens had the following dimensions and strength properties:

Parameter	Value
Span length, L	144 in.
Beam width, b	7.75 in.
Effective depth of the beam, d	12.94 in.
Total depth of the beam, h	15.0 in.
Depth to compression steel, d'	1.5 in.
Area of tension steel, A_s	2.00 $in.^2$
Area of compression steel, A_s'	1.20 $in.^2$
28-day compressive strength of concrete, f_c'	3,660 psi
Yield strength of steel, f_y	67,600 psi
Modulus of elasticity of steel, E_s	29,000,000 psi
Yield strain of concrete, ϵ_{cy}	0.003 in./in.
Density of concrete, ρ	145 lb/ft^3

Tests

The resistance–deflection relationships for WE10 and WE11 were plotted on a common graph. A two-straight-line idealized diagram was constructed through the data Finally, the spring constant, k, was computed from values of resistance, R_m, and deflection, y_y, at the intersection of the straight lines.

$$R_m = wL = (624 \text{ lb/in.})(144 \text{ in.}) = 89{,}900 \text{ lb}$$

$$k = \frac{R_m}{y_y} = \frac{89{,}900 \text{ lb}}{0.92 \text{ in.}} = 97{,}700 \text{ lb/in.}$$

Predictions

Slenderness.

$$\frac{L}{d} = 11.1$$

Modulus of Elasticity.

$$E = E_c = \rho^{1.5} 33 \sqrt{f'_c} = 3{,}460{,}000 \text{ psi}$$

$$n = \frac{E_s}{E_c} = 8.38$$

Neutral Axis by Ultimate Strength Design Method. The ACI[13] requirements for rectangular beams with compression reinforcement can be found in Section 1602 of the Code. By the use of the equations in that section, it was predicted that the compression steel would be elastic at the time of flexural yielding; therefore, a general analysis was made on the basis of the assumptions given in Section 1503. The stress block depth is

$$a = \frac{(A_s f_y - A'_s E_s \epsilon_{cy}) + \sqrt{(A_s f_y - A'_s E_s \epsilon_{cy})^2 + 3.4 f'_c b A'_s E_s \epsilon_{cy} k_1 d'}}{1.7 f'_c b} = 3.08 \text{ in.}$$

Therefore, the depth to the neutral axis is

$$c = \frac{a}{k_1} = \frac{3.08 \text{ in.}}{0.85} = 3.62 \text{ in.}$$

Neutral Axis by Transformed Section Method. By summing statical moments about the neutral axis of a transformed section,

$$\frac{bc^2}{2} + (2n - 1)A_s'(c - d') = nA_s(d - c)$$

With the appropriate substitutions made, only one root of the equation is positive. Thus,

$$c = 4.57 \text{ in.}$$

Moment of Inertia by Ultimate Strength Design Method.

$$I_c = \frac{bc^3}{3} + (n - 1)A_s'(c - d')^2 + nA_s(d - c)^2 = 1{,}620 \text{ in.}^4$$

Moment of Inertia by Transformed Section Method.

$$I_c = \frac{bc^3}{3} + (2n - 1)A_s'(c - d')^2 + nA_s(d - c)^2 = 1{,}601 \text{ in.}^4$$

Gross Moment of Inertia. If it is assumed that no flexural cracks exist prior to loading, the gross moment of inertia, I_g, should be computed from the total depth of the beam. Thus,

$$I_g = \frac{bh^3}{12} = \frac{7.75(15)^3}{12} = 2{,}180 \text{ in.}^4$$

On the other hand, if it is assumed that flexural cracks exist up to the level of the tension steel prior to loading, the gross moment of inertia should be computed from the effective depth of the beam. Thus,

$$I_g = \frac{bd^3}{12} = \frac{7.75(12.94)^3}{12} = 1{,}403 \text{ in.}^4$$

Spring Constant by Nosseir's Method. In accordance with Nosseir's method,

$$k_c = \frac{384\,E\,I_c}{5\,L^3} = 89.2\,I_c$$

$$k = 89.2\,I_c\left[0.13\left(\frac{L}{d}\right) - 0.0058\left(\frac{L}{d}\right)^2\right] = 64.9\,I_c$$

Using ultimate strength design assumptions,

$$k = 64.9(1{,}620) = 105{,}000 \text{ lb/in.}$$

Using transformed section assumptions,

$$k = 64.9(1{,}601) = 104{,}000 \text{ lb/in.}$$

The difference between solutions based on ultimate strength and transformed section assumptions is only about 1%.

Spring Constant by Air Force Design Manual Method. Using ultimate strength design assumptions and a gross moment of inertia based on the total depth of the beam,

$$I = \frac{I_g + I_c}{2} = \frac{2{,}180 + 1{,}620}{2} = 1{,}900 \text{ in.}^4$$

$$k = \frac{384\,E\,I}{5\,L^3} = 89.2\,I = 169{,}000 \text{ lb/in.}$$

The method can be modified by assuming flexural cracking to the level of the tension stuel. In this case, the effective depth is used to compute the gross moment of inertia. Then the spring constant can be calculated as follows:

$$I = \frac{I_g + I_c}{2} = \frac{1{,}403 + 1{,}620}{2} = 1{,}512 \text{ in.}^4$$

$$k = 89.2\,I = 135{,}000 \text{ lb/in.}$$

Results

The spring constant determined from tests was 98 kips/in., and the predictions were:

Method	Spring Constant			
	By Ultimate Strength		By Transformed Section	
	Value (kips/in)	Difference (%)	Value (kips/in.)	Difference (%)
Nosseir	105	7	104	6
Air Force Design Manual (modified method)	135	38	134	37
Air Force Design Manual	169	73	168	72

The accuracy of the test data is about 6%, and computations were carried out with an accuracy of about 2%.

All predictions were high, but the ones obtained from Nosseir's method were near to or within the accuracy of the test data. Nosseir's method produced the best agreement between experiment and theory, and the unmodified Air Force Design Manual method produced the worst. Use of the transformed section assumptions in computing the moment of inertia of a cracked section produced better agreement than use of ultimate strength design assumptions, but the difference in final results due to choice of assumptions was only about 1%.

CONCLUSIONS

1. Of the three methods tested, Nosseir's method is the most accurate.
2. The transformed section assumptions and ultimate strength design assumptions produce predictions with about the same accuracy.

RECOMMENDATIONS

1. Nosseir's method is recommended because it is more accurate than the other methods, and it is just as easy to apply.

2. Ultimate strength assumptions in determining moment of inertia are recommended for the sake of consistency with other parts of the analysis discussed in the main body of this report.

Appendix C

INELASTIC HINGING

INTRODUCTION

The purpose of this appendix is to present the derivation of equations for evaluating the inelastic hinge in order to determine the midspan deflection corresponding to flexural failure in reinforced concrete beams. The equations derived here apply only to slender, doubly reinforced, rectangular, prismatic concrete beams on simple supports and subjected to uniformly distributed static or dynamic loading.

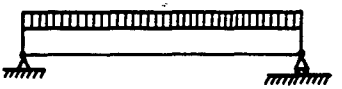

Conditions of Loading and Constraint

The theory is based on the presumption that, for the sake of being consistent in all designs and ease in performing dynamic analysis, all changes in beam behavior, including failures, shall be defined in quantitative terms as values of strain in the various materials. This approach is essential in comparing the shear and flexure capacities of dynamically loaded beams and in comparing the static and dynamic cases. For instance, a concrete strain (ε_{cu} = 0.006 in./in.) at the remote fiber is used to define flexural failure as well as certain types of shear-compression failure. Some minor compromises are made in the elastic range where stress criteria are used and easily converted to strain.

Assumptions regarding distribution of stress and strain outside the hinged length are discussed in the Theory in the main part of the report under Flexural Resistance. They generally follow those of the ACI for ultimate strength design procedure.

Assumptions regarding distribution of stress and strain over the section at the center of the hinged length at the time of flexural failure are shown graphically in the diagram below. The symbols in the diagrams are defined in the derivations that follow.

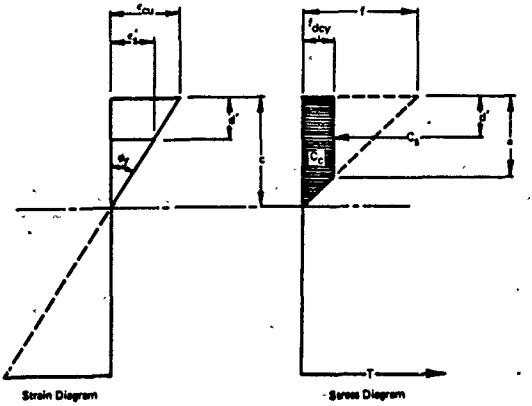

SECTION AT CENTER OF HINGE (MIDSPAN)

Neutral Axis

Flexural failure has been defined in terms of the ultimate strain of concrete, ϵ_{cu}, as

$$\epsilon_{cu} \equiv 0.006 \text{ in./in.}$$

Therefore, at the time of failure and at the center of the hinged length, the strain in the compression steel, ϵ'_s, is

$$\epsilon'_s = 0.006\left(1 - \frac{d'}{c}\right)$$

The fictitious stress, f, is defined here as

$$f \equiv \epsilon_{cu} E_c > f_{dcy}$$

Therefore, at the time of failure, the fictitious stress is

$$f = 0.006\,E_c$$

Furthermore, the dynamic yield strength of concrete, f_{dcy}, has been defined as

$$f_{dcy} = 0.85\,f'_{dc}$$

and, therefore, the stress block proportion, k_1, at the time of failure can be computed as

$$k_1 = \frac{a}{c} = 1 - \frac{f_{dcy}}{f} = 1 - 141.67\,\frac{f'_{dc}}{E_c} \qquad \text{(C-1)}$$

Thus, the stress block dimension, a, can be expressed in terms of the distance to the neutral axis, c, as

$$a = k_1 c = \left(1 - 141.67\,\frac{f'_{dc}}{E_c}\right)c \qquad \text{(C-2)}$$

If underreinforcing is maintained, the longitudinal tension steel is yielded after yielding of the beam, and the total tension force, T, can be expressed in terms of the dynamic yield strength as

$$T = A_s f_{dy} \qquad \text{(C-3)}$$

The compression force provided by the concrete, C_c, is

$$C_c = b f_{dcy}\left(\frac{a + c}{2}\right) = 0.425\,b\,c\,f'_{dc}(k_1 + 1) \qquad \text{(C-4)}$$

The compression force provided by the compression steel, C_s, is

$$C_s = A'_s f'_s < A'_s f'_{dy} \qquad \text{(C-5)}$$

From the above equation, it can be seen that two solutions are possible depending on whether or not the compression steel is yielded.

Assume that the compression steel is yielded. Then,

$$\epsilon_s' > \frac{f_{dy}'}{E_s}$$

Thus,

$$0.006\left(1 - \frac{d'}{c}\right) > \frac{f_{dy}'}{E_s}$$

Solving this inequality for c, the limit on c for the yielded condition can be found as

$$c \leq \frac{d'}{1 - \frac{f_{dy}'}{0.006\,E_s}} \qquad \text{(C-6)}$$

By equilibrium of longitudinal forces,

$$T = C_c + C_s \qquad \text{(C-7)}$$

Assuming the compression steel to be yielded and substituting Equations C-3, C-4, and C-5 into Equation C-7,

$$A_s f_{dy} = 0.425\,b\,c\,f_{dc}'(k_1 + 1) + A_s' f_{dy}'$$

Thus, the distance to the neutral axis is

$$c = \frac{A_s f_{dy} - A_s' f_{dy}'}{0.425\,b\,f_{dc}'(k_1 + 1)} \qquad \text{(C-8)}$$

if the value of c is within the limit specified in Equation C-6.

If the value of c obtained from Equation C-8 does not satisfy Equation C-6, the compression steel is not yielded at the time of failure, and the compression force provided by the steel, C_s, is computed as

$$C_s = A_s' f_s' = A_s' E_s \epsilon_s' = 0.006\,A_s' E_s\left(1 - \frac{d'}{c}\right) \qquad \text{(C-9)}$$

Now, substituting Equations C-3, C-4, and C-9 into Equation C-7,

$$A_s f_{dy} = 0.425 b c f'_{dc}(k_1 + 1) + 0.006 A'_s E_s \left(1 - \frac{d'}{c}\right)$$

By multiplying each term by c and simplifying,

$$0.425 b f'_{dc}(k_1 + 1)c^2 + (0.006 A'_s E_s - A_s f_{dy})c - 0.006 d' A'_s E_s = 0$$

Thus, the distance to the neutral axis is

$$c = \frac{(A_s f_{dy} - 0.006 A'_s E_s) \pm \sqrt{(A_s f_{dy} - 0.006 A'_s E_s)^2 + 0.0102 b d' A'_s E_s f'_{dc}(k_1 + 1)}}{0.85 b f'_{dc}(k_1 + 1)} \quad \text{(C-10)}$$

If the compression steel is not yielded at the time of failure, Equation C-10 should have one positive root inside the dimensions of the beam and outside the limit given by Equation C-6.

It should be remembered that the value for k_1 in Equations C-8 and C-10 is for the inelastic regime and should be obtained from Equation C-1. It is not the value given by the ACI Code equation, which is for the upper bound of the elastic regime.

Curvature

The curvature is equal to the angle of rotation at the neutral axis, and it is essentially equal to the tangent of the angle for small values of the angle. The curvature expressed as a tangent is the ratio of the elongation at the remote fiber and the distance from the remote fiber to the neutral axis. The units are in./in. or radians. The unit curvature, then, is the ratio of the strain at the remote fiber and the distance from the remote fiber to the neutral axis. The units are in./in./in. or radians/in. The unit curvature at the center of the hinge, ϕ_f, at the time of failure is

$$\phi_f = \frac{\epsilon_{cu}}{c} = \frac{0.006}{c} \text{ rad/in.} \quad \text{(C-11)}$$

Moment

The dynamic resisting moment at the center of the inelastic hinge at the time of failure, M_f, can be obtained by summing the moments from the tension steel, compression steel, and concrete about the neutral axis. By summing moments,

$$M_f = T(d - c) + C_s(c - d') + \frac{bc^2}{6} f_{dcy}(2 + 2k_1 - k_1^2) \qquad \text{(C-12)}$$

By substituting Equations C-1 and C-3 into Equation C-12, the moment can be expressed in a more convenient form as

$$M_f = A_s f_{dy}(d - c) + C_s(c - d') + 0.425 b c^2 f'_{dc}\left[1 - 3.97\left(\frac{f'_{dc}}{E_c}\right)^2\right] \qquad \text{(C-13)}$$

Values of C_s are obtained from Equations C-5 and/or C-9, depending on whether or not the compression steel is yielded at the time of failure.

SECTION AT EDGE OF HINGE

Moment

The edge of the hinged length is at the section where the ultimate design, dynamic resisting moment, M_{du}, exists. The moment M_{du} is discussed in the Theory in the main part of the report under Flexural Resistance. Formulas for computing M_{du} are given in Equations 64 and 65 of that discussion.

Neutral Axis

The distance from the remote fiber to the neutral axis, c, at the section where M_{du} exists is also discussed in the Theory under Flexural Resistance. Formulas for computing c are given in Equations 60 and 66 in the main part of the report.

When doing calculations, care must be taken to prevent confusion with regards to values of k_1 *and* c *at the center of hinging and those at the edge of hinging.*

Curvature

The unit curvature of the edge of the hinge length, ϕ_{du}, can be expressed as the ratio of strain in the tension steel, ϵ_s, and the distance from the tension steel to the neutral axis. Thus,

$$\phi_{du} = \frac{\epsilon_s}{d - c} \text{ rad/in.} \qquad \text{(C-14)}$$

where ϵ_s equals f_{dy}/E_s.

DEFLECTION AT MIDSPAN

By assuming linear curvature distribution along the span, a curvature diagram can be constructed as shown below.

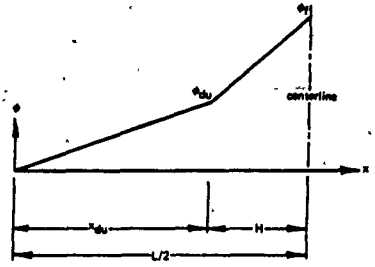

Curvature Diagram

The distance H is the distance from the center of the hinge to the edge of the hinge, and the distance x_{du} is the distance from the support to the edge of the hinge.

The true curvature distribution over the interval x_{du} is proportional to the ratio of moment, M, and stiffness, EI. The modulus, E, is essentially constant when considering the accuracy of the method, but the moment of inertia, I, is not. Thus,

$$\phi \approx \frac{M}{I}$$

Experience has shown that assuming linear distribution produces results about as accurate as those when assuming distribution proportional to M because of the variable nature of I, and the complex relation of I to x precludes I in the assumptions. It is understood that considerable accuracy is sacrificed here to achieve reasonable simplicity.

The deflection at midspan corresponding to failure in flexure (ϵ_{cu} = 0.006 in./in.) can be approximated by determining the hinging length and then summing the moments of areas in the curvature diagram about a point. The point of interest in this case is at the support.

The position along the span where the moment M_{du} exists can be approximated by assuming static moment distribution as shown below.

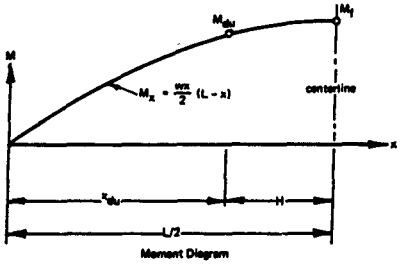

Moment Diagram

From the diagram, it can be seen that

$$M_{du} = \frac{w}{2} x_{du}(L - x_{du}) \qquad \text{(C-15)}$$

and

$$M_f = \frac{w L^2}{8} \qquad \text{(C-16)}$$

The ratio of the dynamic resisting moments at the center and edge of hinging is

$$\frac{M_f}{M_{du}} = \frac{L^2}{4x_{du}(L - x_{du})} \qquad \text{(C-17)}$$

Equation C-17 can be solved for x_{du} in terms of M_f, M_{du}, and L which are known. Therefore, the distance from the support to the edge of hinging, x_{du}, is

$$x_{du} = \frac{L}{2}\left(1 \pm \sqrt{1 - \frac{M_{du}}{M_f}}\right) \qquad \text{(C-18)}$$

Only one of the roots of this equation exists in the half of the beam under consideration; therefore,

$$x_{du} = \frac{L}{2}\left(1 - \sqrt{1 - \frac{M_{du}}{M_f}}\right) \qquad \text{(C-19)}$$

The deflection at midspan, y_f, corresponding to failure in flexure can then be derived by summing the moments of areas in the curvature diagram about a point at the support. Therefore,

$$y_f = \frac{L^2}{24}(\phi_{du} + 2\phi_f) + \frac{L}{12}x_{du}(\phi_{du} - \phi_f) - \frac{1}{6}x_{du}^2\phi_f \qquad \text{(C-20)}$$

CONCLUSION

If the midspan deflection, y, of the beam exceeds the value of y_f, the beam is considered to be failed by crushing of the concrete at the remote fiber at midspan.

REFERENCES

1. J. G. Hammer and A. F. Dill. "Failure criteria as applied to atomic defense engineering," in Department of the Navy, Bureau of Yards and Docks, NAVDOCKS P-290: Studies in atomic defense engineering. Washington, D. C., June 1962, pp. 1-3.

2. Army Corps of Engineers. Engineer Manual EM-1110-345-413 through EM-1110-345-420: Engineering manual for military construction: Engineering and design: Design of structures to resist the effects of atomic weapons. Washington, D. C., Mar. 1957 to Jan. 1960.

3. Department of the Navy. Bureau of Yards and Docks. NAVDOCKS P-81: Personnel shelters and protective construction. Washington, D. C., Sept. 1961.

4. Air Force Special Weapons Center. Technical Documentary Report No. AFSWC-TDR-62-138: Air Force design manual: Principles and practices for design of hardened structures, by N. M. Newmark and J. D. Haltiwanger. Kirtland Air Force Base, N. M., Dec. 1962. (Contract AF 29(601)-2390) (AD 295408)

5. C. H. Norris, et al. Structural design for dynamic loads. New York, McGraw-Hill, 1959.

6. Air Force Special Weapons Center. Technical Documentary Report No. AFSWC-TDR-62-138: Air Force design manual: Principles and practices for design of hardened structures, by N. M. Newmark and J. D. Haltiwanger. Kirtland Air Force Base, N. M., Dec. 1962, p. 7-5. (Contract AF 29(601)-2390) (AD 295408)

7. Cement and Concrete Association. Translation No. 111: The Stuttgart shear tests, 1961, by F. Leonhardt and R. Walther. London, England, Dec. 1964. (Originally appeared in Beton- und Stahlbetonbau, vol. 56, no. 12, 1961; vol. 57, nos. 2, 3, 6, 7, and 8, 1962)

8. National Research Council of Canada. Technical Translation 1172: Contribution to the treatment of shear in reinforced concrete, by F. Leonhardt and R. Walther. Ottawa, Canada, Feb. 1965. (Originally appeared in Beton- und Stahlbetonbau, vol. 56, no. 12, 1961; vol. 57, nos. 2, 3, 6, 7, and 8, 1962)

9. F. Leonhardt. "Reducing the shear reinforcement in reinforced concrete beams and slabs," Magazine of Concrete Research, vol. 17, no. 53, Dec. 1965, pp. 187-198.

10. S. H. Ojha. "The shear strength of rectangular reinforced and prestressed concrete beams," Magazine of Concrete Research, vol. 19, no. 60, Sept. 1967, pp. 173-184.

11. Columbia University. Department of Civil Engineering and Engineering Mechanics. Unnumbered report: Studies of the shear and diagonal tension strength of simply supported reinforced concrete beams, by W. J. Krefeld and C. W. Thurston. New York, N. Y., June 1962.

12. ACI-ASCE Committee 326. "Shear and diagonal tension, pt. 1. General principles," American Concrete Institute, Journal, Proceedings, vol. 59, no. 1, Jan 1962, pp. 1-30.
———: "Shear and diagonal tension, pt. 2. Beams and frames," American Concrete Institute, Journal, Proceedings, vol. 59, no. 2, Feb. 1962, pp. 277-333.
———: "Shear and diagonal tension, pt. 3. Slabs and footings," American Concrete Institute, Journal, Proceedings, vol. 59, no. 3, Mar. 1962, pp. 353-395.

13. American Concrete Institute. Committee 318: Building code requirements for reinforced concrete (ACI 318-63). Detroit, Mich., June 1963.
———: "Amendment," American Concrete Institute, Journal, Proceedings, vol. 60, no. 7, July 1963, pp. 809-815.

14. Naval Civil Engineering Laboratory. Technical Report R-395: Dynamic shear strength of reinforced concrete beams, pt. 1, by W. A. Keenan. Port Hueneme, Calif., Dec. 1965. (AD 627661)

15. J. G. Hammer and A. F. Dill. "Strength of materials under dynamic loadings," in Department of the Navy, Bureau of Yards and Docks, NAVDOCKS P-290: Studies in atomic defense engineering. Washington, D. C., June 1962, pp. 51-55.

16. N. R. Nagaraja Rao, M. Lohrmann, and L. Tall. "Effect of strain rate on the yield stress of structural steels," Journal of Materials, vol. 1, no. 1, Mar. 1966, pp. 241-262.

17. Army Engineer Waterways Experiment Station. Miscellaneous Paper no. 6-609: Dynamic and static tests of plain concrete specimens, by R. L. Lundeen. Vicksburg, Miss., Nov. 1963.

18. S. B. Nosseir. Static and dynamic behavior of concrete beams failing in shear, Ph.D. thesis, University of Texas. Austin, Tex., June 1966.

19. Air Force Weapons Laboratory. Technical Report No. AFWL-TR-67-113: Shear and bond strength of high-strength reinforced concrete beams under impact loads—first phase, by R. W. Furlong, et al. Kirtland Air Force Base, N. M., May 1968. (Contract AF 29(601)-6246) (AD 834407)

20. Iowa State University. Iowa Engineering Experiment Station. Final Report on Contract NBy-32222: The influence of normal pressure on bond between concrete and reinforcing steel in pull-out tests, by R. E. Untrauer, R. L. Henry, and J. F. Harris. Ames, Iowa, June 1964.

21. Naval Civil Engineering Laboratory. Technical Report R-331: NCEL dynamic testing machine, by W. L. Cowell. Port Hueneme, Calif., Oct. 1964. (AD 608173)

22.————: Technical Report R-394: Dynamic tests of concrete reinforcing steels, by W. L. Cowell. Port Hueneme, Calif., Sept. 1965. (AD 622554)

23.————: Technical Report R-502: Dynamic shear strength of reinforced concrete beams, pt. 2, by R. H. Seabold. Port Hueneme, Calif., Jan. 1967. (AD 644823)

24.————: Technical Report R-447: Dynamic properties of plain portland cement concrete, by W. L. Cowell. Port Hueneme, Calif., June 1966. (AD 635055)

25.————: Technical Report R-406: Dynamic compression tests on thin-section reinforced concrete, by D. S. Fuss. Port Hueneme, Calif., Dec. 1965. (AD 624770)

26.————: Technical Report R-534: Dynamic shear resistance of thin-webbed reinforced concrete beams, by D. S. Fuss. Port Hueneme, Calif., June 1967. (AD 655823)

27.————: Technical Report R-121: Design charts for R/C beams subjected to blast loads, by J. R. Allgood and G. R. Swihart. Port Hueneme, Calif., Oct. 1960. (AD 237958; PB 160552)

28. Air Force Special Weapons Center. Technical Documentary Report No. AFSWC-TDR-62-138: Air Force design manual: Principles and practices for design of hardened structures, by N. M. Newmark and J. D. Haltiwanger. Kirtland Air Force Base, N. M., Dec. 1962, pp. B6-B7. (Contract AF 29(601)-2390) (AD 295408)

29. Army Corps of Engineers. Engineering Manual EM 1110-345-414: Engineering manual for military construction: Engineering and design: Design of structures to resist the effects of atomic weapons: Strength of materials and structural elements. Washington, D. C., Mar. 1957.

30. Naval Civil Engineering Laboratory. Technical Report R-226: Blast loading of concrete beams reinforced with high-strength deformed bars, by W. A. Keenan. Port Hueneme, Calif., Apr. 1963. (AD 408447)

31. ———. Technical Report R-371: Plastic hinge formation in reinforced concrete beams, by W. J. Nordell. Port Hueneme, Calif., June 1965. (AD 617246)

32. ———. Technical Report R-489: Hinging in statically and dynamically loaded reinforced concrete beams, by W. J. Nordell. Port Hueneme, Calif., Oct. 1966. (AD 642108)

33. W. A. Shaw and J. R. Allgood. "An atomic blast simulator," Society for Experimental Stress Analysis, Proceedings, vol. 17, no. 1, 1959, pp. 127-134.

34. Naval Civil Engineering Laboratory Technical Note N-941: A versatile data tape system for static and dynamic tests, by R. H. Seabold. Port Hueneme, Calif., Jan. 1968. (AD 826036L)

LIST OF SYMBOLS

A	Area ($in.^2$)
A_s	Area of longitudinal tension steel ($in.^2$)
A_s'	Area of longitudinal compression steel ($in.^2$)
A_v	Stirrup area parallel to the beam axis ($in.^2$)
a	Ultimate design, stress block depth (in.); also shear span (in.)
b	Beam width (in.)
b'	Web width (in.)
C	Coefficient
C_1	Dynamic increase coefficient for concrete in tension
C_2	Dynamic increase coefficient for steel in tension
C_c	Compression force provided by the concrete (lb)
C_p	Load coefficient
C_r	Resistance coefficient
C_s	Compression force provided by the compression steel (lb)
c	Distance from the neutral axis to the remote fiber (in.)
D	Nominal diameter of bar (in.)
DSF	Dynamic shear factor at support
d	Effective depth of the beam (in.)
d'	Distance from the remote fiber to the centroid of the compression steel (in.)
d''	Distance from the remote fiber to the point of rotation (in.)
E	Modulus of elasticity (psi)
E_c	Modulus of elasticity of concrete in compression (psi)
E_s	Modulus of elasticity of steel (psi)
E_t	Modulus of elasticity of concrete in tension (psi)
E_v	Modulus of elasticity of stirrups (psi)
f	Stress (psi)
$\dot{f}$	Stress rate (psi/sec)
f_c	Stress in concrete (psi)
f_c'	Static compressive strength of the concrete at 28 days (psi)
f_{cy}	Effective yield stress of concrete (psi)
f_{cu}	Effective ultimate stress of concrete (psi)
f_{dc}'	Dynamic compressive strength of the concrete at 28 days (psi)
f_{dcy}	Dynamic yield strength of concrete (psi)
f_{dt}'	Dynamic tensile strength of the concrete at 28 days (psi)
f_{dvy}	Dynamic yield strength of stirrups (psi)
f_{dy}	Dynamic yield strength of tension steel (psi)
f_{dy}'	Dynamic yield strength of compression steel (psi)
f_s	Stress in tension steel (psi)
f_s'	Stress in compression steel (psi)
f_t	Tensile stress in concrete (psi)
$\dot{f}_t$	Stress rate of concrete in tension (psi/sec)
f_t'	Static tensile splitting strength of the concrete at 28 days (psi)
f_v	Stress in stirrup (psi)

sticity (psi)	f_{vy}	Static yield strength of stirrups (psi)
sticity of concrete in compression (psi)	f_y	Static yield strength of tension bars (psi)
sticity of steel (psi)	f'_y	Static yield strength of compression bars (psi)
sticity of concrete in tension (psi)	H	Distance from the center to the edge of the hinge (in.)
sticity of stirrups (psi)	h	Total depth of the beam (in.)
	I	Moment of inertia ($in.^4$)
/sec)	I_c	Moment of inertia of a cracked section ($in.^4$)
ete (psi)	I_g	Gross moment of inertia ($in.^4$)
sive strength of the concrete at	jd	Moment arm between centroids of compressive and tensile forces (in.)
stress of concrete (psi)	K_1	y/y_E, deflection ratio
ate stress of concrete (psi)	K_2	ϕ/y, curvature ratio ($rad/in.^2$)
ressive strength of the concrete	K_3	$x_u - x_c$, distance over which stirrups are active (in.)
	K_4	ϕ_E/y_E, curvature ratio at midspan ($rad/in.^2$)
strength of concrete (psi)	$K_{L,m}$	Load-mass factor ($in.\text{-}lb\text{-}sec^2/in.\text{-}lb\text{-}sec^2$)
e strength of the concrete at	k	Spring constant (lb/in.)
strength of stirrups (psi)	k_1	Stress block proportion
strength of tension steel (psi)	k_c	Spring constant of a cracked section (lb/in.)
strength of compression steel (psi)	L	Span length (in.)
n steel (psi)	M	Moment (in.-lb)
tension steel (psi)	M_{du}	Ultimate design, dynamic resisting moment (in.-lb)
) concrete (psi)	M_f	Dynamic resisting moment at the center of the hinge at the at the time of failure (in.-lb)
oncrete in tension (psi/sec)	M_R	Maximum resisting moment (in.-lb)
olitting strength of the concrete	M_x	Moment at distance x (in.-lb)
) (psi)	m	Mass ($lb\text{-}sec^2/in.$)

N	Number of yielded stirrups
n	E_s/E_c, modulus of elasticity ratio, also cycle number in numerical integration
P	Load between supports (lb)
P_c	Cracking load (lb)
p	$A_s/b\,d$, reinforcement ratio
p'	$A_s'/b\,d$, compression reinforcement ratio
p_t	Reinforcement ratio that would produce yielding of the compression reinforcement concurrent with yielding of the tension reinforcement
p_b	Reinforcement ratio that would produce balanced conditions
p_w	Tension reinforcement ratio for steel in the web
Q	Statical moment of the cross section (in.^{3})
q	Uniform load (lb/in.)
R	Flexural resistance (lb)
R_m	Maximum flexural resistance (lb)
R_s	Reaction at support (lb)
r	Radius of compression bar (in.)
r_y	Dynamic yield resistance (lb/in.)
s	Stirrup spacing, center to center, parallel to the beam axis (in.)
T	Load duration (sec); also tension force (lb)
T_n	Natural period of vibration (sec)
t	Time (sec)
u	Bond stress (psi)
u_u	Ultimate bond stress (psi)
V	Shear (lb)
V_b	Maximum allowable shear at the critical section for bond (lb)
V_c	Shear resistance contributed by the concrete (lb)
V_m	Maximum dynamic shear force at the support (lb)
V_s	Shear at the support (lb)
V_{sb}	Shear resistance at the support corresponding to the ultimate bond resistance (lb)
V_{sc}	Shear resistance at the support corresponding to the diagonal tension cracking resistance (lb)
V_{su}	Shear resistance at the support corresponding to the usable ultimate shear resistance (lb)
V_u'	Usable ultimate shear resistance (lb)
V_x	Shear at distance x from the support (lb)
v	Shear stress (psi)
v_c	Shear strength contributed by the concrete (psi)
v_m	Maximum shear stress at the critical section (psi)
v_u	Usable ultimate shear strength (psi)
W	Weight of the beam (lb)
w	Uniformly distributed load (lb/in.)
w_o	Peak uniform load (lb/in.)
x	Distance from the support along the beam axis (in.)
x_b	Distance from the support to the critical section for bond (in.)
x_c	Distance from the support to the critical section for shear (in.)
x_t	Distance from the support to the point where the amount of web reinforcement changes (in.)
x_u	Distanc
y	Deflect
$\dot{y}$	Velocit
$\ddot{y}$	Acceler
y_{ℓ}	Deflect
$\dot{y}_{\ell}$	Velocit
y_f	Deflect flexure
y_y	Yield d
z	Overha
α	Angle b
Δt	Time ir
Σ_o	Sum of
ϵ	Strain (
$\dot{\epsilon}$	Strain r
ϵ_c	Strain i
$\dot{\epsilon}_c$	Strain r
ϵ_{cu}	Ultimat
ϵ_{cy}	Yield st
ϵ_{dvy}	Dynam
ϵ_s	Strain i
$\dot{\epsilon}_s$	Strain r
ϵ_s'	Strain i
$\dot{\epsilon}_s'$	Strain r
ϵ_t'	Strain i cracking

ı the support to the point of rotation (in.)	ϵ_{su} Ultimate strain of steel (in /in)
ı.)	ϵ_{sy} Yield strain of steel (in /in)
sec)	ϵ_v Strain in stirrup (in /in)
(in./sec^2)	$\dot{\epsilon}_v$ Strain rate in stirrup (in /in /sec)
midspan (in.)	ϵ_{vy} Yield strain of stirrup (in /in.)
idspan (in./sec)	ρ Density (lb/ft^3)
midspan corresponding to failure in	σ Direct stress (psi)
on (in)	σ_{dy} Dynamic yield stress (psi)
)	σ_y Static yield stress (psi)
n stirrup axis and beam axis (deg)	ϕ Capacity reduction factor (psi/psi); also unit curvature (rad/in.)
nt (sec)	$\dot{\phi}$ Rate of change of unit curvature with respect to time (rad/in./sec)
eters of effective bars (in.)	ϕ_{ℓ} Unit curvature at midspan (rad/in.)
)	ϕ_{du} Unit curvature at the edge of the hinge (rad/in.)
ı./in /sec)	ϕ_u Unit curvature at the center of the hinge at the time of failure (rad/in.)
crete (in./in.)	
concrete (in./in./sec)	
in of concrete (in /in.)	
d concrete (in./in.)	
d strain of stirrup (in./in.)	
ion steel (in /in)	
tension steel (in /in /sec)	
pression steel (in /in.)	
compression steel (in /in /sec)	
concrete in diagonal tension upon shear in)	

B

Naval Civil Engineering Laboratory
DYNAMIC SHEAR STRENGTH OF REINFORCED CONCRETE BEAMS—PART III (Final), by Richard H. Seabold
TR-695 181 p. illus September 1970 Unclassified

1. Reinforced concrete beams 2. Dynamic shear strength
I. Y-F008-08-02 110 II. DASA SC3318

Shear and diagonal tension in rectangular, reinforced concrete beams on simple supports and subjected to uniformly distributed dynamic and static loads were studied to determine the minimum web reinforcement required for (1) developing the ultimate flexural resistance of beams, and (2) to determine the difference between these criteria for static and dynamic loading. The main experimental work consisted of testing 53 beams; 29 were loaded dynamically and 24 were loaded statically. Forty-seven beams contained web reinforcement and six had none. All of the beams were tested in the NCEL blast simulator. Static loads were applied using compressed air, and dynamic loads were applied using the expanding gas from detonation of Primacord explosive. All of the beams were slender, and all of them were rectangular except 10 that were I-shaped. The shear and the shear strength in the beams were greater under dynamic load than under the same static load. Furthermore, a beam with enough web reinforcement to force flexural failure under static loading might not have enough to force flexural failure under dynamic loading. Theory predicted behavior up to the usable ultimate shear strength within normal engineering accuracy and provided a fair estimate of the time, location, and mode of failure.

Naval Civil Engineering Laboratory
DYNAMIC SHEAR STRENGTH OF REINFORCED CONCRETE BEAMS—PART III (Final), by Richard H. Seabold
TR-695 181 p. illus September 1970 Unclassified

1. Reinforced concrete beams 2. Dynamic shear strength
I. Y-F008-08-02 110 II. DASA SC3318

Shear and diagonal tension in rectangular, reinforced concrete beams on simple supports and subjected to uniformly distributed dynamic and static loads were studied to determine the minimum web reinforcement required for (1) developing the ultimate flexural resistance of beams, and (2) to determine the difference between these criteria for static and dynamic loading. The main experimental work consisted of testing 53 beams; 29 were loaded dynamically and 24 were loaded statically. Forty-seven beams contained web reinforcement and six had none. All of the beams were tested in the NCEL blast simulator. Static loads were applied using compressed air, and dynamic loads were applied using the expanding gas from detonation of Primacord explosive. All of the beams were slender, and all of them were rectangular except 10 that were I-shaped. The shear and the shear strength in the beams were greater under dynamic load than under the same static load. Furthermore, a beam with enough web reinforcement to force flexural failure under static loading might not have enough to force flexural failure under dynamic loading. Theory predicted behavior up to the usable ultimate shear strength within normal engineering accuracy and provided a fair estimate of the time, location, and mode of failure.

Naval Civil Engineering Laboratory
DYNAMIC SHEAR STRENGTH OF REINFORCED CONCRETE BEAMS—PART III (Final), by Richard H. Seabold
TR-695 181 p. illus September 1970 Unclassified

1. Reinforced concrete beams 2. Dynamic shear strength
I. Y-F008-08-02 110 II. DASA SC3318

Shear and diagonal tension in rectangular, reinforced concrete beams on simple supports and subjected to uniformly distributed dynamic and static loads were studied to determine the minimum web reinforcement required for (1) developing the ultimate flexural resistance of beams, and (2) to determine the difference between these criteria for static and dynamic loading. The main experimental work consisted of testing 53 beams; 29 were loaded dynamically and 24 were loaded statically. Forty-seven beams contained web reinforcement and six had none. All of the beams were tested in the NCEL blast simulator. Static loads were applied using compressed air, and dynamic loads were applied using the expanding gas from detonation of Primacord explosive. All of the beams were slender, and all of them were rectangular except 10 that were I-shaped. The shear and the shear strength in the beams were greater under dynamic load than under the same static load. Furthermore, a beam with enough web reinforcement to force flexural failure under static loading might not have enough to force flexural failure under dynamic loading. Theory predicted behavior up to the usable ultimate shear strength within normal engineering accuracy and provided a fair estimate of the time, location, and mode of failure.

Naval Civil Engineering Laboratory
DYNAMIC SHEAR STRENGTH OF REINFORCED CONCRETE BEAMS—PART III (Final), by Richard H. Seabold
TR-695 181 p. illus September 1970 Unclassified

1. Reinforced concrete beams 2. Dynamic shear strength
I. Y-F008-08-02-110 II. DASA SC3318

Shear and diagonal tension in rectangular, reinforced concrete beams on simple supports and subjected to uniformly distributed dynamic and static loads were studied to determine the minimum web reinforcement required for (1) developing the ultimate flexural resistance of beams, and (2) to determine the difference between these criteria for static and dynamic loading. The main experimental work consisted of testing 53 beams; 29 were loaded dynamically and 24 were loaded statically. Forty-seven beams contained web reinforcement and six had none. All of the beams were tested in the NCEL blast simulator. Static loads were applied using compressed air, and dynamic loads were applied using the expanding gas from detonation of Primacord explosive. All of the beams were slender, and all of them were rectangular except 10 that were I-shaped. The shear and the shear strength in the beams were greater under dynamic load than under the same static load. Furthermore, a beam with enough web reinforcement to force flexural failure under static loading might not have enough to force flexural failure under dynamic loading. Theory predicted behavior up to the usable ultimate shear strength within normal engineering accuracy and provided a fair estimate of the time, location, and mode of failure.

Unclassified
Security Classification

DOCUMENT CONTROL DATA - R & D

Security classification of title, body of abstract and indexing annotation must be entered when the overall report is classified.

1 ORIGINATING ACTIVITY (Corporate author)
Naval Civil Engineering Laboratory
Port Hueneme, California 93041

2a. REPORT SECURITY CLASSIFICATION
Unclassified

2b GROUP

3 REPORT TITLE
DYNAMIC SHEAR STRENGTH OF REINFORCED CONCRETE BEAMS—PART III

4 DESCRIPTIVE NOTES (Type of report and inclusive dates)
Final; July 1966–November 1968

5 AUTHOR(S) (First name, middle initial, last name)
Richard H. Seabold

6 REPORT DATE
September 1970

7a. TOTAL NO OF PAGES
181

7b. NO OF REFS
34

8a. CONTRACT OR GRANT NO
DASA SC3318

8b. ORIGINATOR'S REPORT NUMBER(S)
TR-695

b. PROJECT NO Y-F008-08-02-110

c.

d.

9b. OTHER REPORT NO(S) (Any other numbers that may be assigned this report)

10 DISTRIBUTION STATEMENT
This document has been approved for public release and sale; its distribution is unlimited.

11 SUPPLEMENTARY NOTES

12 SPONSORING MILITARY ACTIVITY
Defense Atomic Support Agency
Naval Facilities Engineering Command

13 ABSTRACT

Theoretical and experimental work was done at NCEL to study shear and diagonal tension in rectangular, reinforced concrete beams on simple supports and subjected to uniformly distributed dynamic and static loads. The objective was to determine criteria for the minimum amount of web reinforcement required for developing the ultimate flexural resistance of beams, and to determine the difference between these criteria for static and dynamic loading. The main portion of the experiment work consisted of testing 53 beams; 29 were loaded dynamically and 24 were loaded statically. Emphasis was placed on effectiveness of web reinforcement; 47 beams contained web reinforcement and six had none. All of the beams were tested in the NCEL blast simulator. Static loads were applied using compressed air, and dynamic loads were applied using the expanding gas from detonation of Primacord explosive. All of the beams were slender, and all of them were rectangular except 10 that were I-shaped. It was found that the shear and the shear strength in the beams were greater under dynamic load than under the same amount of load applied statically. Furthermore, it was found that a beam with enough web reinforcement to force flexural failure under static loading might not have enough to force flexural failure under dynamic loading. The theory was found to predict behavior up to the usable ultimate shear strength within normal engineering accuracy, and to provide a fair estimate of the time, location, and mode of failure.

DD FORM 1473 (PAGE 1)
S/N 0101-807-6801

Unclassified
Security Classification

Unclassified
Security Classification

KEY WORDS	LINK A		LINK B		LINK C	
	ROLE	WT	ROLE	WT	ROLE	WT
Reinforced concrete						
Rectangular beams						
Simple supports						
Dynamic loads						
Static loads						
Web reinforcement						
Flexural resistance						
Modal analysis						
Shearing force						
Single-degree-of freedom system						
Stirrup						
I-beams						
Mode of failure						

DD FORM 1 NOV 68 1473 (BACK)
(PAGE 2)

Unclassified
Security Classification